Aerosol-Cloud Radiative Properties and its Impacts on Climate

By

Muhammad Iftikhar

Reg. No. 17-FBAS/PHDPHY/F12

Department of Physics
Faculty of Basic and Applied Sciences
INTERNATIONAL ISLAMIC UNIVERSITY
ISLAMABAD

2020

I Atmospheric Aerosols

II Clouds

III Environmental

IV Atmospheric physics

Aerosol-Cloud Radiative Properties and its Impacts on Climate

By

Muhammad Iftikhar

17-FBAS/PHDPHY/F12

This thesis is submitted to the Department of Physics, International Islamic University, Islamabad.

For the award of degree of

Doctor of Philosophy in Physics

Signature: _____

Chairman
Department of Physics, FBAS
International Islamic University
Islamabad

Chairman, Department of Physics

International Islamic University, Islamabad

Signature: _____

Dean, Faculty of Basic and Applied Sciences,

International Islamic University, Islamabad

Department of Physics
Faculty of Basic and Applied Sciences
International Islamic University, Islamabad

Dated: 24 February 2021

FINAL APPROVAL

It is certified that the work presented in this PhD thesis entitled "**Aerosol-Cloud Radiative Properties and its Impacts on Climate**" by **Muhammad Iftikhar**, Registration No.**17-FBAS/PHDPHY/F12** is of sufficient standard in scope and quality for award of Degree of PhD in Physics from the Department of Physics, International Islamic University, Islamabad, Pakistan.

VIVA VOCE COMMITTEE

Chairman
Dr. Wiqar Hussain Shah
Associate Professor, Department of Physics,
International Islamic University, Islamabad.

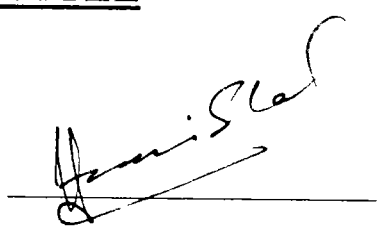

Supervisor
Dr. Khan Alam
Assistant Professor, Department of Physics,
University of Peshawar

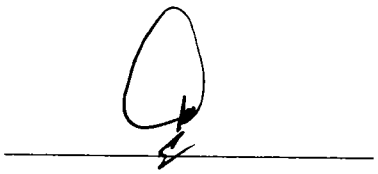

Co Supervisor
Dr Waqar Adil Syed
Associate Professor, Department of Physics,
International Islamic University, Islamabad

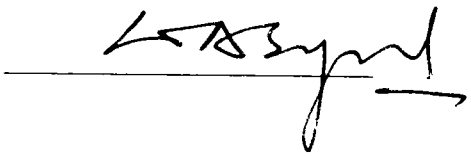

External Examiner-I
Dr. Javed Iqbal Saggu
Associate Professor, Department of Physics,
Qaid-e-Azam University, Islamabad

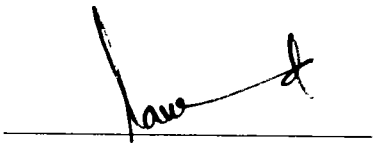

External Examiner-II
Prof. Dr. Sajid Qamar
Professor, Department of Physics,
Comsats University, Islamabad

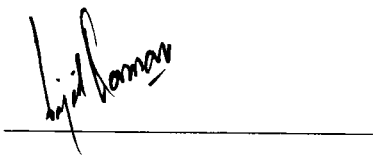

Internal Examiner
Dr. Sardar Sikandar Hayat
Associate Professor, Department of Physics,
International Islamic University, Islamabad

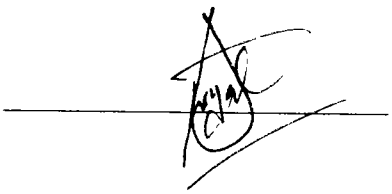

DECLARATION

I, Muhammad Iftikhar, hereby declare that the research work presented in this thesis is produced by me during the scheduled course of time. My name in all the publications is written as Iftikhar, M. It is further declared that this thesis neither as a whole nor as a part thereof has been copied out from any source except referred by me whenever due. No portion of the work presented in this thesis has been submitted in support of any other degree or qualification of this or any other university or institute of learning. If any violation of HEC rules on research has occurred in this thesis, I shall be liable to punishable action under the plagiarism rules of Higher Education Commission (HEC) Pakistan.

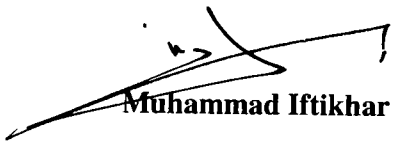

Muhammad Iftikhar

17-FBAS/PHDPHY/F12

Dedicated to

My Mother, Wife, and Kids (Somama, Esa, Simal and Rizma)
For Their Love, Support and Prayers

ABSTRACT

In this thesis, aerosol and cloud optical characteristics were analyzed using remote sensing observations in various cities of Pakistan. This study is carried out in two different phases. At the first phase, aerosol characteristics were analyzed during extreme episodes (EE) of haze and dust in two major cities, namely Karachi and Lahore. In the second phase, cloud optical characteristics were studied in three mountainous locations of Gilgit, Skardu, and Diamir situated in the glacier region of Northern Pakistan.

Aerosol optical properties and radiative forcing were investigated during the EE of haze and dust in Lahore and Karachi during 2010–2014. During the EE, the dust and haze particles have high Aerosol Optical Depth (AOD) and low Ångström Exponent (AE), and high AOD and high AE, respectively. The aerosol optical characteristics, such as AOD, AE, aerosol volume size distributions, single scattering albedo, asymmetry parameter, and refractive index showed contrasting variations during the EE of haze and dust.

The results of AOD-AE relationship and remote sensing observations depicted that dust was the major type of aerosol during dust episodes, and urban industrial and biomass burning were dominant aerosol types during the haze episodes. In order to calculate the climatic effects of aerosol, the Santa Barbra DISORT Atmospheric Radiative Transfer (SBDART) model was used to calculate the aerosol radiative forcing (ARF) at the surface (SUR), top of the atmosphere (TOA), and within the atmosphere (ATM). The model results showed negative ARF both at the TOA and SUR during both haze and dust episodes. The large differences between SUR and TOA forcing revealed positive ARF within the ATM, which produced significant heating of the lower atmosphere.

The assessment of varying cloud optical properties and their sensitivity to meteorological parameters and radiation fluxes is gaining concern to investigate climate change. For this purpose,

this study is carried out at high altitudes of Diamir, Gilgit and Skardu in the Himalaya Karakoram (HK) region of Northern Pakistan. The spatio-temporal variations in cloud optical properties and the impacts of radiation feedback and meteorological parameters were investigated for the period from 2004 to 2016. The obtained results revealed high values of cloud fraction (CF), cloud water path (CWP) and cloud optical depth (COD) in winter months, while contrasting response was observed in summer months. Due to Twomey effect, clouds become thicker and brighter with maximum COD and liberation of latent heat, which modifies temperature gradient of vertical profile. Similarly, an uneven distribution of cloud effective radius (CER) was observed throughout the study period. Whereas, the reduced CER makes possible to lift up a large quantity of water vapor. An increasing trend of cloud top temperature (CTT) from February to September was observed, while an opposite response was found from September to January. Cold clouds with CTT less than 273K were observed in all seasons over all study areas. Likewise, minimum and maximum cloud top pressure CTP was found in February and November, respectively. However, the relationship between CER and CTP clearly depicted the curvature effect. In addition, a positive relationship was found for COD and CTP against top of the atmosphere shortwave cloud radiative forcing (TOASWCRF), depicted the cooling effect due to increasing COD and CTP. With TOASWCRF, a variation in CWP and CER may also lead to cooling effect due to the reflection of solar radiations. While the meteorology depicted an uneven relationship with cloud optical properties at observation sites.

LIST OF PUBLICATIONS

1. Iftikhar, M., Alam, K., Syed, W. A., Ahmad, M., Zeb, B., Liu, Y., & Gulistan, N. (2021). Contrasting changes in cloud optical properties and the influence of aerosols, meteorology and radiation feedback in the Himalaya Karakoram region. Atmospheric Research, 248, 105210.
2. Iftikhar, M., Alam, K., Sorooshian, A., Syed, W. A., Bibi, S., & Bibi, H. (2018). Contrasting aerosol optical and radiative properties between dust and urban haze episodes in megacities of Pakistan. Atmospheric environment, 173, 157-172.
3. Iftikhar, M., Alam, K., Syed, W. A. (2016). Analysis of aerosol characteristics over two mega cities of Pakistan using long term AERONET observations. Journal of GeoSpace Science, 1(2), 14-30.

Acknowledgement

To start and complete thesis is not only a difficult, but also an uphill task. However, Allah almighty made this task easy for me and today I have completed this thesis with the blessing of Allah almighty who bestowed upon me the strength and wisdom to complete this tough task. Today I am going to acknowledge the able and timely guidance and advise of Dr. Khan Alam, my supervisor and mentor who fully supported and guided me in completion of this thesis, here I am frankly conceded that without the active support, guidance and advise of Dr. Khan Alam, the present task was not possible. I also acknowledge the support, guidance and encouragement of Dr. Waqar Adil Syed, my Co-supervisor made this difficult task possible to complete with triumph. Here, I also acknowledge the support of Dr. Atif Elahi, Ms. Maryam Faheem, Mr. Kashif Ahmad, Mr. Yasir Ahmad, Mr. Khalid Asad, Mr. Fazli Subhan, Mr. Wajid, and Mr. Iftikhar Khan Khalil, who whole heartedly supported me and always boosted my courage for the completion of this task. I also whole heartedly extend my thanks and gratitude to my family members who always supported and co-operated with me and always appreciated and acknowledged my hard work, struggle and efforts towards the present task.

I am grateful to NASA for providing the AERONET data, MODIS data and CERES data product for five observational sites (Karachi, Lahore, Diamir, Gilgit and Skardu). I also grateful to CALIPSO mission scientists for the provision of data utilized in this research work. We gratefully acknowledge the working team for the global HYSPLIT data set.

Muhammad Iftikhar

TABLE OF CONTENTS

LIST OF FIGURES

LIST OF TABLES

List of Abbreviations/Acronyms

AERONET	AErosol RObotic NETwork
MODIS	MODerate Resolution Imaging Spectroradiometer
CALIPSO	Cloud-Aerosol Lidar and Infrared Pathfinder Satellite Observation
TOMS	Total Ozone Mapping Spectrometer
AVHRR	Advanced Very High Resolution Radiometer
AS	Arabian Sea
EIO	Equatorial Indian Ocean
BBI	Bay of Bengal, India
R	Correlation Coefficient
BC	Black Carbon
AOD	Aerosol Optical Depth
AVSD	Aerosol Volume Size Distribution
AE	Angstrom Exponent
AAE	Absorption Angstrom Exponent
EAE	Extinction Angstrom Exponent
SSA	Single Scattering Albedo
PF	Phase Function
AP	Asymmetry Parameter
RRI	Real Refractive Index
IRI	Imaginary Refractive Index
AI	Aerosol Index
GCOS	Global Climate Observing System
LaRC	Langley Research Center
COD	Cloud Optical Depth
CF	Cloud Fraction
CWP	Cloud liquid Water Path

CER	Cloud Effective Radius
CTT	Cloud Top Temperature
CTP	Cloud Top Pressure
T_{max}	Maximum Temperature
T_{min}	Minimum Temperature
MTR	Monthly Total Rain
RH	Relative Humidity
WS	Wind Speed
RF	Rainfall
OPAC	Optical Properties of Aerosols and Clouds
SBDART	Santa Barbra DISORT Atmospheric Radiative Transfer
SW	Short Wave
LW	Long Wave
ATM	Atmosphere
SUR	Earth's Surface
TOA	Top Of the Atmosphere
HR	Heating Rate
AFE	Absorption Forcing Efficiency
PM	Particulate Matter
UV	Ultraviolet
IGP	Indo-Gangetic Plain
NMP	Nucleation Mode Particles
AMP	Accumulation Mode Particles
CMP	Coarse Mode Particles
FMP	Fine Mode Particles
CERES	Clouds and the Earth's Radiant Energy System
EBAF	Energy Balanced and Filled product

ARFE	Aerosol Radiative Forcing Efficiency
ARF	Aerosol Radiative Forcing
DARF	Direct Aerosol Radiation Forcing
ERBE	Earth Radiation Budget Experiment
NSR	Net Surface Radiation
DE	Dust Episode
HE	Haze Episode
TOASWCRF	Top of the Atmosphere Shortwave Cloud Radiative Forcing
NOAA	National Oceanic and Atmospheric Administration
HYSPLIT	Hybrid Single Particle Lagrangian Integrated Trajectory
IMR	Indian Monsoon Region
EC	Eastern China
CBT	Cloud Based Temperature
MT	Meteorological Temperature
NASA	National Aeronautics and Space Administration
MISR	Multi-angle Imaging Spectroradiometer
SUPARCO	Space and Upper Atmosphere Research Commission
ISCCP	International Satellite Cloud Climatology Project

Chapter 1

Introduction

1.1 Aerosols

Aerosols are considered as a significant part of global environmental system, having significant variation in their size, nature, optical properties and emission sources; they are basically a composite mixture of liquid or solid particle present in the earth's atmosphere. The lifetime of aerosols varies from few hours to several days and their size changes from nanometers to micrometers in diameter wise. The aerosols are emitted to the atmosphere both naturally and anthropogenically. Naturally, the aerosols are originated from dust, volcanic aerosols, natural sulfates and sea salt, while anthropogenically originate from soot, sulfates and organics [1, 2]. The natural aerosols are uncontrollable unlike anthropogenic aerosols; they are larger in concentration than anthropogenic aerosols on global scale, while on regional scale, the emission from transportation and industrial sectors, can contribute to increase the concentration of anthropogenic aerosols [3, 4]. The contribution of aerosols extended from regional to global scale. There are many adverse effects of aerosols on health, for example, respiratory infection, allergies, harmful cardiovascular, strokes and premature deaths. Besides health effects, aerosols are polluting air with associated impacts on air quality and climate change. It is concluded that comprehensive knowledge and understanding about aerosol sources, composition and transportation require special attention in order to quantify the air quality and global warming issues [5].

1.2 Types of Aerosol

On the basis of composition, aerosols are classified into primary and secondary aerosols. The directly emitted aerosols which are produced from the combustion, biomass burning, and fragmentation processes are called primary aerosols, while the aerosols formed by combining primary aerosols with other atmospheric particles are called secondary aerosols [6, 7]. Aerosols are divided into three types according to their morphology (size, shape and structure) [8]. These three types are: nucleation mode, accumulation mode, and coarse mode particles. Nuclei mode particles are usually produced by the transformation process of gas to particle and are usually ranges from 0.001-0.1 μm. AMP ranged from 0.1-1.0 μm, while coarse mode particles are larger than 1.0 μm. The coarse mode particles are produced by mechanical process, while the other particular size aerosols are formed by both chemical and mechanical ways during nucleation and accumulation processes [9].

1.3 Aerosols processes

Aerosols can be transported to short or long distances within the atmosphere and their compositions are variable. They are removed by two processes; wet deposition and dry deposition. The removal of aerosols by rain drops from the atmosphere is known as wet deposition, while settlement of aerosols on the earth surface due to the Brownian motion of the particles or the gravitational force is called dry deposition. The atmospheric aerosol processes are shown in the figure 1.1 [10].

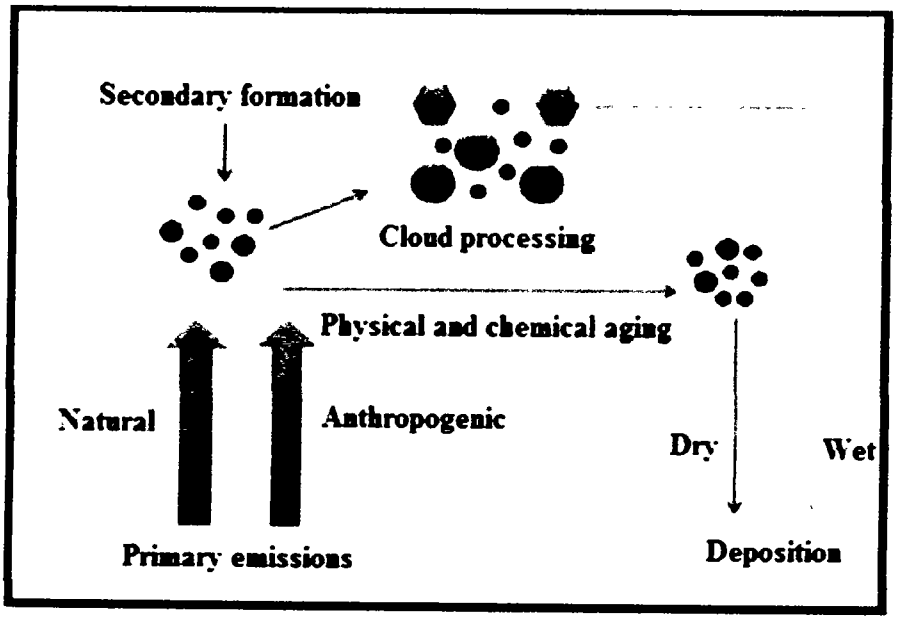

Figure 1.1 Aerosol process in the atmosphere [10]

1.4 Optical Characteristics of Aerosol

Aerosol optical properties play a significant role in the assessment of the earth's radiation budget, environmental health and air quality. The most important optical characteristics of aerosols are Aerosol Optical Depth (AOD), Angstrom Exponent (AE), Aerosol Volume Size Distribution (AVSD), Single Scattering Albedo (SSA), Asymmetry Parameter (AP), Phase Function (PF) and Refractive Indices (RI), which are discussed in detail in chapter 3. These optical properties are important for the estimation of radiative fluxes and heating rate.

1.5 Aerosols over Pakistan

Due to the large urbanization, population, industrialization, and diverse topography, Pakistan is severely affected by natural and anthropogenic aerosols. Different types of aerosol have different environmental consequence due to the size and absorption nature, for example shortwave radiation can be scattered by large size dust particle, while it can be absorbed by small size aerosols like

carbon particle. The sulfate particles reflect the solar radiation back to space. The loading of each type of aerosol and its spatial distribution changes seasonally can cause global as well as regional climate changes [11].

Aerosol has deteriorated air quality in Pakistan during the last few decades. It has also affected the monsoon circulation in the country. Pakistan is prone to both natural and anthropogenic aerosols. Therefore, in-depth analysis is of vital importance of aerosol characteristics both in natural and anthropogenic aerosol events.

1.6 Clouds

The water droplets or icy water particles suspended in the atmosphere in collective form or a mixture of both (mixed phase clouds), constitute clouds. Those clouds, which contain ice particles are called cold cloud, whereas cloud having liquid droplet are said to be warm clouds [12]. Cold or warm clouds' composition depends on clouds height and atmospheric temperature. Regardless of clouds influence and countless significance, the understanding of cloud micro and macro physics require more attention of the researchers for better understanding of the weather and climate.

1.7 Classification of clouds

Classification of clouds depends on appearance, atmospheric height and composition. Cloud can be classified on the bases of texture, e.g., Cirrus (hair's curl), Cumulus (pile), Stratus (layer), and Nimbus (rain), and on the bases of height , e.g., low level (Stratus and Stratocumulus clouds), mid level (Altocumulus), and high level (Cirrus) clouds [13].

1.8 Cloud Process

The Earth's climate and weather are regulated and controlled by clouds [4, 14]. Clouds cool the atmosphere of the Earth. Aerosols are produced naturally or anthropogenically. The aerosol acts as condensation nuclei for cloud and helps in the development of clouds. The clouds cool the surface of earth by back scattering of shortwave solar radiation to space and warm the atmospheric by trapping the longwave radiation. The cloud radiative properties depend on the size/number of these particles. When the size of cloud particle becomes 10 μm, they appear in the form of rain, colliding with one another and fall rapidly. The cloud particles formation, growth rate and rain fall is the function of aerosol particles concentration, chemical composition and dimension.

Clouds depend on thermodynamical processes (temperature, pressure, moisture, and air vertical velocity). Therefore, the chemical composition and modification of the aerosols significantly affect development of the cloud as well as weather and climate [15].

1.9 Optical characteristics of Cloud

The optical characteristics of clouds are very useful for the analysis and determination of cloud micro & macro physics and radiative properties. The important cloud optical characteristics included, the Cloud Optical Depth (COD), Cloud Fraction (CF) or Fractional Cloud Cover, Cloud liquid Water Path (LWP), Cloud Effective Radius (CER), Cloud Top Temperature (CTT) and Cloud Top Pressure (CTP). The mentioned optical characteristics are discussed in detail in chapter 3.

1.10 Motivation and Scope of research work

Pakistan is one of the most vulnerable countries to climate change. Climate change is not just an environmental challenge, but a serious issue impacting our economy, agriculture, human health, energy and ecosystem. Recent studies showed that aerosol is an important factor that contribute to

climate change. Variations in aerosol and cloud can be understood in a better way by including and analyzing aerosol and cloud microphysical properties, which play key roles in various processes, such as the hydrological cycle, energy budget, and monsoon circulation, etc.

Keeping the importance of aerosol and cloud in various processes, the major objectives of this study are summarized below:

- To analyze the spatio-temporal and synoptic variability of aerosol and cloud concentration/amount.
- To characterize anthropogenic and mineral dust aerosols from aerosol optical properties.
- To investigate urban-industrial/mineral dust aerosols' warming or cooling effect at the earth's surface, top of atmosphere, and within the atmosphere.
- To investigate the effects of aerosols –cloud radiative properties in different regions of Pakistan.

1.11 Layout of the study

The present study exhibits the detailed analysis of ground and satellite observations to assess/quantify the optical/radiative properties of aerosols and clouds in Pakistan. Apart from the introduction chapter, the remaining thesis is organized as follows:

Chapter 2: This portion focuses on the significant contextual information about aerosol optical and radiative properties, and cloud optical and radiative properties.

Chapter 3: This section will comprise of instrument/methodology used in the present research.

Chapter 4: This chapter is aimed to analyze the contrasting changes in aerosol characteristics during extreme episodes of haze and dust over Karachi and Lahore. This work has been published in Atmospheric Environment.

Chapter 5: This section deals with the detailed analysis of Long-term changes in cloud optical properties in the Himalaya Karakoram region, northern Pakistan. Monthly/seasonal variation of cloud optical properties (CF, COD, CER, CWP, CTT, and CTP) are subsequently discussed over Diamir, Gilgit and Skardu during the period of 2004-2016. The impacts of meteorology on cloud properties were thoroughly analyzed. Finally, the impacts of cloud radiation feedback on cloud properties were also discussed. This work is accepted in Atmospheric Research and will be available online soon.

Chapter 6: This chapter is of great concern to summarize the thesis results and further providing future valuable recommendations.

Chapter 2

Literature Review

The analysis of the aerosol-cloud optical characteristics, aerosol-cloud radiative properties, and aerosol-cloud interaction plays a critical part in realizing the impacts of aerosol and cloud in the earth's atmosphere system. In the context of the aforementioned facts, a comprehensive analysis of the available sources in respect of the co-relation of satellite and ground-based data regarding optical and radiative properties of aerosol, and cloud are accumulated in detail through various sub-sections as given below:

2.1 Aerosol optical properties

The solar radiation is significantly affected by the variation of aerosol particles. As upward terrestrial thermal radiation absorbed by the aerosols, they become the origin of modifications in local and global albedo. Aerosol particles both scatter and absorb the solar radiation through direct and indirect effect. Aerosol affects directly the radiation balance and indirectly the cloud condensation nuclei and its optical properties. Numerous studies have been conducted to investigate the optical properties of atmospheric aerosol and their impacts on climatic dynamics.

Dubovik *et al.* [16] worked on the optical properties of desert dust, urban and industrial aerosols, mineral dust and biomass burning aerosols' utilizing ground based data retrieved from the Aerosol Robotic Network (AERONET) over various locations of the world-wide for a time span of 8 years from 1993 to 2000. The authors investigated RI, VSD, phase function, AE and AOD and concluded that substantial variations in the absorbing characteristics of the same type of

aerosols are based on characteristics of its origin and diversity in the meteorological conditions. Similarly, Toledano *et al.* [17] examined the optical characteristics of atmospheric aerosols for the period 2000 to 2004 utilizing AERONET data for AE and concluded that coarse particles have maximum and minimum values of AOD and AE respectively.

The influences of dust episodes on aerosol optical properties such as AOD, AE, AVSD, SSA, and RI (both imaginary and real) were examined through utilization of AERONET data over the Kanpur city during the period of 2001 to 2003. The results depicted distinct differences of the visual properties of the aerosols. The aforesaid analysis also showed that dust loading and aerosol optical properties show significant seasonal fluctuations [18]. The climatological and influencing features of atmospheric aerosols were analyzed over Beijing, Ilorin and Kanpur. Based on the results it was reported that the external linear mixing of particles with diversity in size and physical properties significantly affects the variation of SSA [19].

In a study carried out over Karachi, Pakistan, Alam *et al.* [20] investigated few characteristic properties of aerosols from August 2006 to July 2007 using AERONET data. The results showed that for longer wavelength the AOD is lower. However, for shorter wavelength, higher AOD is observed. In the same year, Gautam *et al.* [21] examined AOD distribution in pre-monsoon during 2009 over the Southern slope of the Himalayas and Indo-Gangetic Plains (IGP) and reported that the transportation of dust from arid regions of southwest Asia into the IGP is the cause of the increase in the average value of seasonal AOD by 0.6 to the highest value noted over southern Asia. They also reported that the noticeable coarse mode peak in AVSD and spectral SSA is due to enhancement of dust loading and high concentration of absorbing aerosol recorded at the western part of the IGP. Dumka *et al.* [22] worked on the optical properties of aerosols latitudinal wise, included the solar spectral disparities of AE, AOD, and SSA along with a dual mode of

distribution of probability in the context of volume size distribution, over central Himalayas foothills and IGP for the period 2008-2009 during pre-monsoon season. The authors reported that AOD increases from central Himalayas to IGP region. While, the observed variation in the VSD showed that coarse and fine particles are dominant at Kanpur and Nainital, respectively.

Alam *et al.* [20] employed SSA and VSD analysis to look into several properties of aerosols over an urbanized and industrialized environment of Karachi. The researchers reported that the coarse particles were more dominant in summertime as compared to other seasons. Similarly, Alam *et al.* [23] reported that angstrom exponents of extension and absorption may be employed as an indicator of minerals and urban-industrial aerosols for Karachi and Lahore during 2010–2011.

Using data retrieved from AERONET for the period July-December, 2012 over Gorongosa (central Africa), Adesina *et al.* [24] observed high and low AOD in September and November, respectively, and VSD has a maximum fine mode fraction due to biomass burning in September other than in the remaining months. An extreme dust happened in March, 2012 in the Middle East and Southwest Asia, the AOD was maximum with values greater than 4.9 and the other optical properties (AVSD, SSA) showed the presence of thick dust in the environment [25]. Similarly, during spring 2001-2014, the higher AOD and lower AE values were reported over Beijing (China), which suggested the presence of the dominant coarse-mode particles [26]. Furthermore, high values of SSA and RI demonstrated the presence of dust aerosols over the observation site.

2.2 Aerosol radiative properties

Two important effects, which played a crucial role upon the planetary radiation fluxes, are direct and indirect effects. In direct effect, the solar fluxes are directly scattered or absorbed. However,

negative at SUR, in time period 2001-2005 over Kanpur and Delhi, having maximum values in pre monsoon [33, 34]. The ARF calculated at 25 stations in China during 2006 suggested overall negative ARF at SUR (-15.7 ± 8.9 Wm^{-2}). While, a positive value of ARF was recorded at the TOA (0.3 ± 1.6 Wm^{-2}) and within the ATM ($16.0 \pm 9.2 Wm^{-2}$), consequently produced cooling and warming effects at the SUR and within the ATM, respectively [35]. Likewise, maximum values of seasonal ARF at TOA, SUR and within the ATM have been taped in summertime. While, minimum values have been noticed in winter season. The ARF over Delhi for the period from 2006 to 2007 was analyzed by Singh *et al.* [36]. The results showed positive ARF in June at the TOA (21 ± 2 Wm^{-2}) and negative at the SUR ($-46 \pm 8 Wm^{-2}$) in August, while contrasting behavior was found in November.

The aerosol radiative forcing for a time span of one year starting from August,2006 to July,2007 over megacity Karachi (Pakistan) was estimated by Alam *et al.* [20] and reported the negative ARF at TOA (mean $-22 \pm 6 Wm^{-2}$) and surface (SUR) (mean $-73 \pm 12 Wm^{-2}$), while positive ARF within the ATM (mean $+51 \pm 13 Wm^{-2}$). Furthermore, a noteworthy statistical association among the SBDART and AERONET radiative forcing at TOA and SUR was also calculated.

Pandithurai *et al.* [34] observed increasing pattern of negative forcing at SUR that can produced positive ARF with heating rate (HR) up to 2.5 $Kday^{-1}$. Similarly, HR of ~0.3 $Kday^{-1}$ was calculated over Bay of Bengal that is higher than for the Arabian Sea in pre-monsoon [37]. Likewise, Kumar and Devara, [38] worked on the calculation of radiative forcing at SUR, TOA and within the ATM with their associated HR over Pune from 2004 to 2009 and observed negative ARF at both SUR and TOA, and positive within the ATM during all seasons. Their study depicted highest HR of 0.95 $Kday^{-1}$during pre-monsoon with consequent decreasing trend in winter seasons and post-monsoon with HR values of 0.84 and 0.86 $Kday^{-1}$, respectively. Similarly, Alam *et al.* [23] studied

ARF in summer and winter in Karachi and Lahore and observed positive atmospheric forcing producing HR in the range 1.1-1.8 $Kday^{-1}$ in winter season and 1.2-2.3 $Kday^{-1}$ in summer season. Valenzuela *et al.* [39] calculated ARF during dust episodes from 2005-2010 over Granada and reported negative ARF both at SUR and TOA, which produced positive atmospheric forcing in the region. Srivastava and Ramachandran, [40] reported negative ARF at both SUR and TOA with maximum ($-44Wm^{-2}$) and minimum ($-24Wm^{-2}$) at SUR over Kanpur and Ghandi College respectively. The large SUR and TOA forcing produced HR of 0.75 $Kday^{-1}$ (in pre-monsoon) and 0.5 $Kday^{-1}$ (in monsoon), respectively over the locations under study.

Likewise, ARF and ARFE were analyzed over the western Mediterranean during the period 2003-2011 and observed TOA and SUR forcing ranged from -1.5 to -3.9 Wm^{-2} and from -6 to-29 Wm^{-2}, respectively. Similarly, the recorded ARFE at TOA and SUR was -19.2 ± 0.3 Wm^{-2} and-139 ± 3 Wm^{-2}, respectively. The observed negative statistics indicated that the solar radiation is absorbed by the airborne aerosols, which conforms the significant features of environmental aerosols at the selected area [41].

Taneja *et al.* [42] estimated direct aerosol radiation forcing (DARF) over Delhi in 2013. The DARF at TOA, ATM and SUR was ranging from, -14.8 W m^{-2} to -48.8 W m^{-2}, 18.8 W m^{-2} to 90.6 W m^{-2} and -33.6 W m^{-2} to -117 W m^{-2}, respectively. Generally, it was found that DARF values were minimum during winter and maximum in summer season. Bhaskar *et al.* [43] in a study over Jodhpur, India computed ARF for the period from May 2011 to April 2012 and reported negative ARF, both at the TOA and SUR during the whole period, suggesting the dominance of scattering dust particles. However, these parameters showed positive values at the ATM, indicating atmospheric heating effect, particularly higher during pre-monsoon (+40.5 W/m^2) as to other seasons. The ARFE observed values at TOA and SUR were -63.2 W/m^2 and -4.2 W/m^2,

respectively, showing the cooling effect. While, the ARFE within the ATM was found to be +59 W/m^2, indicated warming of the atmosphere. The variation in HR from post to pre monsoon were in the range from 0.49 $Kday^{-1}$ to 1.13 $Kday^{-1}$. Patel & Kumar, [44] worked out the ARF during May, 2012, over Dehradun, India, and reported the ARF at TOA and SUR to be –14.49 W m^{-2} and –53.29 W m^{-2}, respectively. The average net ARF within the ATM was 38.79 W m^{-2} indicating a high positive value with associated HR of ~1.1 $Kday^{-1}$.

Kalluri *et al.* [45] analyzed the DARF over Anantapur (India), and reported that the averaged DARF values within the ATM were found to be +26.9 ± 0.2 W m^{-2}, +36.8 ± 1.7W m^{-2}, +18.0 ± 0.6 W m^{-2} and +18.5 ± 3.1 W m^{-2}, during winter, summer, monsoon and post monsoon, respectively. The significant variation between DARF at TOA and SUR was detected during the summer due to more absorption of solar radiation (36.80 W m^{-2}) with corresponding HR ~1 K/day, in the presence of black carbon mass concentration (BC) in the study area. Similarly, Singh *et al.* [46] analysed ARF during severe dust storm over Patiala (India) in March, 2012. They reported the negative ARF at surface (-96.71 W m^{-2}) and positive ARF within the ATM ranging from +45 to +77 W m^{-2}, associated to the HR of 2.2 $Kday^{-1}$ in the said period. The results indicated that the dust may change the regional environment and hence affected local climate.

2.3 Cloud optical properties

Clouds have covered approximately 70% of the earth's surface. Therefore, they contribute a substantial role to interact with shortwave (SW) and longwave (LW) solar fluxes meaningfully [47]. They keep the atmosphere cold by reflecting the solar SW radiations and warm when they trap the LW solar fluxes. That is why clouds are known to be an integral part of the global radiation budget [48]. Cloud optical properties consist of micro/macro physical parameters and there are

numerous studies that have focused on these properties. This section comprises of a number of literatures that deals with the cloud optical properties.

Cossu *et al.* [49] reported CF statistics for Bern, Switzerland in the period (2004–2013) using Ground-Based Microwave Radiometer, and found CF of 60.9% and 42.0% in December and Jul, respectively. Dong *et al.* [50] analyzed the CF data obtained from the Atmospheric Radiation Measurement (ARM) from June 1998 to May 2008 over Alaska and the NOAA Barrow Observatory (BRW). The CF significantly increases from a minimum value of 0.57 to a maximum value of 0.9 from March to October. However, a fluctuated decrease was observed from November to March. While, the average value of CF per annum was found to be 0.76. Similarly, Seiz *et al.* [51] worked on the analysis of CF from March 2000 to February 2010, using MODIS data over Switzerland and reported the highest CF 0.71 in January (winter) and lowest 0.52 in July (summer). Furthermore, the authors compared MODIS data to ground-based Global Climate Observing System (GCOS Switzerland) observations and observed a good agreement with an average difference of $-2\% \pm 6\%$.

Yin & Min, [52] analyzed COD from 2001 to 2009 for the Barrow and Atqasuk sites. They observed that the COD increases from spring to summer due to the increase of surface temperature and sunshine hours. They also suggested in their analysis that the decrease in the CER values from March to July is an indication of a polluted atmosphere due to the high aerosol loading. The higher value of COD means greater thickness of clouds, which shows the high probability of precipitation with large intensity [53]. Bennartz,*et al* [54] used MODIS data and found that the difference in COD values were small as compared to the CER.

Kawamoto and Suzuki [55] compared the COD, CER and CWP along with droplet number density (Nd) for continental clouds (over China) and oceanic clouds (over the northwest Pacific),

using radiometer and space-borne radar radiometer data. They concluded that cloud parameters (excluding Nd) were significantly higher for oceanic clouds than for continental for the precipitating class of the clouds. Lin *et al.* [56] examined the variations of CWP with meteorological (MT) and cloud temperature (CT) using satellite and ground-based data for the year 1998 over the Arctic Ocean. The results show that due to growth in the thickness of cloud by the increase in surface moisture during the thaw season, CWP is primarily positively correlated to the temperature.

Niu and Li, [57] analyzed the MODIS and the Cloud-Aerosol Lidar and Infrared Pathfinder Satellite Observations (CALIPSO) satellite data for the year 2007 over the tropical region. They reported two distinctive correlations of aerosol loading with clouds and rainfall; (1) Analyzing the mixed phase clouds, it was found that AI and AOD showed negative correlation with CTT over tropical oceans and tropical land, respectively, (2) However, the rate of rainfall showed positive association with AI for mixed phase clouds, while negative for warm clouds. Liu *et al.* [58] analyzed the relation between AOD and cloud optical properties and found that cloud optical properties depend on the quantity of aerosol particles. They also observed that COD is negatively correlated with AOD due to the radiative effects caused by absorbing aerosol. While, the positive correlation between AOD and CTP showed that the aerosol is not always inclined to grow in the upright direction. Further, a nonspecific relationship between COD-CER and CWP-CER is indicated, which could be affected by the loading of aerosol. The changes in cloud optical properties with AOD in the presence of larger RH resulted high probability of cloud formation and greater cloud droplet particles, regardless of vertical or horizontal cloud's level. The CF expands horizontally during stable atmospheric condition. However, unstable atmospheric conditions and upward motion of air parcels were favorable for the formation of thicker and high-level clouds.

Similarly, Patil *et al.* [59] examined the correlation of cloud properties with AOD for the period 2000-2009 (from June to September) over the monsoon region of India using MODIS Level-3 data. They reported an increase in CTP, decrease in CER and IWP during monsoon deficient seasons with higher AOD. These results suggest the suppression of clouds. The opposite was observed during heavy monsoon seasons indicated the cloud invigoration. Furthermore, CTP and CER was positively and negatively correlated with AOD. While, insignificant correlation recorded between IWP and AOD.

Alam *et al.* [25] examined the impact of AOD on cloud properties, i.e., water vapor (WV), CF, COD, LWP, CTT, and CTP over the selected locations in Pakistan using MODIS data during the period 2001–2011. They reported high correlations (> 0.6) for AOD and WV in some locations and moderate (0.4 to 0.6) in other sites. CF turned out to vary directly with AOD over urban location during the whole study period. CWP is positively correlated with AOD both in winter and autumn seasons. While, CWP and COD (except Karachi) were negatively correlated during spring and summer seasons for all the selected sites. Furthermore, CTT and CTP and depicted positive relationships with AOD during spring and negative correlation during summer for study sites.

2.4 Cloud Radiative Properties

The radiative properties of cloud elaborate the differential response of the radiation fluxes which, varies in respect of cloud amount and its types. The radiative properties of clouds are complex. However, their investigation is significant due effective influence on climate. The global climate is significantly affected due to the variation in the reflection of SW radiations and absorption of LW radiation by the cloud, especially in the Himalaya region. The summary of some numerous studies regarding cloud radiative properties is discussed in the following paragraphs.

Liou *et al.* [60] analyzed the variation in the absorption, transmission and reflection of solar radiation by interaction with different types of cloud and concluded that the wave properties of solar radiation varies with water and ice content of clouds and solar zenith angle. Ramanathan *et al.* [61] worked on radiative properties of cloud using the space borne Earth Radiation Budget Experiment (ERBE), and calculated that the negative global SW cloud radiative forcing (SWCRF) producing cooling effect and positive LW cloud radiative forcing (LWCRF) give heating effect. They estimated global SWCRF was -44.5 W/m^2 and LWCRF was 31.3 W/m^2 during April 1985, producing net cooling effect.

Rucong *et al.* [62] reported the highest negative SW, positive LW and negative net cloud radiative forcing (CRF) in the Indian monsoon region (IMR) and Eastern China (EC) during the summer for the period February 1985 to December 1989. In EC highest negative CRF recorded at the start of the summer season. While, the average value of the aforementioned parameter was found to be larger than IMR during the entire year, due to the diverse topography and its effects on monsoon, cloud dynamics and circulation in Asia.

Machado and Rossow, [63] examined the radiative and structural characteristics of clusters of tropical cloud and their variation with system size in tropical convective systems (CS). They used a radiative transfer model to analyze the CS radiative effects. The researchers found that the mesoscale anvil cloud increases the adiabatic heating of the atmosphere by convection and maintain these CS at night.

Yin and Min, [52] reported the positive correlation between COD and LWP with the surface temperature during the frozen season, and observed the positive impact of the clouds on the net surface radiation (NSR). While, during the thawed season, the clouds impact on the NSR is negative because of the dominance of ice cloud and arctic haze. Similarly, Somerville and Remer

(1984) suggested that due to the increase of atmospheric CO_2, the cloud optical properties act like a thermostat, and as a result the negative radiative feedback observed.

Lin *et al.* [56] studied the variations of CWP with meteorological temperature (MT) and cloud base temperature (CBT) using satellite and ground-based data for the year 1998 over the Arctic Ocean. They reasoned that with larger relative humidity (RH) and MT, the condensation levels and cloud base altitudes reduce and the mean change rate of CWP with CT is 3.3% K^{-1}.

Li *et al.* [64] worked on change in the radiative properties of cloud due to mixing with black carbon (BC). They reported that mixing of the BC in the cloud droplets was significantly affecting the HR and solar fluxes. For the solar zenith angle (SZA) of 53° and BC fractional volume of 10^{-7}, the increase in the HR of 0.08 K/d and decrease in the solar flux at the top of the atmosphere of 0.5 W/m2 was estimated during the study.

Xi *et al.* [65] analyzed the CRF obtained from the Atmospheric Radiation Measurement (ARM) from June 1998 to May 2008 over Alaska and the NOAA Barrow Observatory (BRW). They reported that all sky SWCRF and LWCRF was negatively and positively correlated with cloud fraction, respectively. LWCRF was found to be minimum (6 W/m^2) in the month of March and maximum in August (63 W/m^2) with corresponding CF of 57 % and 90 %, respectively.

Chapter 3

Site Description, Instrumentation and Methods

This chapter contains the study locations, instruments and methodology used in the study of interest.

3.1 Site Description

In this thesis, we have conducted study over the urban (Lahore and Karachi) and high altitude (Diamir, Gilgit and Skardu) locations as shown in Figure 1, whose details are given below:

3.1.1 Urban Locations

Lahore and Karachi are known as the largest urban cities with dense population in Pakistan. The area has a semi-arid climate with cold and dry winters, hot summers, and significant rain during the monsoon season. There is a high propensity for dust storms during the hot summers, while heavy haze is common during the winter season owing to a shallower boundary layer and more residential wood burning for heating purposes. The major sources of air pollution are vehicular and industrial emissions, biomass burning, and road dust [20].

Karachi is a mega city in the southeastern part of Pakistan, geographically situated on the coast of Arabian Sea (24° N, 67° E, 8 m above sea level). It is highly populated with more than 17 million inhabitants, covering an area of around 3500 km^2. Similarly, Lahore is another high populated megacity location in the central part of the country (31° N, 74° E; 210 m above sea level). There are over 10 million inhabitants with the city covering 404 km [23].

25th May-2011, 25th June-2011, 21st March-2012, 27th December-2012, 25th June-2013, 11th October-2013 and 06th October-2014 due to high concentration of coarse and fine particles. It was observed that daily averaged visibility varied between 3.9 and 6.5 km during DE over Karachi, whereas over Lahore it is fluctuated from 0.9 to 4 with lower values during HE and higher values during DE.

3.1.2 High Altitude Locations

The northern areas of Pakistan are less populated as compared to urban areas, and significantly affected from the global warming, have strategic and geographic important for the whole south Asia. The Diamer District (35.43° N, 73.93° E) is situated in the northern part of Pakistan. The Karakoram highway passes through this district. Chilas is the district headquarter of the Diamer District. Diamer in the east touches Astore district, Khyber Pahktunkhwa (KPK) Province in the southwest, Nilam district of Azad Kashmir lies in the south, Ghizar district lies in the north and northwest, and the Gilgit district in the north and northeast.

Gilgit (35° N, 74° E) is the provincial headquarter of Gilgit-Baltistan territory of Pakistan. The elevation ranges from 1600 to 3000 m (above sea level). The area of Gilgit district is 3800 Km^2. In its periphery, Gilgit district is covered with three giant snow mountain ranges. According to the published report in 2015, the population of Gilgit district is approximately 1,800,000 [66].

Skardu (35.29° N, 75.62° E) district is also located in the Gilgit-Baltistan region. Skardu is situated in the foothill of the great Karakoram mountain range. The width and length of Skardu are 10 and 40 km, respectively. The meteorological statistics for Diamir, Gilgit and Skardu are given in Table 3.1.

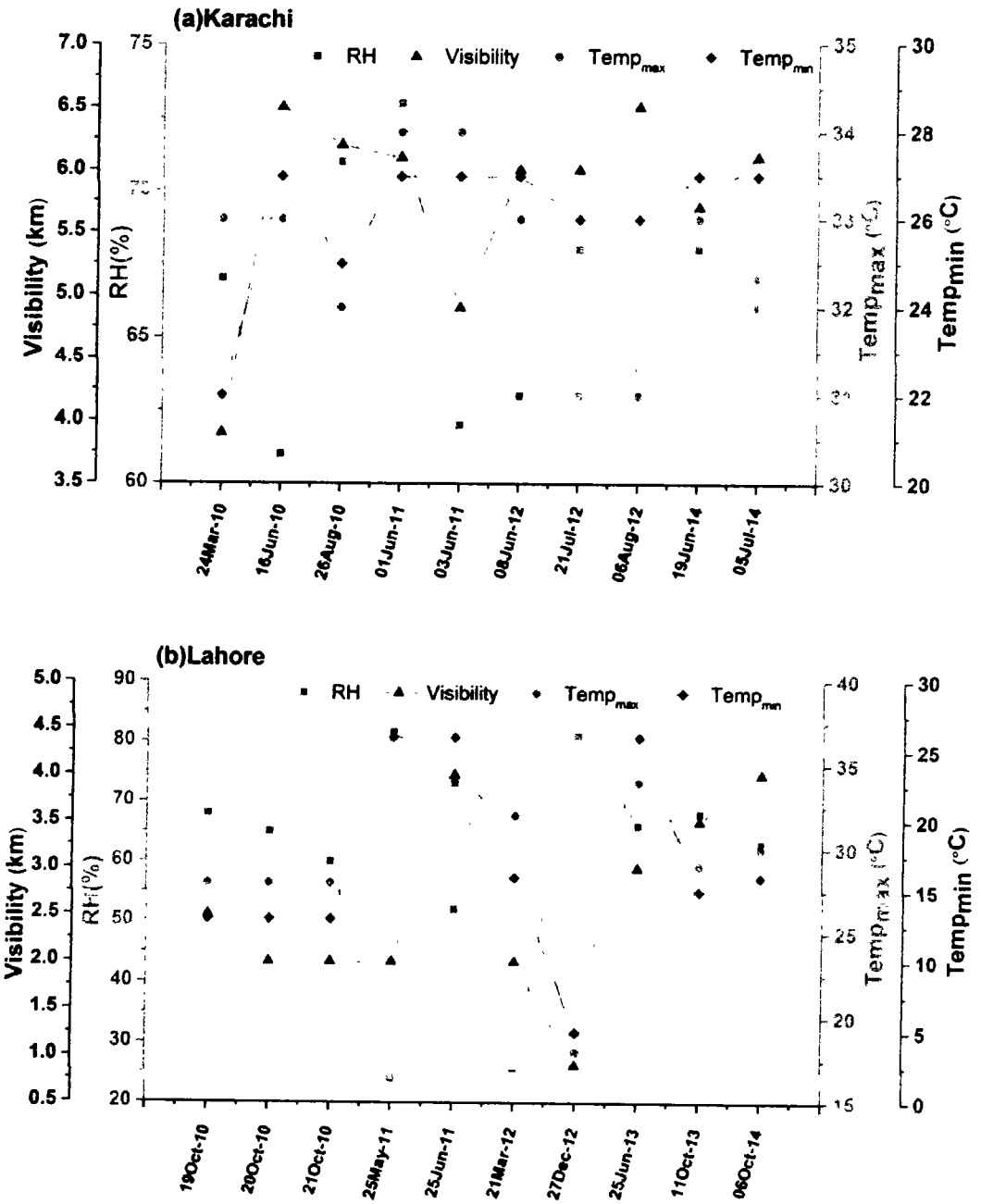

Figure 3. 2 Daily variation of RH, visibility, $Temp_{max}$ and $Temp_{min}$ over (a) Karachi and (b) Lahore during the study period.

Table 3.1. Details about the seasonal and annual values of meteorological parameters in the selected study areas during 2004-2016. The values of (± SD) represents the standard deviation values.

	Parameters	Winter ± SD	Spring ± SD	Summer ± SD	Autumn ± SD	Annual ± SD
Diamir	Humidity (%)	58.00 ± 9.0	43.55 ± 8.6	37.40 ± 7.5	43.14 ± 6.2	46.58 ± 4.1
	Monthly Total Rain (mm)	16.61 ± 17.5	23.63 ± 19.0	15.42 ± 14.3	4.68 ±7.8	15.09 ± 3.1
	$Temperature_{min}$ (°C)	2.53 ± 1.8	14.08 ± 4.5	25.00 ± 2.3	14.40 ± 5.7	14.00 ± 0.8
	$Temperature_{max}$ (°C)	13.59 ± 2.0	26.74 ± 5.0	37.34 ± 1.9	28.09 ± 5.4	26.44 ± 0.8
	Wind Speed (m/s)	0.30 ± 0.2	0.72 ± 0.2	1.14 ± 0.4	0.41 ± 0.2	0.64 ± 0.1
Gilgit	Humidity (%)	78.0 ± 7.1	62.5 ± 5.1	65.8 ± 8.5	78.5 ± 3.8	71.2 ± 2.7
	Monthly Total Rain (mm)	6.52 ± 11.1	19.42 ± 19.0	14.81 ± 14.1	8.72 ± 11.3	12.9 ± 3.6
	$Temperature_{min}$ (°C)	-1.3 ± 2.5	9.2 ± 2.6	16.7 ± 1.6	6.8 ± 5.0	7.82 ± 0.3
	$Temperature_{max}$ (°C)	12.31 ± 2.0	25.07 ± 4.5	34.68 ± 1.8	25.35 ± 4.8	24.35 ± 0.5
	Wind Speed (m/s)	0.17 ± 0.2	0.28± 0.1	0.24± 0.2	0.06± 0.1	0.19 ± 0.05
Skardu	Humidity (%)	81.48 ± 4.4	52.54 ± 10.1	48.75 ± 7.3	61.96 ± 8.7	61.18± 2.7
	Monthly Total Rain (mm)	33.68 ± 37.1	32.56 ± 36.1	12.30 ± 10.2	11.05 ± 23.5	8.7 ± 8.7
	$Temperature_{min}$ (°C)	-6.68 ± 2.6	5.70 ± 3.2	14.08 ± 1.5	3.73 ± 5.9	4.33 ± 0.5
	$Temperature_{max}$ (°C)	6.25 ± 2.2	19.30 ± 4.7	30.16 ± 1.9	20.37 ± 5.3	19.02 ± 0.7
	Wind Speed (m/s)	0.06 ± 0.05	0.26 ± 0.2	0.34 ± 0.3	0.07 ± 0.1	0.19 ± 0.1

3.2 Instrumentation

In this section the description about the satellite and ground-based instruments used in the study period is presented.

3.2.1 Aerosol Robotic Network

Aerosol Robotic Network (AERONET) is a global network of ground based observation that provide standardized aerosol data [67]. The AERONET inversion algorithm [16, 25, 68] was used to calculate AVSD, SSA, ASY and RI. AERONET takes measurements of the direct sun and diffused sky radiances within the spectral range (340−1020 nm) [67]. AERONET provides data at

level 1.0, level 1.5 [69] a[redacted]evel 2.0 [25, 67], which are raw data, cloud processed, and cloud processed and quality ass[redacted]data, respectively. The AERONET is also called collimated radiometers, which ca[redacted]used to collect sky irradiances.

We used Level 2.0 dai[redacted]eraged AOD and other optical properties (AVSD, SSA, ASY, PF, RRI, and IRI) data for the[redacted]ervation period from two AERONET sites of Lahore and Karachi. The two sites are operate[redacted]ce 2006 with the collaboration of National Aeronautics and Space Administration (NASA) [redacted] Pakistan Space and Upper Atmosphere Research Commission (SUPARCO). The AER[redacted]ET data can be easily accessed for the NASA website at http://aeronet.gsfc.nasa.g[redacted]

Table 3.2. Data set used t[redacted]racterize the clouds and radiation properties.

Product	Parameters	Resolution	Data Source
Clouds (MOD 06_M3)	Cloud Fraction (CF)	1 × 1 km	MODIS
	Cloud Optical Depth (COD)	1 × 1 km	
	Cloud Effective Radius (CER)	1 × 1 km	
	Cloud Water Path (CWP)	1 × 1 km	
	Cloud Top Pressure (CTP)	5 × 5 km	
	Cloud Top Temperature (CTT)	5 × 5 km	
TOA fluxes (CERES_EBAF)	Shortwave flux (Clear and all sky)	$1^o \times 1^o$	MODIS (Terra +Aqua)
Meteorological Data	Maximum Temperature (T_{max})	Point Data	Pakistan Meteorological Department
	Minimum Temperature (T_{min})		
	Relative Humidity (RH)		
	Monthly Total Rain (MTR)		
	Wind Speed (WS)		

3.2.2 Moderate Resolution Imaging Spectroradiometer

The MODerate resolution Imaging Spectroradiometer (MODIS) sensors were launched by NASA in 1999 and 2002 on Terra and Aqua satellites, respectively. There are two separate algorithms used by MODIS to detect aerosol over land and ocean [70]. MODIS provide data in 36 spectral bands in the wavelength range from 400 to 1440 nm [71]. Out of 36 bands, two bands have nominal resolution of 250 m, along with five bands at 500 m, and 29 bands at 1 km. The timing for the Aqua overpass is 13:30 LT and that for the Terra is 10:30 LT. In the current study, true colour images were obtained for the verification of aerosol types in the extreme episodes of haze and dust over studied sites. Furthermore, the cloud parameters data were also obtained from MOIDS as given in Table 3.2. MODIS data are available at https://earthdata.nasa.gov/earth-observation-data/near-real-time/rapidresponse/modis-subsets.

3.2.3 Clouds and the Earth's Radiant Energy System

Clouds and the Earth's Radiant Energy System (CERES) was launched by Langley Research Center (LaRC) in NASA. A biaxial scanner with three channels is mounted on it to collect various samples of clouds. The reflected sunlight, earth emitted thermal radiation and radiation in the context of all wavelengths are measured by shortwave channel (first), long wave channel (second) and total channel (third). CERES is used to measure the cosmic as well as the terrestrial radiation from the top of the atmosphere (TOA) to the surface. In addition, it is used to measure the Earth's energy balance to enhance the understanding of global climate change. In this study, CERES Energy Balanced and Filled product (CERES-EBAF) was used to evaluate the instantaneous direct shortwave cloud radiative forcing (SWCRF) over the study area from 2004 to 2016 using Eq. (3.1) [72].

$$SWCRF = SW_{clr} - SW_{all} \quad (3.1)$$

Where SW_{clr} and SW_{all} represents the short wave at clear and all sky conditions.

A biaxial scanner is mounted on it for sampling. CERES data are available at https://ceres.larc.nasa.gov/order_data.php.

3.2.4 Hybrid Single Particle Lagrangian Integrated Trajectory

The origin of air masses can be traced by the cluster analysis of back trajectories using HYSPLIT model [73]. The airmass backward trajectories were computed from the source point to the receptor sites. We run the HYSPLIT model for 72 h back cluster trajectories of air masses at 1000 m during DE and HE over the studied sites.

3.3. Methodology

In this section, a comprehensive description about the methods that are used in the present research work as given in below section and subsections.

3.3.1. Aerosol optical properties

A major source of uncertainty in predicting the state of climate is variability in spatio-temporal distribution and optical properties of aerosol. Aerosol particles affect the troposphere by various scattering and absorption processes, resulted changes in solar radiation and cloud microphysics, which can in turn affect the cloud albedo and their lifetime [74]. The aerosol optical parameters are described below.

3.3.1.1. Aerosol Optical Depth

AOD is the aerosol concentration in vertical column from the surface to TOA. Mathematically, AOD can be defined as the integrated extinction between two heights in the atmosphere.

$$\text{AOD}\ (\tau_\lambda) = \int_{h_i}^{h_{ii}} \gamma_{ext,\lambda}(h)\ dh \tag{3.2}$$

where "λ" represents the wavelength, γ_{ext} the particle extinction efficiency, h_i and h_{ii} are the low and high altitudes in the units of length, respectively.

3.3.1.2. Angstrom Exponent

The aerosol size distribution is indirectly measured by Angstrom Exponent (α). It is calculated by an equation called Ångström equation [75]:

$$\text{AOD}\ (\tau_\lambda) \sim \lambda^{-\alpha} \tag{3.3}$$

The wavelengths (λ) have the range of 440-870 nm

3.3.1.3 Single Scattering Albedo

SSA is termed as the ratio between scattering coefficient (Qsca) and total extinction coefficient (Qext):

$$\text{SSA} = \text{Qsca/Qext} \tag{3.4}$$

3.3.1.4 Aerosol Volume Size Distribution

The AVSD is bimodal (fine mode and coarse mode) and can be explained by the sum of two log-normal distributions as follows:

$$\frac{dV(r)}{d\ln r} = \sum_{i=1}^{2} \frac{C_{v,i}}{\sqrt{2\pi}\sigma_i} \exp\left[-\frac{(\ln r - \ln r_{v,i})^2}{2{\sigma_i}^2}\right] \tag{3.5}$$

In the above expression $r_{v,i}$ is the volume median radius, $C_{v,i}$ is the volume concentration, and σ_i is the geometric standard deviation for mode i. The fine mode aerosol particles are those having radii less than 0.6 μm, while radii greater than 0.6 μm are associated with coarse mode aerosol particles [16].

3.3.1.5 Phase Function

PF is the angular distribution of scattered intensity relative to the incident beam at a given angle "θ" and normalized by the integral of the scattered intensity at all angles, given by the equation:

$$PF(\theta) = \frac{f(\theta)}{\int_0^{\pi} f(\theta) \sin\theta \, d\theta} \tag{3.6}$$

where f(θ) is the intensity of scattered radiation and "θ" is the scattering angle.

3.3.1.6. Asymmetry Parameter

"The intensity weighted average cosine of the scattering angle" is called the Asymmetry Parameter (AP). The variation in AP ranges from +1 to -1. The "+1" value of AP, indicates forward scattering and "-1" indicate backward scattering of radiation, while "0" value of AP shows symmetrical scattering of solar radiation [76]. AP mathematically defines as:

$$AP = \int_0^{\pi} \cos\theta \, PF(\theta) \sin\theta d\theta \tag{3.7}$$

where PF(θ) is the Phase Function and "θ" is the angle between transmitted and scattered radiation.

3.3.1.7. Refractive Indices

Mathematically refractive index is given as

$$RI = n + ik \tag{3.8}$$

In the above equation 'n' and 'k' denote the real and imaginary parts of RI. The real part depicts the scattering while the Imaginary part shows the absorption of radiation [77-79].

3.3.2. Cloud Optical Properties

The cloud plays a vital role in the earth radiation budget, and can be examine from the data acquire by remote sensing [49]. The cloud optical properties are discussed below.

3.3.2.1. Cloud Fraction

The Cloud Fraction (CF) is an important earth radiative fluxes modulator that is being examined from the remote sensing data. The radiative fluxes through the atmospheric and at the surface can be determined by using CF in the climate models.

3.3.2.2. Cloud Optical Depth

The Cloud Optical Depth (COD) is the extinction of solar radiation due the absorption by cloud and can be calculated by equations 3.9 and 3.10.

$$P_{ext}(\lambda) = \int_0^{R_{max}} \pi R^2 \rho_{ext}(M, R, \lambda)\, n(R)\, dR \tag{3.9}$$

Where n(R) is a concentration of droplet number distribution and ρ_{ext} the extinction efficiency for a water droplet. The COD is the product $\tau_c(\lambda)$:

$$\tau_c(\lambda) = P_{ext}(\lambda)\, H \tag{3.10}$$

In eq (3.11) 'H' is the width of a spatially uniform cloud. The COD is the most significant optical property for the characterization of cloud in term of their various types. The COD is derived from widely used and effective method called solar reflective method. The accuracy for the method of interest depends upon different atmospheric and surface conditions [80].

3.3.2.3. Cloud Effective Radius (CER)

The significant property of cloud that leading their radiative transfer is the cloud effective radius CER, which is define as the ratio of the third to second moments of the size distribution of the cloud drop number concentration. For homogeneous cloud, CER can be represented by equation (3.11).

$$CER = \frac{\mu_3}{\mu_2} = \frac{\int n(R)\, R^3\, dR}{\int n(R)\, R^2\, dR} \tag{3.11}$$

Where n(R) is size distribution of the cloud drops and r is the cloud drop radius. For readily extended to vertically inhomogeneous clouds, the CER can be expressed by equation.

$$CER = \frac{\mu_3}{\mu_2} = \frac{\iint n(R,z)\, R^3 dRdz}{\iint n(R,z) R^2 dRdz} \quad (3.12)$$

The integral are taken over the radius of the droplet and over the cloud thickness [81].

3.3.2.4. Cloud Water Path

The Cloud water path (CWP) is an important parameter in different cloud physical processes like condensation, evaporation, and precipitation, and widely used to control cloud shortwave radiative forcing. CWP can be calculated from the retrieved COD (τ_c) and CER (R_e) by using the relationship

$$CWP = C_v D_w \tau_c R_e \quad (3.13)$$

where Dw is the water density 1gm/cm^3, Cv is a constant that depends upon the assumed vertical stratification. For 1 km resolution and presumed vertical homogeneity Cv = 2/3, while for cloud where water content linearly increases from base to top with associated constant droplet concentration with respect to height Cv= 5/9 [82].

3.3.2.5. Cloud Top Temperature

The estimated temperature measured at the top of a cloud is termed as CTT and it is measured in kelvin, usually thicker clouds have low CTT which may consequences to heavy surface rainfall [83].

3.3.2.6. Cloud Top Pressure

The estimated pressure observed at the top of all clouds (liquid and ice) is known as CTP and it is measured in hPa. It is based on the absorption of the solar radiation. Generally, high level clouds have low CTP. The CTP is calculated by inverting a model of the atmospheric optical properties

and clouds, using a neural work (https://envisat.esa.int/handbooks/meris/CNTR2-7-2-2-3-3.html). Through thermal infrared rays, the satellite measurement of CTP is also obtained by using the known atmospheric temperature profile, this well-known methodology is also applicable by the International Satellite Cloud Climatology Project (ISCCP). The limitation in the accurate measurement of CTP included the spectral resolution of the instrument, the surface albedo's uncertainties, and multiple scattering and absorption inside clouds [84].

3.3.3. Santa Barbara DISORT Atmospheric Radiative Transfer (SBDART) Model

SBDART model is developed by Ricchiazzi *et al.* [85] in the University of California which calculates the plane parallel equation at the surface of the earth and within atmosphere in clear and cloudy environment. A module called DISORT used in SBDART model for the integration of radiative transfer equation and is developed by [86]. SBDART is rendered for six atmospheric profiles e.g. tropics, mid latitude summer, mid latitude winter, subarctic summer, sub-arctic winter, and US62. Variety of problems can be solved by using this model in the context of atmospheric radiative energy balance as well as in remote sensing. There are six basic parameters used in SBDART model, which are AOD, SSA, AP, surface albedo, ozone and water vapour. In addition to the above parameters, other two key input parameters are solar geometry and atmospheric profiles.

3.4 Calculation of Aerosol Radiative Forcing

For the better estimation of the aerosol effects on local as well as in global scale, accurate calculation of ARF is necessary. ARF is the net difference between incoming and outgoing solar fluxes and is measured in the unit of W/m^2. The SBDART model calculates ARF in the absence as well as in the presence of aerosols. For the study in hand, in order to estimate the ARF, the AERONET retrieved aerosol optical properties (AOD, SSA, AP, Water Vapour), surface albedo

and columnar ozone from MODIS and OMI were obtained. We have used this model for the estimation of radiative forcing at the Top of the Atmpshere (TOA), Surface (SRF) and within atmosphere (ATM) in short wavelength range (0.2 – 4.0 μm) over the study area for the study period. For the estimation of ARF, we consider mid latitude summer (March to September) and mid latitude winter (October to February) according to the meteorological situations of study locations. Figure 3.3 represents the methods to calculate the short wave radiative forcing at the SUR, TOA and within the ATM and their corresponding heating rate.

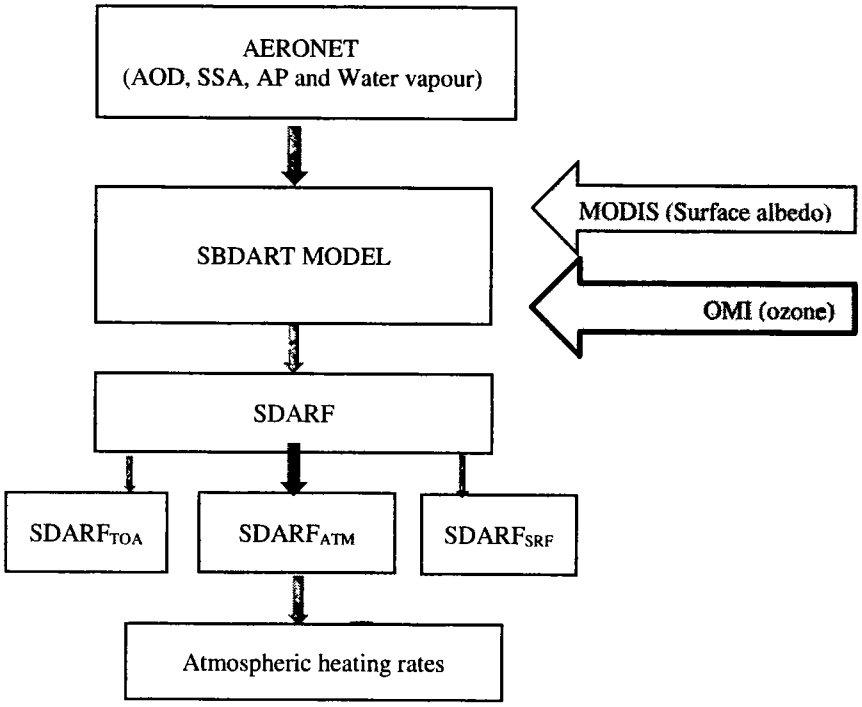

Figure 3. 3 Diagram shows radiative forcing and heating rates using SBDART model.

Chapter 4

Variability in aerosol optical characteristics between Dust and Urban Haze in two cities of Pakistan

4.1. Aerosol Optical Properties during the High Pollution Episodes

Daily averaged characteristics of aerosol optical properties such as AOD, AE, SSA, PF, ASY, RRI, and IRI are subsequently discussed during dust episodes (DE) and haze episodes (HE) over Karachi and Lahore.

4.1.1. Aerosol Optical Depth (AOD) and Ångström Exponent (AE)

Fig. 4.2 (a & b) shows the daily averaged variability of AOD and AE during the heavy pollution episodes (AOD > 1) over Karachi and Lahore. AOD and AE provide details associated with aerosol loading and the size distribution of aerosol, respectively. Eck *et al.* and Holben *et al.* [87, 88] reported that for fine particles, AE is greater than 1 and less than 1 for coarse ones.

In the present study, the detection of DE was associated with AOD500 > 1 and AE440–870 < 0.37 over Karachi and AOD500 > 1.34 and AE440–870 < 0.88 over Lahore. The case with AOD500 > 1.41 and AE440–870 > 1.21 corresponds to HE over Lahore, while no HE were detected over Karachi. Ten and four DE were observed in Karachi and Lahore, respectively. Also, six HE over Lahore were identified during the studied period with associated AOD and AE value summarized in Table 4.1. During DE, AOD values were high with low AE, while during HE the AOD values were high with enhanced values of AE. Tariq et al. [89] and Alam et al. [25] pointed out that the daily averaged AOD reached maximum values of 3.70 and 2.7 during intense HE and DE, respectively, over Lahore.

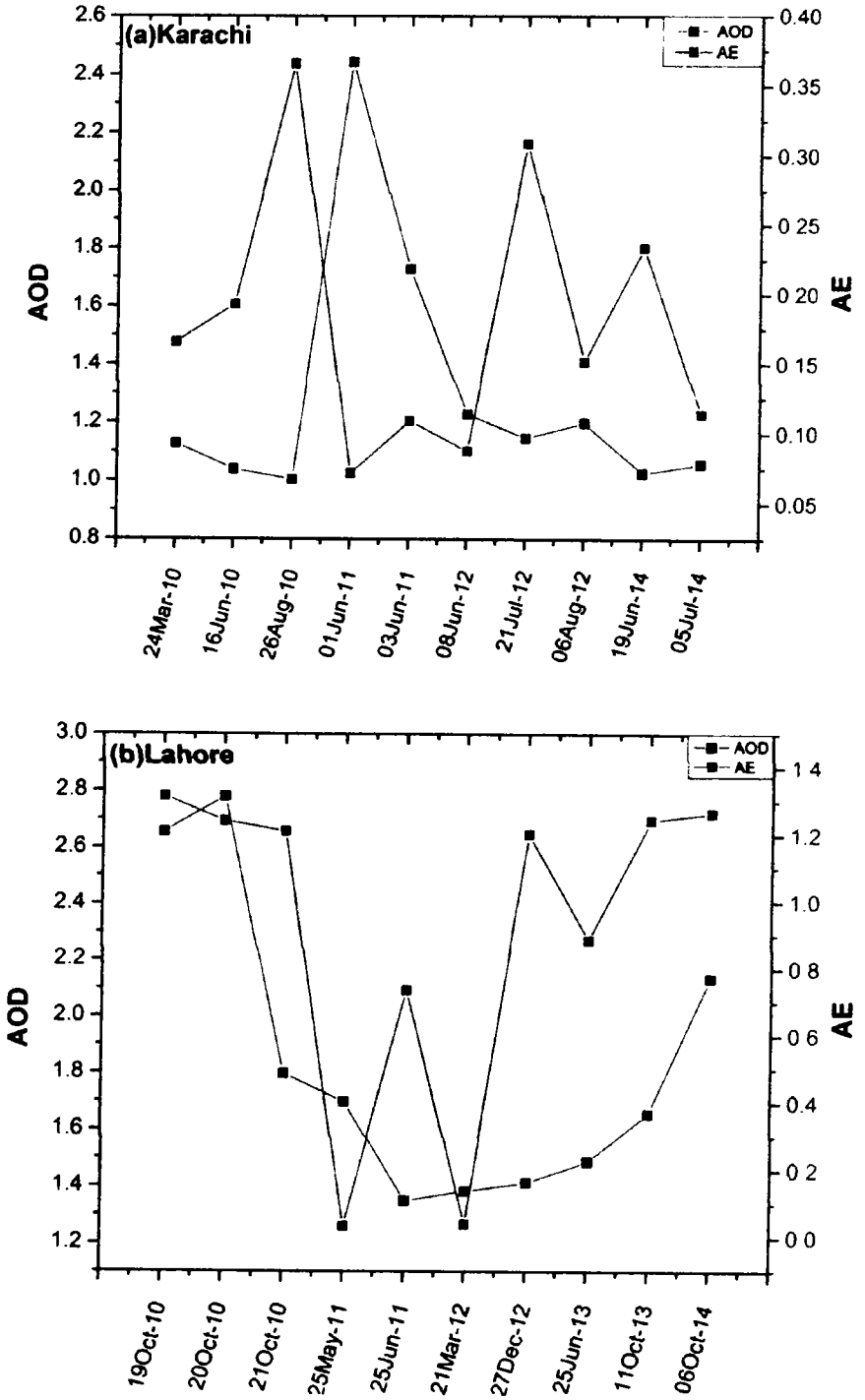

Figure 4. 1 Daily averaged variation of AOD at 500 nm and AE in the range of 440–870 nm over (a) Karachi and (b) Lahore during DE and HE.

Table 4. 1. Daily averaged values of AOD and AE of each heavy pollution episode over Karachi and Lahore during the study period from 2010 to 2014.

Karachi				Lahore			
Days	AOD	AE	Episode	Days	AOD	AE	Episode
24Mar-10	1.108	0.165	DE	19Oct-10	2.342	1.313	HE
16Jun-10	1.019	0.192	DE	20Oct-10	2.469	1.240	HE
26Aug-10	0.968	0.365	DE	21Oct-10	1.600	1.210	HE
01Jun-11	2.425	0.071	DE	25May-11	1.691	0.033	DE
03Jun-11	1.709	0.109	DE	25Jun-11	1.257	0.735	DE
08Jun-12	1.217	0.087	DE	21Mar-12	1.377	0.039	DE
21Jul-12	1.112	0.308	DE	27Dec-12	1.309	1.202	HE
06Aug-12	1.180	0.151	DE	25Jun-13	1.366	0.885	DE
19Jun-14	1.002	0.233	DE	11Oct-13	1.471	1.243	HE
05Jul-14	1.045	0.113	DE	06Oct-14	1.893	1.264	HE

The low values of AE with corresponding high AOD signify the dominance of coarse mode dust particles, while the high values of both AE and AOD indicate the high influence of fine mode particles. These results are also supported by Bibi *et al.* [90], as they documented that high AOD with low AE and high AOD with high AE were due to coarse and fine mode aerosol, respectively. Alam *et al.* [25] also observed the anti-correlation in AOD and AE during a dust storm on 20 March 2012 in the Middle East and Southwest Asia. Similarly, an inverse relationship between AOD and AE was reported in June 2002 over the western Mediterranean where coarse particles were dominant [91]. There was observed negative correlations among AOD and AE for the different dust storm episodes implying the presence of coarse particles over the Indo-Gangetic Plan (IGP) [34, 92, 93]. The results for HE are similar with finding of Che *et al.* [94] during severe HE in January 2013 over Beijing, where there were predominantly fine particles [95].

4.1.2. Aerosol volume size distributions (AVSD)

Aerosol radiative forcing depends on size of aerosol as well as their chemical composition. For various types of aerosol, the AVSD rely on sources, transport, composition, and scavenging mechanisms [96].

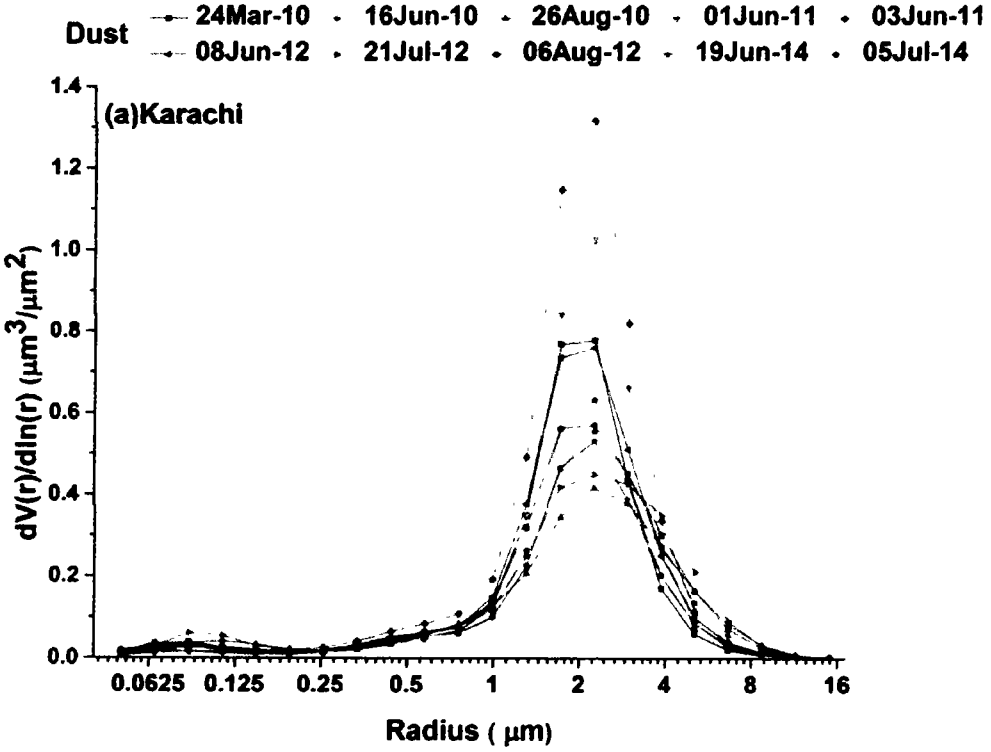

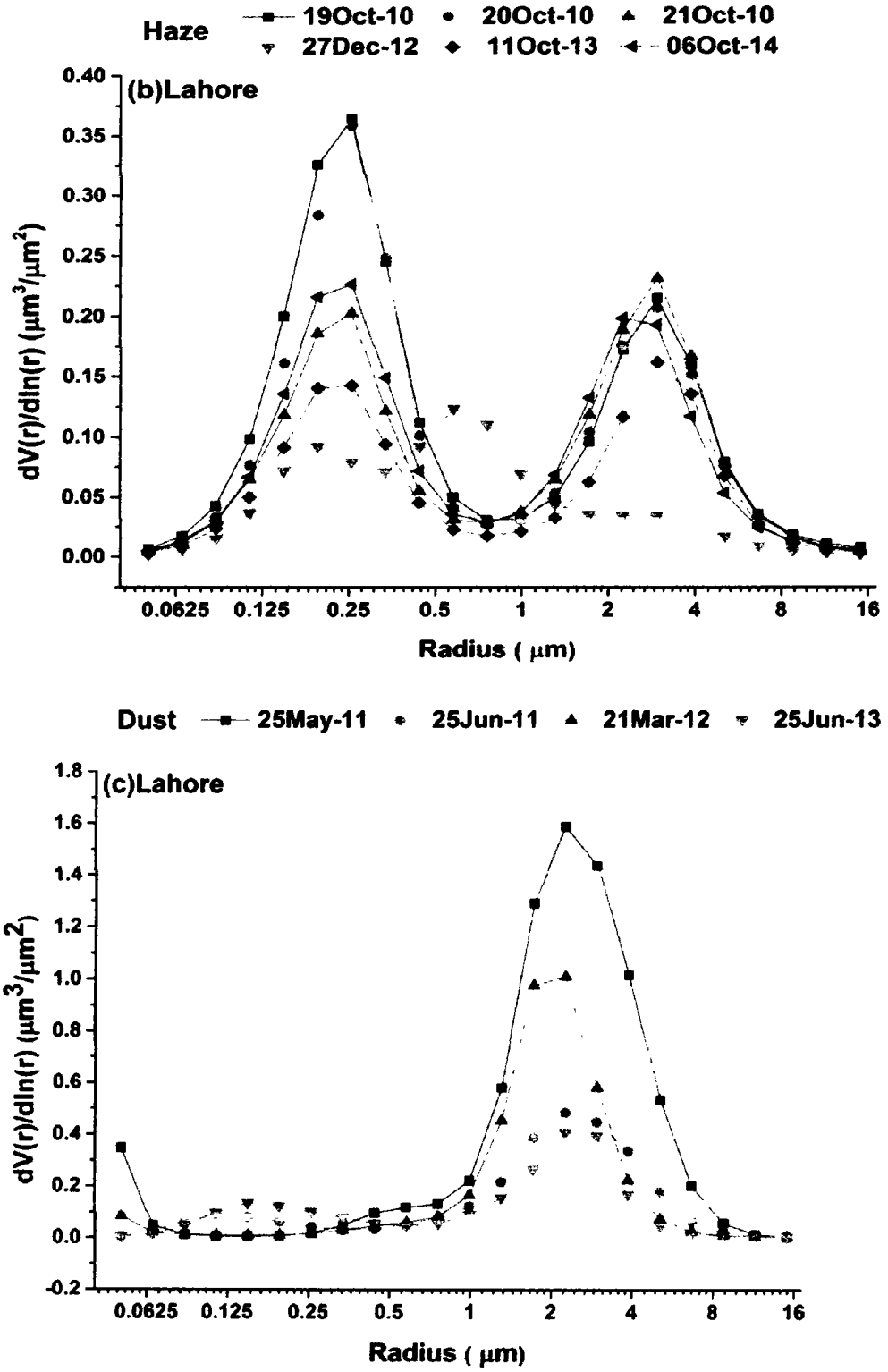

Figure 4. 2 Daily averaged profiles of AVSD over (a) Karachi during DE, (b) Lahore during HE and (c) Lahore during DE.

The daily averaged profiles of ASVD obtained for the studied DE and HE are shown in Fig. 4.2 (a, b & c). The coarse mode peaks were more pronounced around a radius of 2.24 μm over Karachi and Lahore during DE (see Fig. 4.2a). In contrast, a bimodal lognormal distribution was reported with the prominent fine mode peaks at a radius 0.25 μm over Lahore during HE, indicative of the dominance of fine particles (see Fig. 4.2b). During DE, the fine mode peaks varied from 0.1 to 0.4 μm over both sites, which is at least partly due to the background aerosol upon which dust is superimposed (see Fig. 4.2c). Previously, Tan *et al.* [97] noted a bimodal structure of AVSD and reported the significant contribution of fine mode aerosols during HE over Guangzhou. The local HE stem from anthropogenic aerosols originating from industrial emissions, agriculture and residue burning [98].

4.1.3. Single Scattering Albedo (SSA)

The SSA provides detailed information related to scattering and absorbing characteristics of various types of aerosol and used in ARF calculations. SSA values for purely absorbing and completely scattering particles are 0 and 1, respectively. It can be used as indicator to determine size and composition of aerosol [99]. Fig.4. 3 (a & b) shows the spectral variation of SSA for selected days during the heavy pollution episodes over Karachi and Lahore.

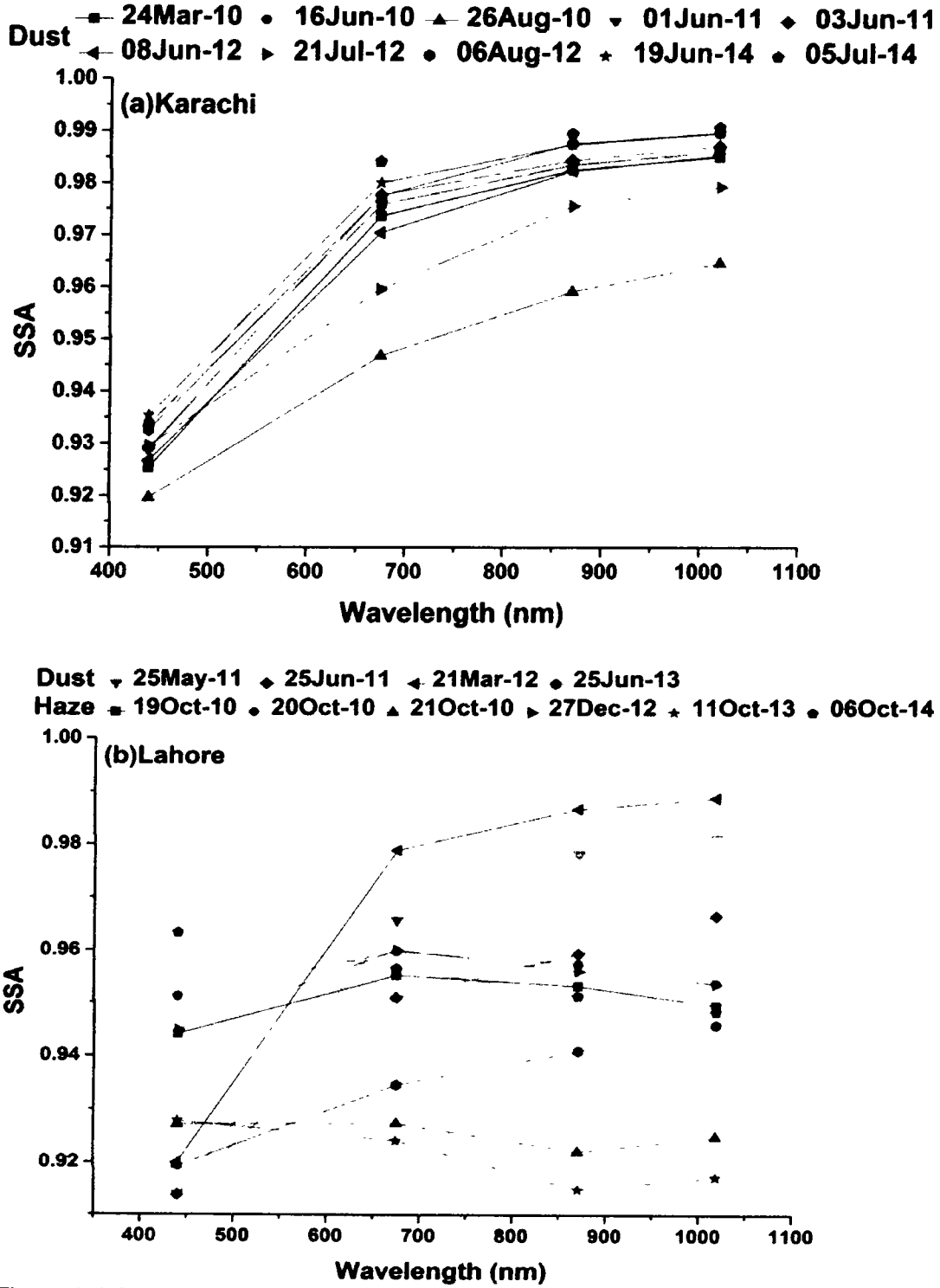

Figure 4. 3 Spectral variation of SSA over (a) Karachi and (b) Lahore during DE and HE.

The spectral variation of SSA exhibits an abrupt increase as a function of wavelength for DE over Karachi and Lahore owing to the presence of coarse particles. This increase in SSA with increasing wavelength was similar for all DE examined but with varying magnitude. Higher SSA values and the increasing behavior with wavelength, displays the dominance of coarse dust particles [16, 21]. Similar increasing trends of SSA with increasing wavelength are common during DE, as documented by others too [20, 34, 93, 100].

In contrast, during some HE (i.e. 21 October 2010, 11 October 2013 and 06 October 2014), SSA decreases with increasing wavelength, suggestive of the contribution of fine particles (see Fig. 4.3(b)). During other HE (i.e. 19 October 2010 and 20 October 2010, 27 December 2012), SSA steeply increases between 440 and 675 nm and then decreases from 675 to 1020 nm. Recently, similar behaviour of increasing SSA at shorter wavelengths followed by reductions at longer wavelength was documented by Bibi *et al.* [101] during the winter over Lahore. Our results are analogous to Bibi *et al.* [102] over Beijing during January 2013, who observed a decreasing pattern of SSA with increasing wavelength from 440 nm to 675 and increased from 675 to 1020 nm, which is mainly due the presence of organic matter.

The existence of fine mode aerosols during October and December are mainly due to the vehicular/industrial emissions and biomass burning [101]. Aerosols originating from anthropogenic emissions have greater absorbing potential [93]. Our results are similar to the result carried out by Che *et al.* [94] during HE in Beijing. The high AOD having low AE and increase in SSA confirms the existence of coarse particles, with fine particles showing the opposite behavior [78].

4.1.4. Phase Function (PF)

Fig. 4.4(a & b) reveals the variability of the PF of aerosol particles versus scattering angle (θ) over Karachi and Lahore during DE and HE. At $\theta = 0°$, the values of PF were in the range of 91 to 113 for Karachi DE, 72 to 114 for Lahore DE, and 25 to 63 for Lahore HE.

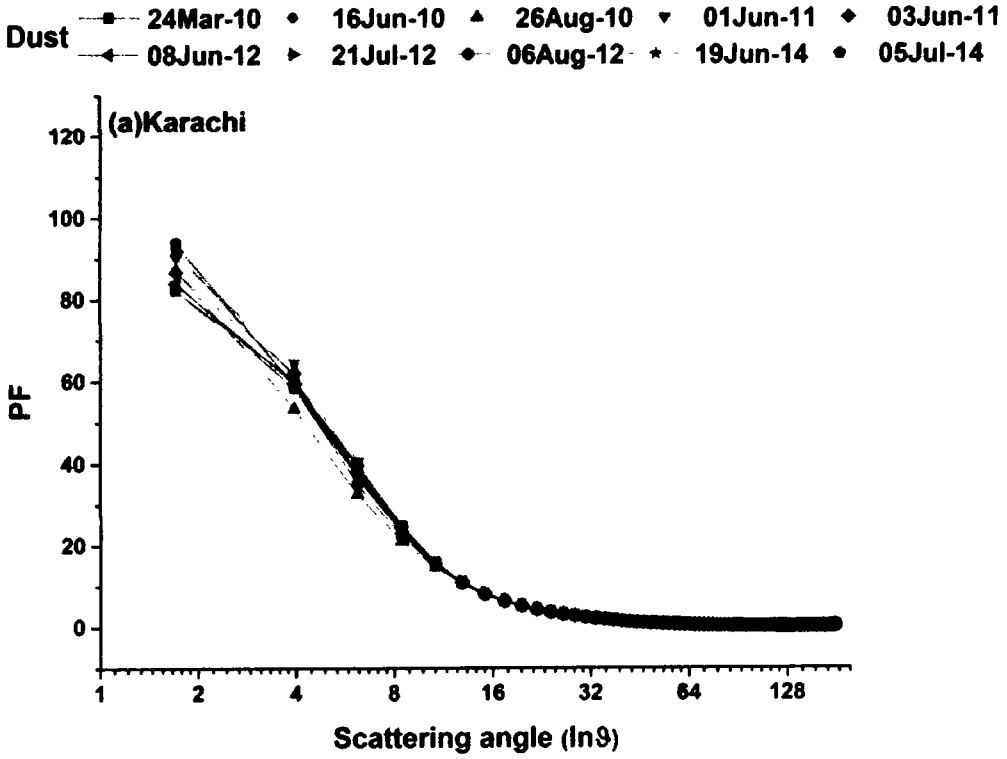

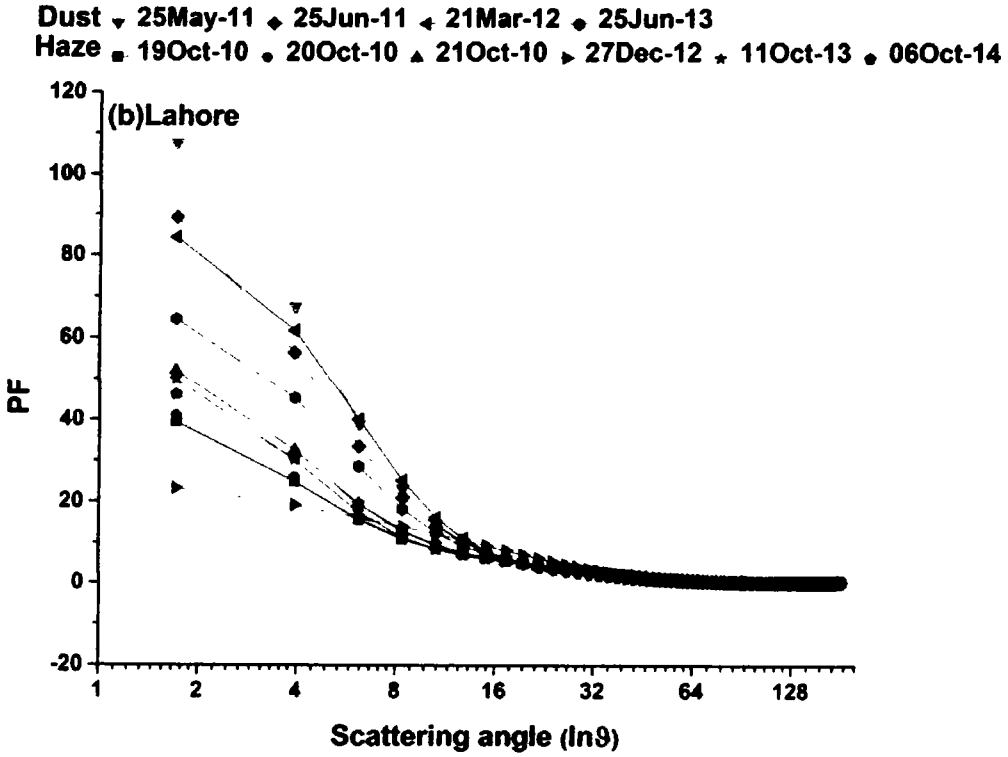

Figure 4. 4 Daily averaged variation of PF over (a) Karachi and (b) Lahore during DE and HE.

The results show that PF values were relatively higher at angle $\theta = 0°$ during the DE over Karachi and Lahore. This reflects the dominance of large dust particles. Conversely, HE over Lahore with relatively low values of PF clearly represents the presence of small particles. It shows that the PF has a high sensitivity to the scattering angles for both DE and HE. The PF values were a maximum at a scattering angle of 0° and then decreased to a minimum at angles of 131° during all the episodes. A uniform PF was observed at scattering angles > 131°. 77. Bohren and Singham [77] analyzed non-spherical dust particles and found that at greater scattering angles uniform scattering and backscattering were observed. The PF of fine particles is smaller than coarse particles for both forward and backward directions [103]. It is directly related to particle size while inversely related to wavelength [104]. At larger scattering angles, there is uncertainty in PF due to multiple interactions and greater absorption at shorter wavelengths [105]

4.1.5. Asymmetry Parameter (ASY)

The ASY parameter summarizes the angular distribution of light scattering by particles and is a crucial factor used for ARF estimation. Values of ASY vary between −1 to +1; ASY = -1 indicates completely back-scattered radiation, while ASY = +1 represents fully forward-scattered radiation, and ASY = 0 denotes symmetric scattering. Similar to SSA, ASY also depends on wavelength, size, as well as on composition of particles [106].

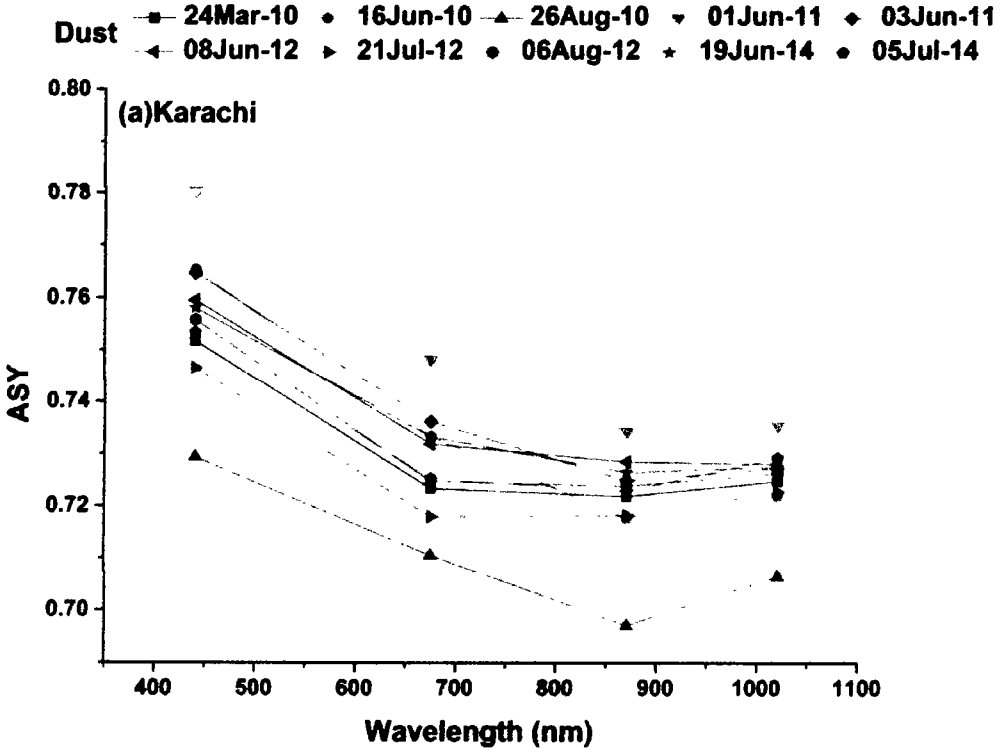

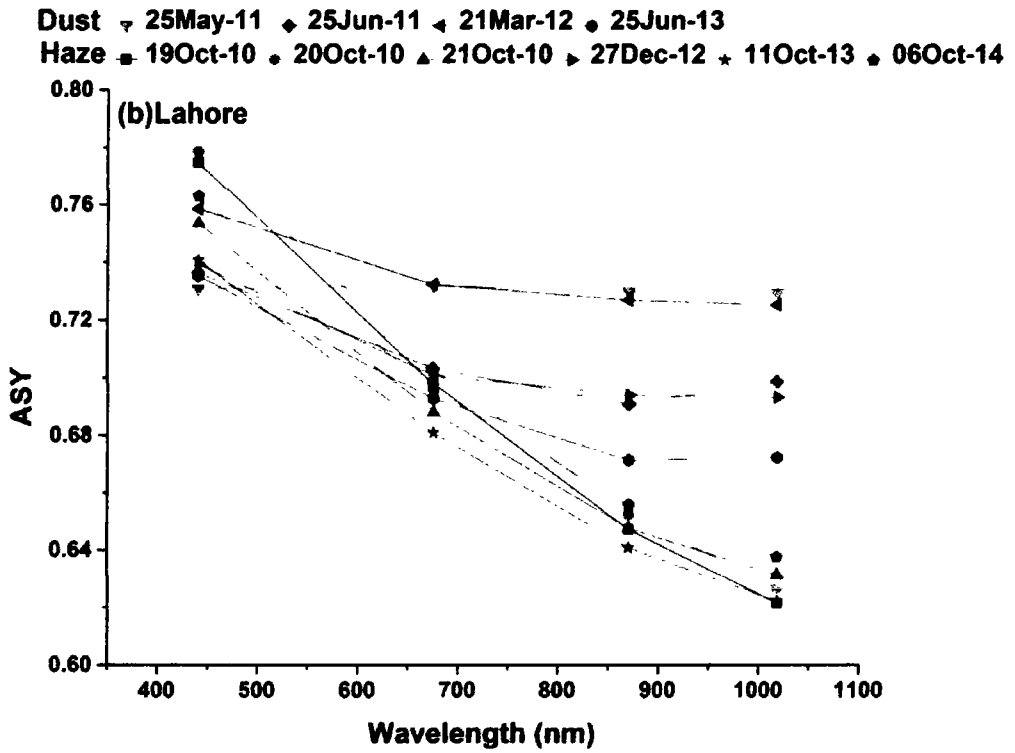

Figure 4. 5 Spectral profile of ASY over (a) Karachi and (b) Lahore during DE and HE.

Fig. 4.5 (a&b) shows that for DE over Karachi and Lahore, ASY decreases with increasing wavelength at shorter wavelengths (visible region) and slightly increases at longer wavelengths (near-infrared region which is attributed to the presence of dust particles as reported by Srivastava *et al.* [93]. Over Lahore for HE, ASY decreases abruptly with increasing wavelength suggestive of the presence of fine aerosols exhibiting high AE, similar to the findings of Pandithurai *et al.*[34]. Our results for HE are supported by Yu *et al.* [95] for severe haze over Beijing. The ASY of fine particles is smaller than that of coarse particles for a particular AOD [103].

4.1.6. Refractive Index (RI)

Refractive index, comprised of real (RRI) and imaginary (IRI) parts, is another optical property that gives information about the nature of aerosol particles. It depends on the chemical composition of aerosol particles and gives information related to the nature of particles. The RRI is related to

the scattering property whereas IRI is linked to absorption. Fig. 4.6(a & b) depicts the spectral variation of RRI during DE and HE over Karachi and Lahore. RRI remains smooth from 440 to 870 nm, and then drops at 1020 nm during DE at both studied sites, which represents the enhanced contribution of dust particles. The results are comparable to former published results reported by Alam *et al.* [25] for a South Asian dust episode. Prasad *et al.* [78, 103] documented enhanced RRI between 441 to 673 and decreased values at higher wavelengths during dust episodes over the IGP.

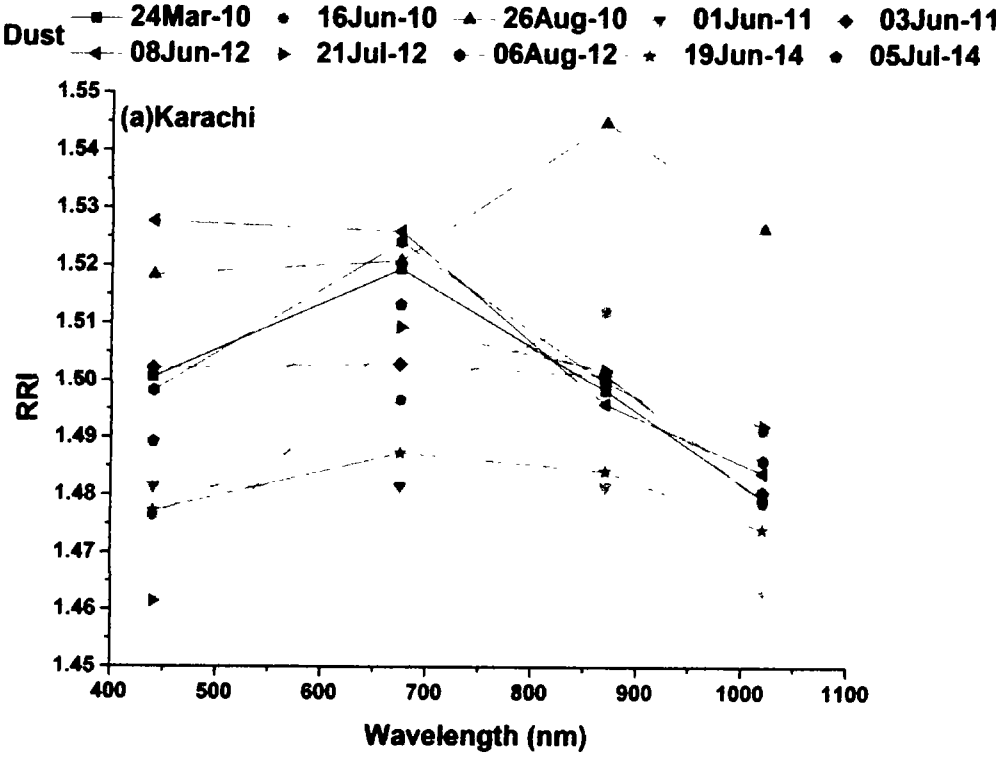

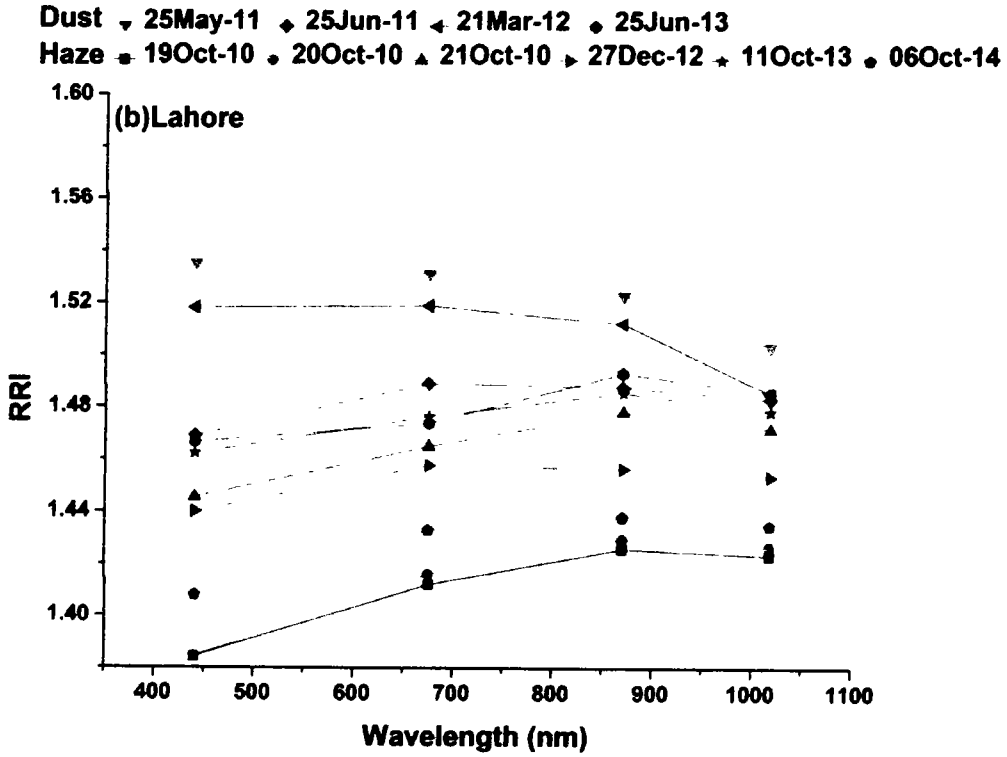

Figure 4. 6 Spectral profile of RRI over (a) Karachi and (b) Lahore during DE and HE.

Higher RRI was observed at shorter wavelengths as compared with longer wavelengths, which is supported by Singh *et al.* [107]. During HE over Lahore, RRI increases as a function of wavelength, signifying the presence of fine particles. RRI values for larger particles during DE are relatively higher as compared with fine particles during HE. The RRI at shorter wavelengths was less than the reported values for haze in China [95].

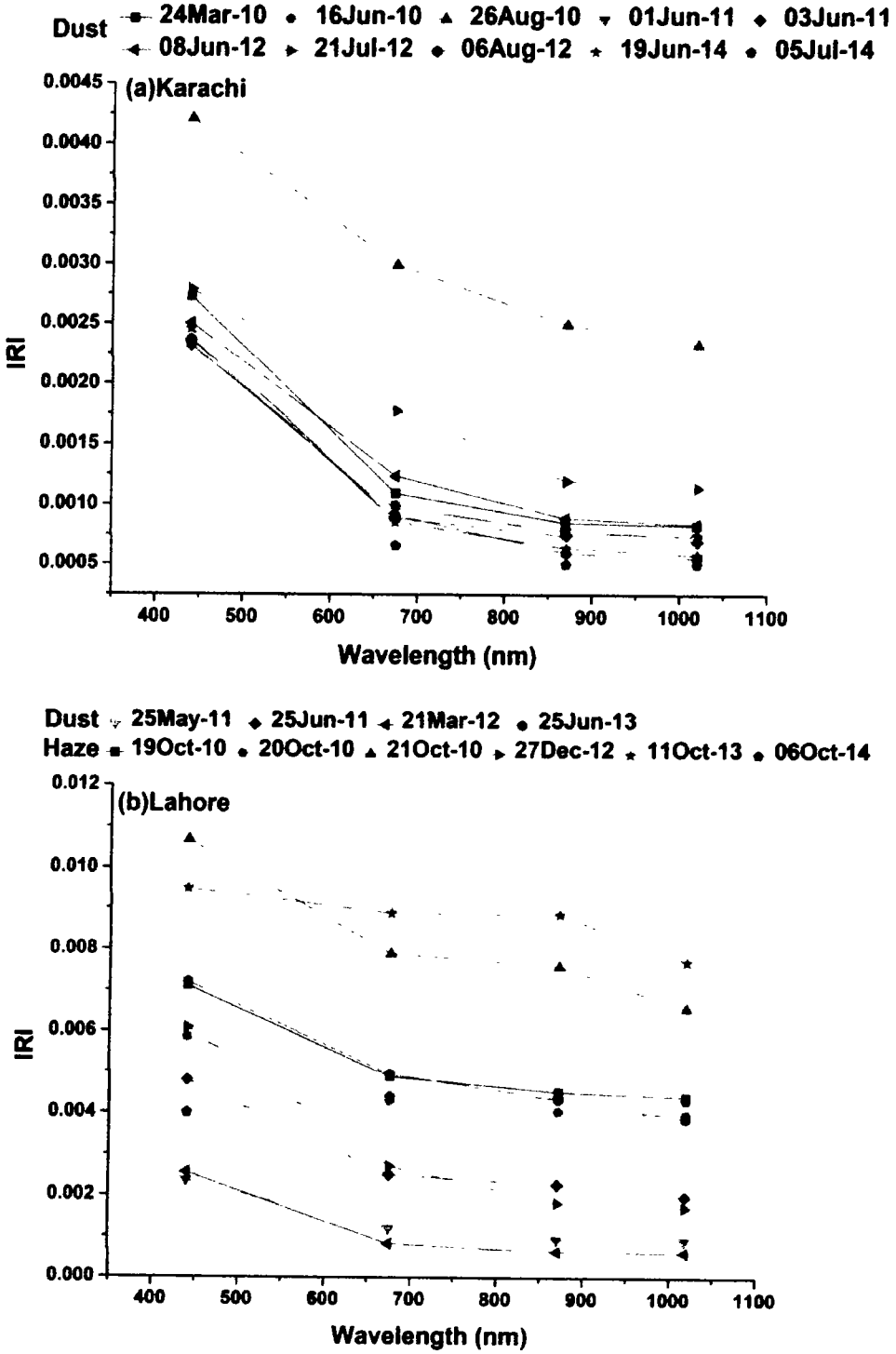

Figure 4. 7 Spectral profile of IRI over (a) Karachi and (b) Lahore during DE and HE.

The spectral variation of IRI during heavy pollution episodes of DE and HE are shown in the Fig. 4.7 (a & b). The IRI was found to decrease with increasing wavelength opposite to the spectral variation of SSA during the DE of Karachi and Lahore, suggestive of the presence of coarse dust particles. During HE, the IRI displayed no significant spectral dependency at longer wavelengths and is more challenging to explain. Generally, during HE, IRI decreases with wavelength at shorter wavelengths, but at longer wavelengths the variation was not pronounced. Singh *et al.* [107] reported the similar decrease in IRI with wavelength during post monsoon over Kanpur. IRI for HE was comparatively higher than that for DE as higher values show the dominance of fine particles and lower values confirm the presence of coarse particles.

4.2. Identification of Aerosol Types in High Pollution Episodes

It is very necessary to identify the types of atmospheric aerosols because they originate from different sources simultaneously with diverse physical and optical properties that could lead to impact atmosphere in different aspects [16]. Variation of aerosol types and their optical characteristics during high pollution episodes with changing meteorology will be useful to assess the ARF and will be utilized in the climate models in order to reduce the uncertainties. In order to better understand types of aerosol, optical characteristics are selected with threshold values that can be used to differentiate various aerosol types [108-112]. Prevailing aerosol types were characterized by leveraging the correlation between absorption and size [108]. Several methods can be used to identify aerosol types that originate naturally as well as anthropogenically. The commonly used clustering technique for classification of different types is the correlation of AOD with AE (both wavelength dependent), as has been demonstrated for different regions [89, 90, 110, 113, 114]. Likewise, the aerosol's discrimination can be rendered through clustering techniques with correlation to other optical properties.

During the episodes of high pollution, identification of aerosol types were selected for the given threshold values of AOD and AE as: Dust: 1 < AOD < 3.7 and 0.01 < AE < 0.4; Mixed-type aerosols: 1 < AOD < 1.7 and 0.5 < AE < 1; Biomass burning and urban/industrial: 1.2 < AOD < 3.8 and 1.1 <AE < 1.4. Fig 4.8 (a & b) reveals the relationship between AOD and AE, in which specific clusters represent different aerosol types over Karachi and Lahore during DE and HE. Dust particles were prominent during all DE over Karachi and over Lahore, especially during 25 May 2011 and 21 March 2012. During HE, especially occurring in the month of October, biomass burning, and urban/industrial fine particles were detected over Lahore. The remaining scattered points (25 June 2011, 25 June 2013, and 27 December 2012) were placed in mixed type of aerosols group which resulted from mixed natural and anthropogenic aerosols [95]. Recently, Tariq *et al.* [89] used AERONET data and reported that biomass burning was dominant types of aerosol during HE in Lahore. Kumar *et al.* [110] analyzed the AOD-AE relationship and classified aerosol into various types such as clean marine, continental clean, biomass burning/urban industrial, and desert dust over Durban, South Africa. Similarly, Sharma *et al* [115] discriminated the aerosols in various sub-types of clean marine, anthropogenic, biomass burning, mostly dust and mixed aerosols over Greater Noida. Further, using similar clustering technique, the classification of aerosols was carried out by numerous researchers [12, 114, 116].

4.3. Aerosol radiative Forcing and Heating Rate during High Pollution Episodes

The corresponding values of atmospheric heating rate are shown as well. During DE, the daily averaged ARF_{TOA}, ARF_{BOA}, and ARF_{ATM} were in the range of -7 to -25 W/m^2, -38 to- 76 W/m^2, and 25 to 52 W/m^2, respectively, over Karachi. The associated atmospheric heating rates ranged from 0.7 to 1.4 K/day over Karachi. Similarly, during DE over Lahore, the daily averaged values varied from -19 to -51 W/m^2, -66 to -128 W/m^2, and 47 to 77 W/m^2 at ARF_{TOA}, ARF_{BOA}, and

ARF_{ATM}, respectively. Correspondingly, the atmospheric heating rates during the DE over Lahore were between 1.3 and 2.2 K/day.

For a major dust storm over IGP, Prasad *et al.* [78] reported values of ARF_{BOA} in the range of -29.5 to -87.5 W/m^2 with an average of -57.5 W/m^2, while ARF_{TOA} values were in the range of -2.9 to -26 W/m^2 having an average of -13.5 W/m^2. The ARF for the three dusty days were -17.99, -65.77, and 47.78 W/m^2 at TOA, BOA, and within the atmosphere, respectively, with peak values reaching -40.59, -101.60, and 75.11 W/m^2, respectively, over IGP [117]. Patel and Kumar, [118] reported for maximum value of ARF_{ATM} (38.79 W/m^2) in May with associated atmospheric heating rates of 1.06 K/day over Dehradun in pre-monsoon where the dust aerosol types was prominent.

Table 4. 2. Average values of ARF_{TOA}, ARF_{BOA}, and ARF_{ATM}, in addition to their corresponding heating rate during DE and HE over Karachi and Lahore

Sites	Episodes	ARF_{TOA} (W/m^2)	ARF_{BOA} (W/m^2)	ARF_{ATM} (W/m^2)	Heating rate K/day
Karachi	DE	-15	-49	34	1.0
Lahore	DE	-34	-93	58	1.6
Lahore	HE	-38	-88	51	1.4

Singh *et al.* [46] found that ARF_{ATM} ranged from 45 to 77 W/m^2 and the atmospheric heating rates touched the value of 2.2 K/day during DE over Patiala, which depicts the potent atmospheric heating through dust particles. Srivastava *et al.* [93] also noted the higher values of ARF_{ATM} (71.6 and 68.4 W/m^2) in the period of dust events (March 2012), with estimated atmospheric heating rates of 2.0 and 1.9 K day^{-1} over Jodhapur and Delhi, respectively.

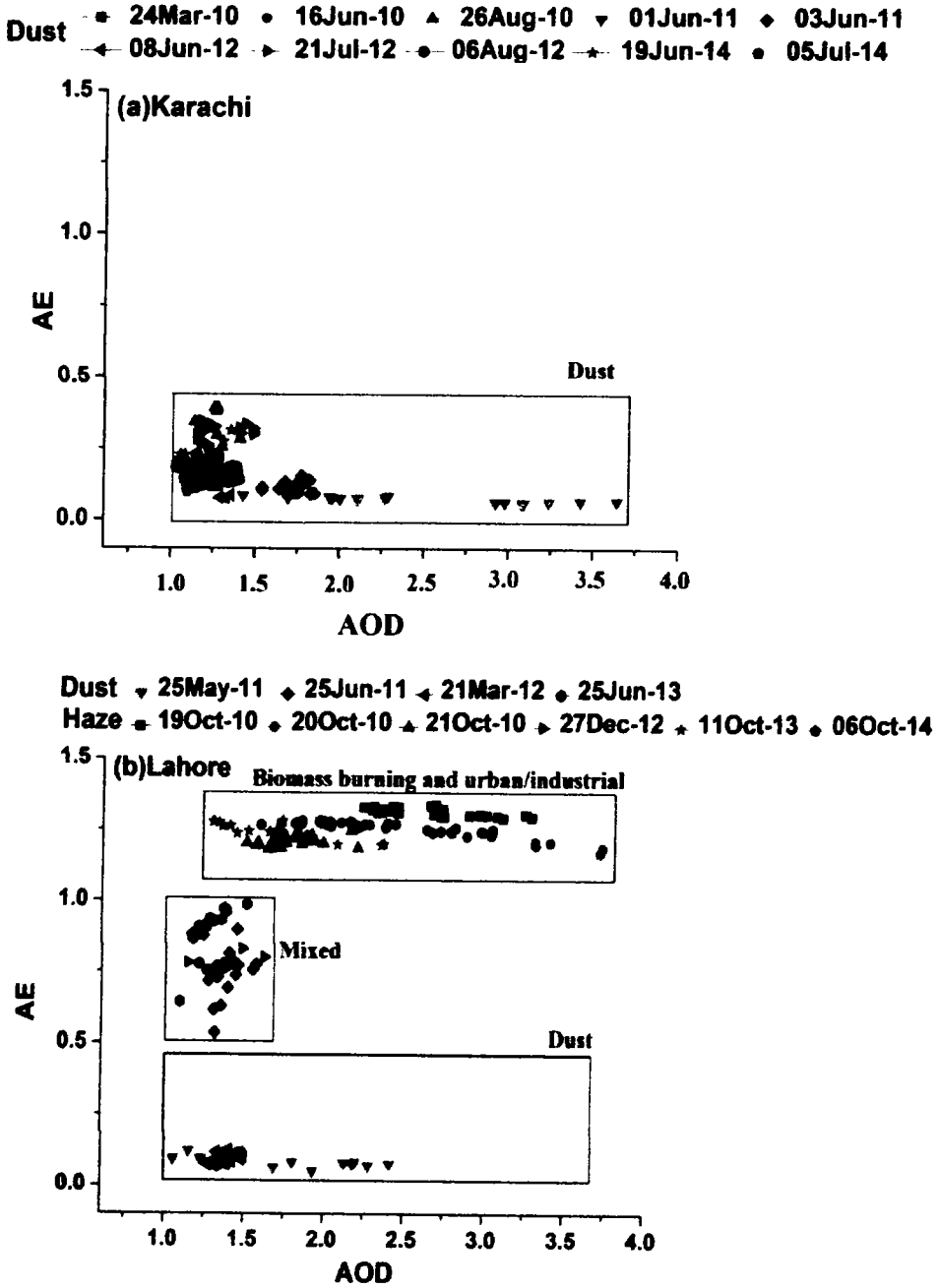

Figure 4. 8 Scatter plot showing clusters of aerosol types for AOD and AE over (a) Karachi and (b) Lahore during DE and HE.

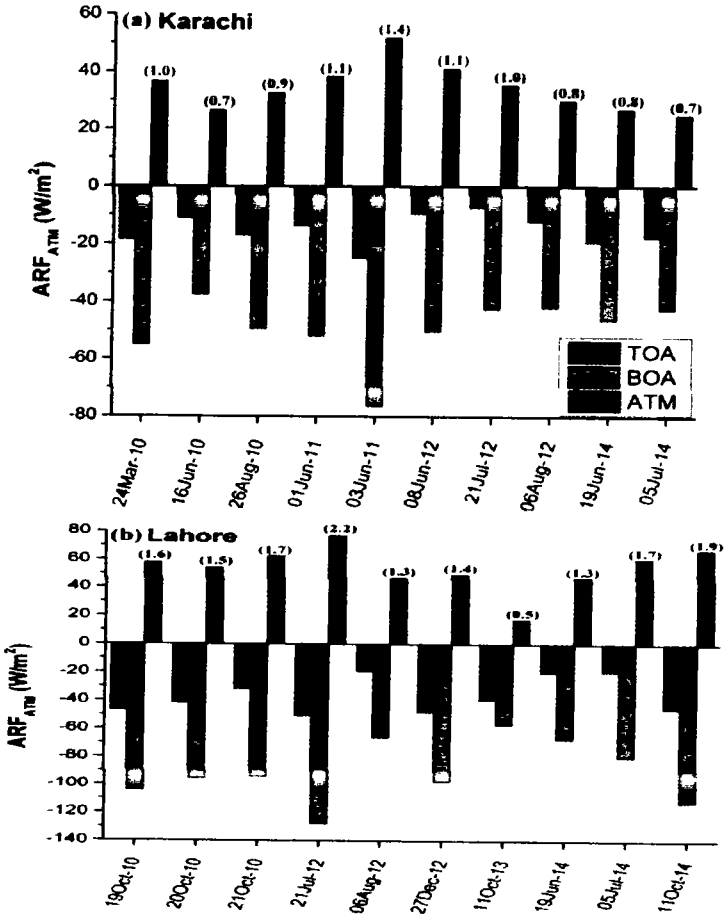

Figure 4. 9 Daily averaged variation in ARF_{TOA}, ARF_{BOA} and ARF_{ATM} with corresponding heating rate in the parenthesis over (a) Karachi and (b) Lahore during DE and HE.

Pandithurai *et al.* [34] computed ARF_{BOA} values from -39 W/m^2 (in March) to -99 W/m^2 (in June), and ARF_{ATM} from +27 W/m^2 (in March) to +123 W/m^2 (in June), with an associated atmospheric heating rate of 0.6 to 2.5 K/day over New Delhi. Due to significant impacts of DE, numerous other works calculated the ARF at different locations [25, 112, 119, 120]. For HE, the daily averaged ARF ranged between -20 and -47 W/m^2 at ARF_{TOA}, -57 and -112 W/m^2 at ARF_{BOA}, and 17 and 67 W/m^2 in ARF_{ATM}, with an associated atmospheric heating rate in the range of 0.5 to 1.9 K/day. Recently, Yu *et al.* [94] observed the ARF_{TOA}, ARF_{BOA}, and ARF_{ATM} with values of -45.78, -112.29, and 66.51 W/m^2, respectively, with a corresponding atmospheric heating rate of

1.61 K/day recorded at heavy haze in Beijing. Similarly, Jose *et al.* [121] observed the large negative ARF_{BOA} (-87 W/m^2) and positive ARF_{ATM} (30 W/m^2) during haze days over Hyderabad.

A significant difference was observed between ARF_{TOA} and ARF_{BOA}, pointing to solar radiation absorbed in the atmosphere, leading to a warmer atmosphere and cooler surface. Table 4.2 summarizes the averaged values of ARF_{TOA}, ARF_{BOA}, and ARF_{ATM}, along with associated heating rates, during DE and HE over the studied sites. During both DE and HE, aerosol particles produced a net warming effect within ATM over Karachi and Lahore.

To assess the reliability of the model calculations, estimated values of atmospheric forcing were compared with measured values. Fig. 4.10 (a & b) shows the validation of daily averaged ARFATM estimated from SBDART and retrieved from AERONET during the DE and HE over Karachi and Lahore. The correlation coefficient (R2) between AERONET and SBDART within the atmosphere were 0.92 and 0.52 over Karachi and Lahore, respectively, during the study period. The AERONET-SBDART ARF analysis revealed relatively better correlation over Karachi than Lahore. Overall, a significant correlation was observed for AERONET-SBDART derived ARF despite the uncertainties and assumptions in the data. A similar comparison between ARF (at BOA) derived from AERONET and SBDART yielded good correlations of 0.98 and 0.99 during summer and winter seasons over Karachi and Lahore [23]. Alam *et al.* [122, 123] compared AERONET ARF with SBDART ARF at BOA (R^2 = 0.92) and TOA (R^2 = 0.82) over Karachi showing good correlation. Recently, Kumar *et al.* [110] observed a strong relationship (R=0.89 at BOA and R=0.78 at TOA) for AERONET-SBDART derived ARF in the pre-monsoon over Kanpur.

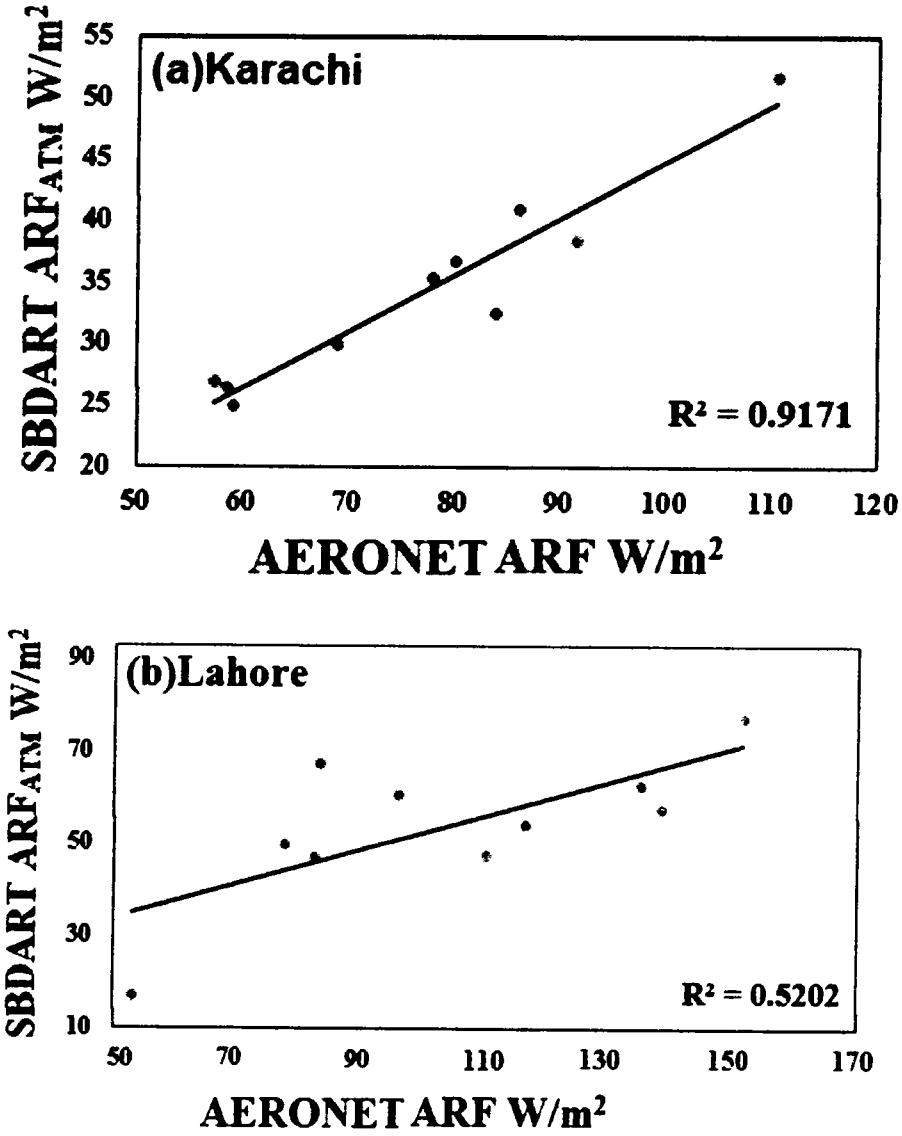

Figure 4. 10 Scatter plots of AERONET with SBDART ARF within atmosphere over (a) Karachi and (b) Lahore during DE and HE.

4.4. Satellite Monitoring and Aerosol Transport During High Pollution Episodes

The DE and HE were verified with MODIS active fire images. Fig. 4.11 (a-d) shows the MODIS true color images during the DE of 24 March 2010, 16 June 2010, 26 August 2010, and 19 June 2014 over Karachi. These images are the representative for the rest of the episodes. The dense layer of dust plumes over Karachi and across the Arabian Sea was clearly seen during DE.

Similarly, Alam *et al.* [25] also reported the dense layer of dust plumes during dust events over Lahore.

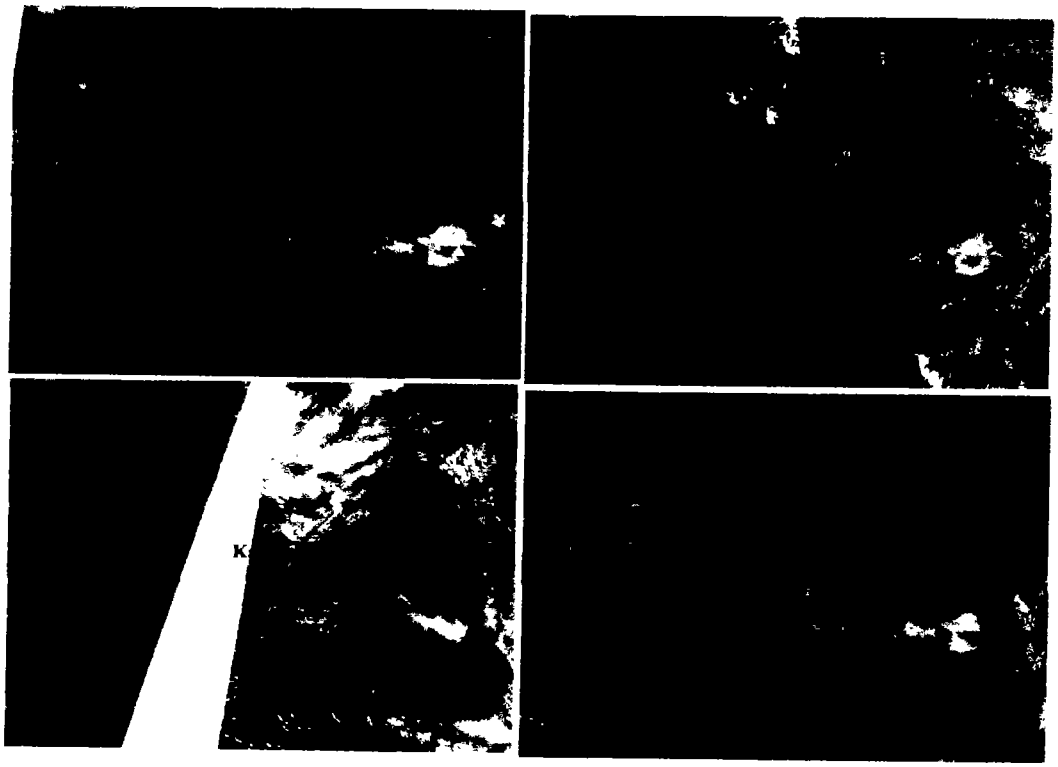

Figure 4. 11 True color images derived from MODIS Terra during the DE over Karachi.

Fig. 4.12 (a-d) illustrates the MODIS true color images during the HE of 19-21 October 2010 and 06 October 2014 over Lahore. For the rest of the DE and HE, no images were available. The biomass burning (red marks) areas were coupled with visible plumes of greyish haze, resulting in the reduction of visibility during HE over Lahore. The red dots in haze images show the hotspots area, where MODIS has detected uneven events of surface temperature. The hotspots are probably agriculture residue burning, which contributed to the haze significantly.

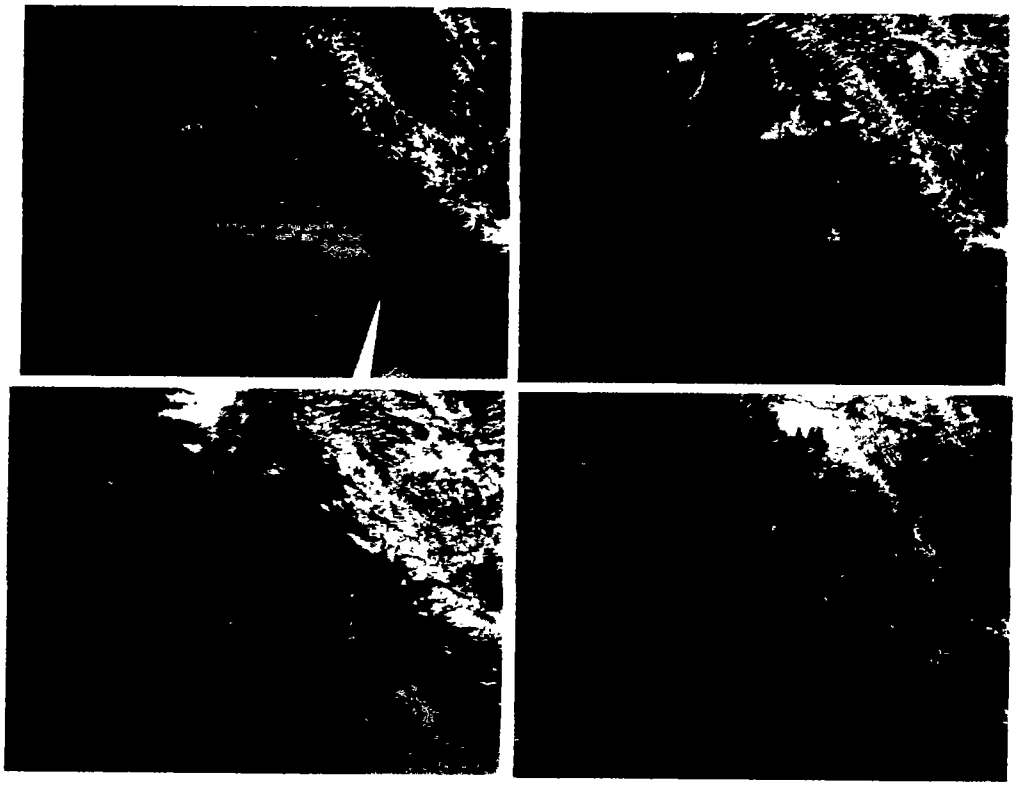

Figure 4. 12 True color images derived from MODIS Terra during the HE over Lahore.

To examine the long distance transport and possible source regions of air masses, cluster analysis of back trajectories was conducted based on the HYSPLIT model [73]. The activated meteorological data used in the trajectory simulations were retrieved from the Air Resources Laboratory (ARL). The trajectories near each other were merged into individual clusters. Differences between these trajectories within a cluster were minimized while differences between clusters were maximized. The spatial variance was calculated between each endpoint along trajectories within a cluster. The cluster spatial variance is the sum of the spatial variance of all trajectories within its cluster.

Fig. 4.13 (a & b) show the 72 h back cluster trajectories of air mass at 1000 m during DE and HE over the studied sites. During DE over Karachi and Lahore are receiving almost the air masses

from arid/semi-arid regions (Arabian Sea, India, Turkmenistan, Yemen and Oman) covering long distances and transporting coarse particles to the studied sites. Some of the trajectories originated from local sources. During HE over Lahore, local air masses arrive along fine particles, with less contribution from coarse particles originating over India and Afghanistan.

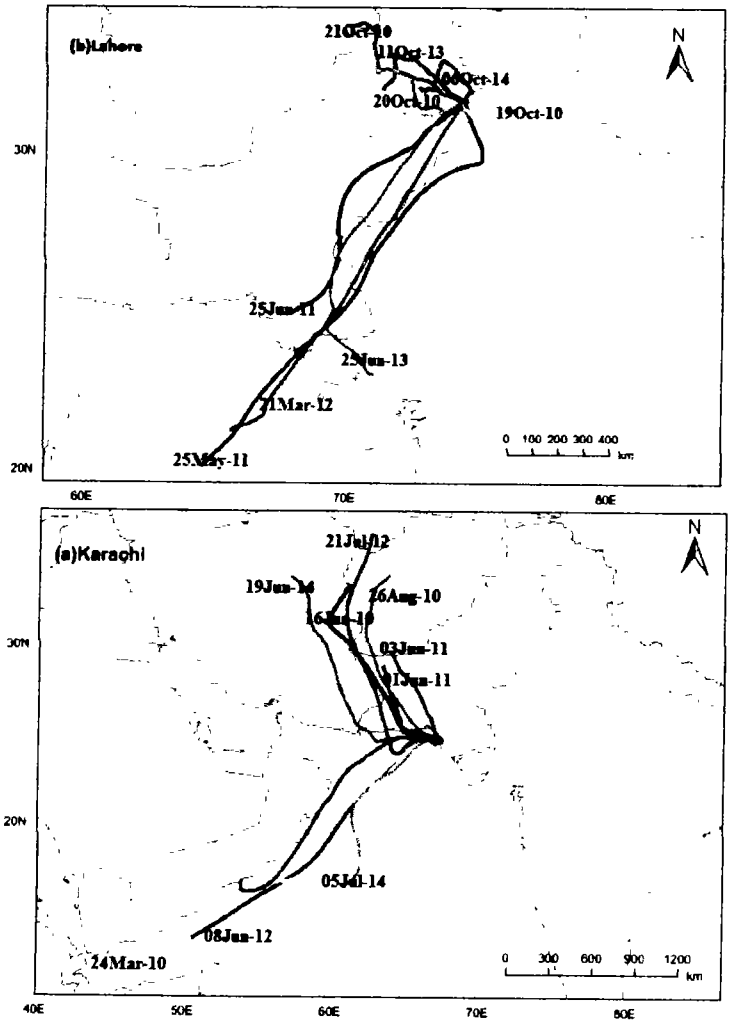

Figure 4. 13. 72 h back trajectories using HYSPLIT model showing air masses origins and pathways at 1000 m above ground level (AGL) over (a) Karachi and (b) Lahore during DE and HE.

Chapter 5

Influence of meteorological parameters and radiation feedback on cloud optical properties in the Himalaya Karakoram region

5.1. Variations in the Optical Properties of Clouds

The long-term temporal variations of cloud optical properties (e.g. CF, COD, CER, CWP, CTT and CTP) were investigated over three sites of Diamir, Gilgit and Skardu in Pakistan during 2004-2016. The changes in radiation fluxes over TOA due to these patterns were also analyzed. Furthermore, the impacts of meteorological parameters on cloud properties were also investigated.

5.1.1. Cloud Fraction

CF is being considered as the dominant modulator of the radiative fluxes of the earth. Major effect of cloud cover is warming of the climate. However, sometimes surface albedo also plays its role to cool the environment [124]. CF ranges from 0.28 - 0.84, 0.34 - 0.86 and 0.34 - 0.91 at Diamir, Gilgit and Skardu, respectively, with their corresponding averaged values of 0.54 ± 0.15, 0.60 ± 0.14 and 0.65 ± 0.13 (see Figs 5.1a, 5.2a, 5.3a). The high CF values were observed in winter. Where, Tao *et al.* [125] and Oreopoulos *et al.* [126] linked invigorated expansion and vertical thickness of clouds with aerosol loadings. Massive loading of aerosols provides an ample bit of cloud condensation nuclei which reduces CER. In this process clouds become thicker and brighter with maximum COD [127]. Whereas, the reduced CER makes possible to lift up a large quantity of water vapor, which releases latent heat upon freezing in the upper atmosphere [128]. This liberation of latent heat modifies temperature gradient of vertical profile. Low values in summer have been recorded over the study areas. Which drive to increase the proportion of solar fluxes to

reach the earth's surface [129]. The uneven fluctuations in CF during the study period were due to the evaporation caused by solar heating, cloud formation, cloud evolution and transportation. However, these variations can also be associated with local thermodynamic parameters, radiation fluxes, large-scale atmospheric circulation, turbulent fluxes, and atmospheric moist convection [49]. Cossu *et al.* [49] reported the highest and lowest CF value of 0.60 and 0.42 during December and July, respectively in Bern (Switzerland). Seiz *et al.* [51] investigated the mean monthly CF values of 0.71 and 0.52 during January and July over Switzerland from March 2000 to February 2010. Their results are in agreement with our results.

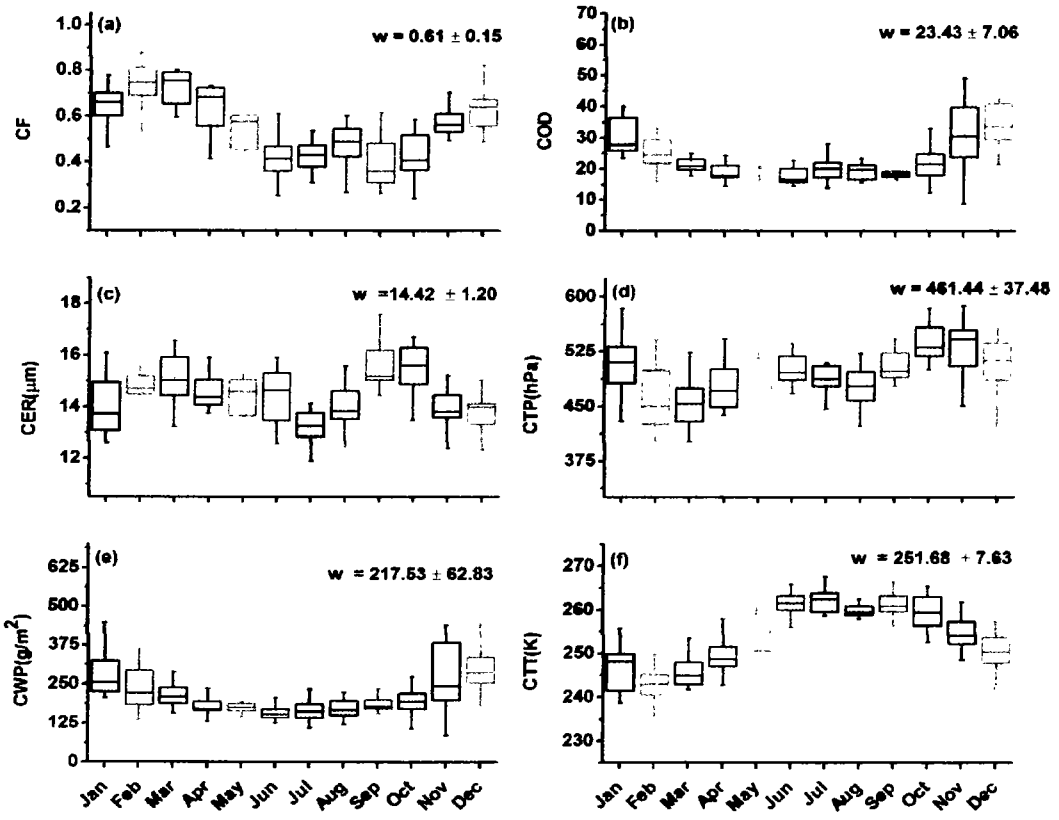

Figure 5. 1 Box-whisker plots shows the average monthly variation in cloud optical properties over Diamir during 2004-2016. Each box and the whisker represent as 25th and 75th percentiles, and the 5th and 95th percentiles, respectively. The horizontal and vertical lines show the mean and standard deviation, respectively. The small circle in each box represent median value and the cross above and below the box corresponds to maximum/minimum values. The monthly averaged values for each parameter are given in each panel.

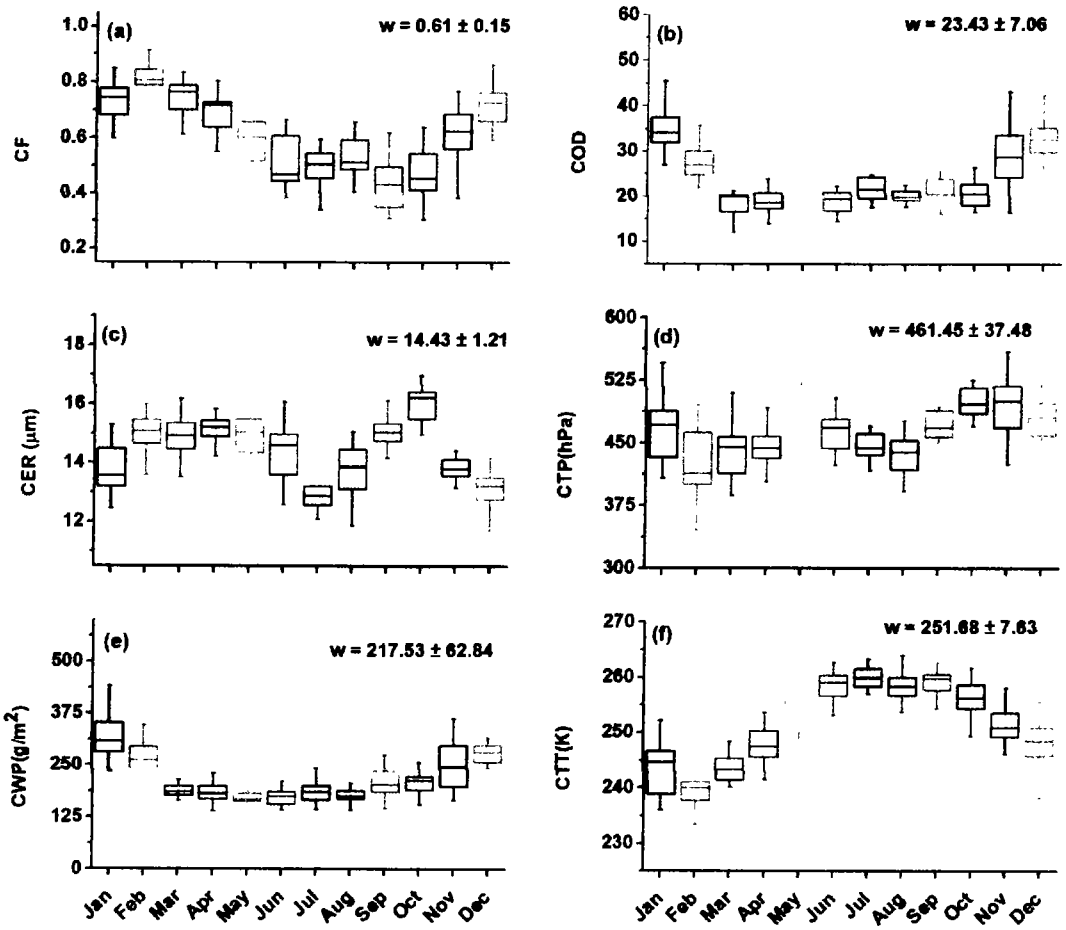

Figure 5. 2 Same as Figure 5.1, but for Gilgit.

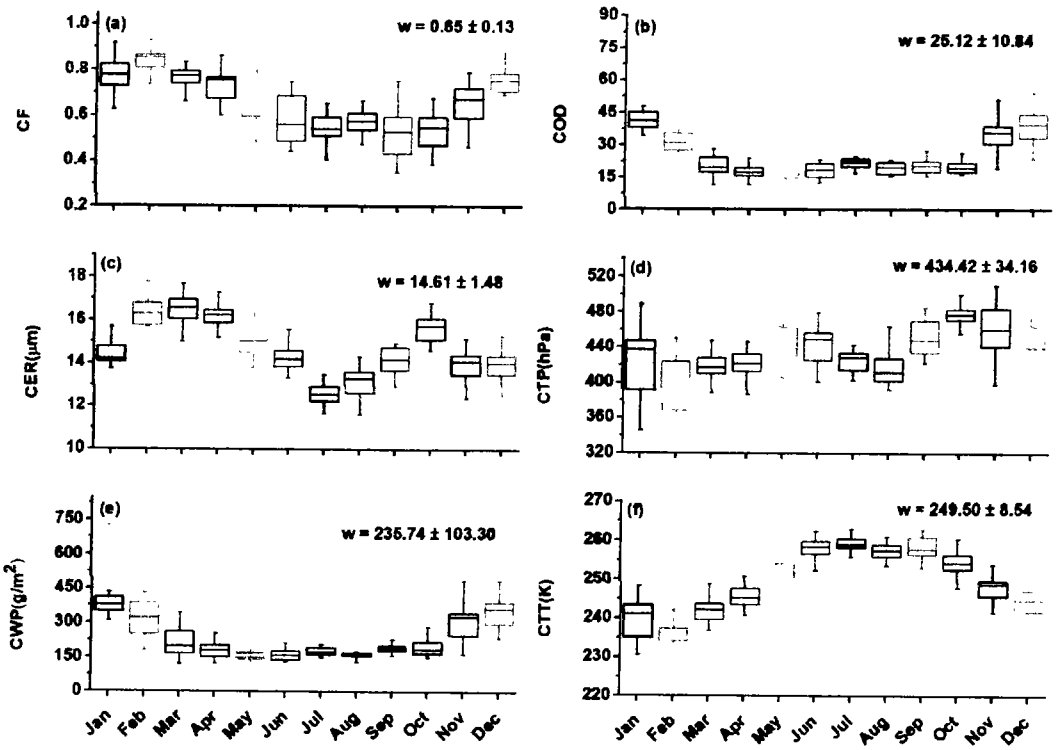

Figure 5. 3 Same as Figure 5.1, but for Skardu.

5.1.2 Cloud Optical Depth

COD and CER are two main optical cloud parameters to control radiative forcing [81]. Whereas, a linear relationship exists between COD and CWP [130]. For Diamir, Gilgit and Skardu the COD values range from 8.66-59.62, 11.94-50.57 and 11.78-74.39 respectively, with their corresponding averaged values of 23.24 ± 8.14, 23.43 ± 7.06 and 25.12 ± 10.84 (see Figs 5.1b, 5.2b, 5.3b). At each location, the COD values were found to be low and high during warm and cold months, respectively. The minimum values of COD during spring and summer months show the existence of thin clouds in the study locations. Yin and Min, [52] observed that COD from spring to summer decreases due to the increase of surface temperature and sunshine hours in the study regions of Barrow and Atqasuk. The variations in COD indicate for the types and thickness

of clouds and consequent chances of precipitation [131]. Whereas, Kobayashi *et al.* [130] identified the non-precipitating clouds with maximum values of COD and CER. Therefore, the maximum values of COD and CER suggest non-precipitating clouds over study regions in the months of winter season. However, Boers *et al.* [132] found that the correlation between COD and CER for precipitating clouds is negative. Similarly, increased COD may direct towards a strong convection. Our analysis is consistent with Jin *et al.* [133], who reported the maximum (25) and minimum (5) inter-annual COD during winter and summer seasons, respectively.

5.1.3 Cloud Effective Radius

CER values fluctuate between 11.83-17.58 μm, 11.64-17.55 μm and 11.37-17.79 with an averaged value of 14.42 ± 1.15 μm, 14.42 ± 1.20 μm and 14.61 ± 1.48 μm over Diamir, Gilgit and Skardu, respectively (see Figs 5.1c, 5.2c, 5.3c). Whereas, these variations in CER are a function of CWP and cloud condensation nuclei [132, 134]. At each location, CER has minimum values in the month of July and August and maximum values in March, September and October. Monthly variations in CER and CTP above all regions show a negative correlation (see Fig 3, 4 and 5) which is in accord to curvature effect (Kelvin Effect) demonstrating greater vapour pressure over droplets with smaller radii. However, both aerosol loading and cloud water path also affect the CER values. Yin *et al.* [52] investigated the decrease trend of CER from March to July, which shows the polluted environment and high aerosol loading over the region. Our obtained results of CER are similar to the results of Yin *et al.* [52].

5.1.4 Cloud Water Path

The average monthly variations in CWP over three locations during the study period are shown in the Figs (5.1e, 5.2e, 5.3e). The CWP value varies from minimum values of 86 to maximum value of 626 gm/m^2, from 103 to 497 gm/m^2 and from 121 to 726 gm/m^2 with averaged values of

217.57 ± 81.58 gm/m2, 217.53 ± 62.83 gm/m2 and 235.74 ± 103.30 gm/m^2 over Diamir, Gilgit and Skardu, respectively. At each location, minimum CWP was found in summer, while maximum in winter. According to Albrecht, [135], when cloud microphysical parameters i.e., cloud droplet number concentration increases, size of the cloud droplet decreases that suppresses formation of precipitation that leads to produce larger amount of CWP. Yet, few authors found that CWP may also decrease with the increasing trend in cloud number concentration [136]. Our findings of CWP are similar to Yin and Min, [52] who attributed the decrease in CWP from spring to summer due to the increase in sunshine hours and surface temperature over two locations i.e. Barrow and Atqasuk. Likewise, Bodas-Salcedo *et al.* [137] showed the positive response of CWP due to the cloud regime.

5.1.5 Cloud Top Temperature

One of the fundamental parameters, that is responsible for climate modification and worldwide weather conditions is the variation in CTT, governed by solar insolation [138]. CTT values ranged from 232.98 to 267.56 K (averaged value of 254.20 ± 7.68 K), from 230.60 to 263.62 K (average value of 251.68 ± 7.63 K) and from 229.04 to 263.82 K (average value of 249.50 ± 8.54 K) over Diamir, Gilgit and Skardu, respectively (see Figs 5.1f, 5.2f, 5.3f). An increasing trend of CTT from February to September and a decreasing trend from September to January has been observed over all sites during the study period. Heavy rainfall results due low CTT and vice versa. The clouds in the Skardu area were found to be cooler than Diamir and Gilgit which shows the presence of thicker clouds capable of heavy rainfall. Low value of CTT corresponds to the greater thickness of clouds with high cloud tops and greater probability of rain [139]. Hanna *et al.* [140] reported that the CTT cause heavy, moderate and light rain for 223.15 K, 226.15 K and 228.15 K, respectively. Liu and Fu, [141] attributed the low CTT to heavy rainfall rate for convective cloud.

Nonetheless, seasonal fluctuations in atmospheric temperature are the primary cause of variation in CTT [142].

5.1.6 Cloud Top Pressure

The CTP varies between 365.40-586.60 hPa, 345.8-559.4 hPa and 342.40-510.60 hPa with an average value of 495.41 ± 41.46 hPa, 4661.44 ± 37.48 hPa and 434.41 ± 34.16 hPa over Diamir, Gilgit and Skardu, respectively (See Figs 5.1d, 5.2d, 5.3d). The minimum and maximum CTP was found in February and November, respectively. The low values of CTP suggested clouds at high elevations of atmosphere and vice versa. Nevertheless, the low values of CTP may also be due to heterogeneous nucleation of cloud droplet and dominancy of salt effect (Raoult's effect). According to solute effect, the water molecules are prohibited to escape due to dissolved aerosols on the surface of the cloud droplet. Bharti, [143] reported the CTP values of 256.8 hPa over Kedarnth and 183.60 hPa over Leh in the north-west Himalaya region of India that consequently cause thunderstorm and heavy rainfall.

5.2 Seasonal Variations in Cloud Optical Properties

Thermodynamical variations in climate are linked with seasonwise variations of atmospheric aerosols. Such inter-seasonal variations made the analysis of cloud macro-microphysics more complicated [144]. Seasonal variations in cloud optical properties such as CF, COD, CER and CWP depend on changes in local temperature and humidity level. Whereas, cloud cover is ace of the significant cloud optical properties that plays vital role in modulation of energy budget and solar fluxes [145]. Similarly, Ceppi et al. [146] found that long and shortwave raddiative feedback is proportional to cloud fraction and is controlled by the Clausius-Clapeyron equation.

Figure 5.4 revealed the averaged seasonal variations in the selected locations during the period (2004–2016). The CF values were found to be high during winter and low during summer saosons.

The high (low) CF averaged values were 0.69±0.10 (0.44±0.09), 0.75±0.08 (0.51±0.13), and 0.79±0.08 (0.56±0.09) over Diamir, Gilgit and Skardu. The high CF corresponds to high RH during winter and low CF due to low RH in summer. Table 5.1 also depicted good corelations between CF and RH (correlation coefficient 0.62 and 0.64) over Diamir and Skardu. Similarly, COD and CWP have high values in winter season as compared to other seasons. There is a strong postive correlation between COD and RH (see Table 5.1), which suggested that the rich humid air may cause high values of COD. Likewise, CWP is strongly dependent on RH and high values of CWP observed in winter season as compared to other seasons. The seasonal changes in CWP ranged from 169±34.22 gm^{-2} in summer to 280.92±97.43 gm^{-2} in winter, 178.43±22.19 gm^{-2} in summer to 287.56±65.73 gm^{-2} in winter, and 167.84±21.74 gm^{-2} in summer to 363.69±101.22 gm^{-2} over Diamir, Gilgit and Skardu respectively.

It is evident from Fig 5.4 that there is small seasonal fluctuation in CER, CTP and CTT throughout the study period. The seasonal averaged CER ranged from 13.82±1.06 μm (in summer) to 14.95±1.24 μm (in autumn), 13.75±1.13 μm (in summer) to 15.04±0.86 μm (in spring) and 13.30±1.13 μm (in summer) to 15.87±0.98 μm (in spring) over Diamir, Gilgit and Skardu respectively. However, due to collision coalescence process during precipitation formation CER slightly increases with the decrease in COD in spring and summertime (see Fig 5.4). Similarly, seasonal averaged changes in CTP range from 478.18±39.01 hPa in spring to 523.94±31.88 hPa autumn, 447.36±24.22 hPa in summer to 487.95±28.01 hPa in autumn, and 419.00±39.25 hPa in winter to 462.93±25.24 hPa in autumn, over Diamir, Gilgit and Skardu respectively. The seasonal variations in CTT ranged from 246.83±6.17 K in winter to 261.13±2.90 K in autumn, 243.84±6.00 K in winter to 258.84±2.70 K in summer, and 239.18±5.66 K in winter to 258.11±2.58 K in summer over Diamir, Gilgit and Skardu respectively. Referable to the high values of CTT in

summer season over Gilgit and Skardu, it may result in dominance of Kelvin effect and precipitation formation. Where, the decreased value of CWP and CER suggest thin clouds with short lifetime [150, 151]. In winter season, COD over all the study sites is proportional to the water content present in the air column, which is similar to the results reported by Ceppi et al. [146] and Li et al. [144] that COD is directly proportional to CWP. Nevertheless, Li et al. [144] also corroborated that in the episodes of high concentration of aerosols, the high value of COD is not due to CWP but linked with microphysical variations and larger fraction of smaller CER. Thus, in summer season, the smaller value of CER over Skardu may also be due to the first indirect effect [127]. The smaller cloud droplets resist the precipitation formation and cause second indirect effect [135]. Where, the comparative high values of CER in spring season over all regions also manifest the presence of hydrophilic aerosols and dominance of Kelvin effect over solute effect. Since, clouds with CTT < 273K are cold clouds [152, 153]. Therefore, in all seasons cold clouds have been observed over all study regions (see Fig 5.4). The lowest value of CTP over Diamir, Skardu and Gilgit has been read in spring, summer and winter season, respectively. Where, the lower CTP causes the strong updraft of intense air currents, resulting in very thick clouds [154].

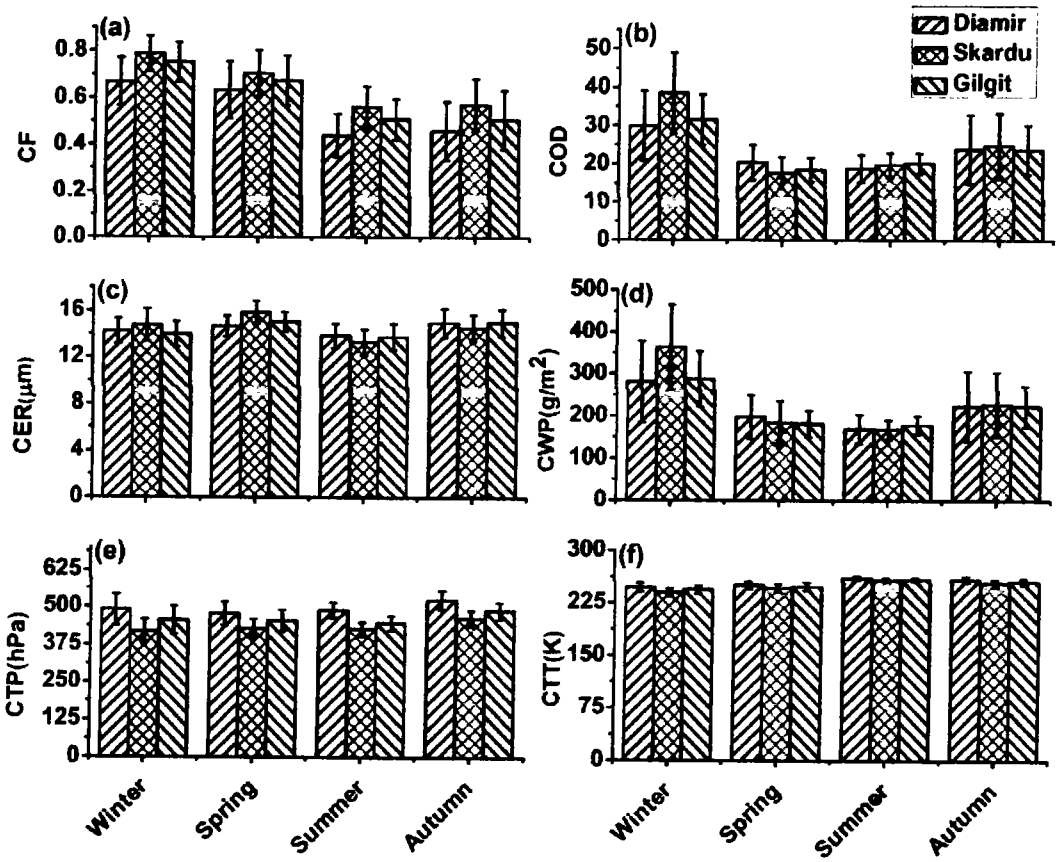

Figure 5. 4 Seasonal Variations in optical properties of clouds.

5.3 Cloud Radiative Feedback

The global climate is significantly affected by cloud radiation feedback, particularly in the HK region. Cloud sensitivity is a critical factor in the cloud-radiation feedback that represents the differential response of the radiation fluxes [155]. The cloud radiation feedback was analyzed in numerous studies and found negative feedback at different latitudes [52]. We are interested to analyze the linkage of radiation feedback to cloud parameters in the HK region of the northern Pakistan, as the global climate is more affected by cloud radiation feedback, particularly in the HK region. In this section, the influence of cloud optical properties on the TOA shortwave radiative fluxes has been analyzed by utilizing the monthly mean cloud properties. The correlations between

COD with TOASWCRF were found to be 0.35, 0.11 and 0.32, while CF correlations with TOASWCRF were reported to be -0.05, 0.19 and 0.36 over Diamir (see Figure 5.5a), Gilgit (see Figure 5.5b) and Skardu (see Figure 5.5c), respectively. A positive relationship was found for COD and CTP against TOASWCRF, indicating that the cooling effect increases with the increase in COD and CTP. The COD depends on the particle concentration, the geometrical depth and particle-radiation interaction. Thus, the larger the COD, greater will be the interaction with radiation [156]. Colman et al 2001 [157] studies reported associated the large negative and positive contributions of TOASWCRF with CF. Weare, [158] also related the atmospheric cooling to the high cloud amount and COD. Li *et al.* [159] also reported a good correlation of -0.73, -0.67 between CF and TOASWCRF over Central Asia and East Asia, respectively, with a strong correlation (-0.94) over North America. Sathiyamoorthy *et al.* [160] investigated a comparison between High CF and TOASWCRF and found a moderate correlation (-0.51 and -0.66) over the Arabian Sea (AS) and Equatorial Indian ocean (EIO), whereas, a relatively high correlation (-0.86) over the Bay of Bengal, India (BBI). They also reported a negative, but good association of the TOASWCRF with COD (R = -0.86, -0.75 and -0.83) over the AS, BBI and EIO.

Similarly, the correlation of CTP and CER with TOASWCRF over Diamir, Gilgit and Skardu were found to be 0.006 and 0.58 (see Figure 5.5d), 0.02 and 0.46 (see Figure 5.5e), 0.40 and 0.05 (see Figure 5.5f), respectively. Figure 5 (g-i) shows the correlation between cloud microphysical properties (CTT, CWP) and the TOASWCRF. The correlation coefficients of CTT and CWP with TOASWCRF were found to be -0.24 and 0.32, 0.044 and 0.02, 0.-0.64 and 0.38 over Diamir, Gilgit and Skardu, respectively. An increase in CWP with TOASWCRF lead to the enhanced reflection of solar radiation, resulting in the atmospheric cooling effect [3].

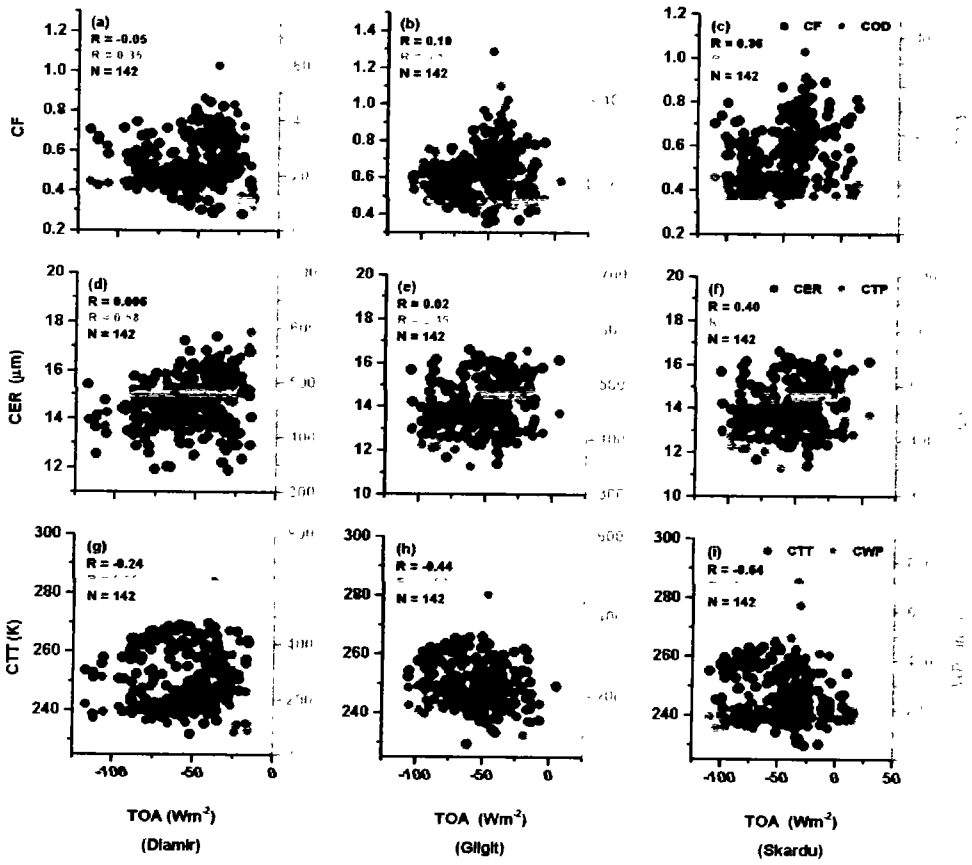

Figure 5. 5 Relationship between TOASWCRF and the cloud optical properties at the Diamir, Gilgit and Skardu during 2004-2016.

5.4 The Impact of Meteorological Parameters on Cloud Optical Properties

The cloud optical properties were analyzed with their associated influencing meteorological parameters, e.g. surface temperature (maximum, T_{max}, and minimum T_{min}), relative humidity (RH), monthly total rain (MTR) and wind speed (WS) over Diamir, Gilgit and Skardu during 2004-2016 (see Table 5.1).

Table 5. 1 Correlation between meteorological parameters and cloud optical properties for period (2004-2016).

Sites	Variable	T_{max}	T_{min}	RH	MTR	WS
Diamir	CF	-0.64	-0.57	0.62	0.38	-0.24
	COD	-0.59	-0.56	0.59	0.16	-0.39
	CER	-0.04	-0.05	-0.08	0.005	-0.13
	CWP	-0.59	-0.56	0.58	0.18	-0.38
	CTT	0.84	0.78	-0.71	-0.33	0.38
	CTP	-0.11	-0.21	-0.23	-0.52	-0.53
Gilgit	CF	-0.66	-0.44	0.21	0.14	-0.14
	COD	-0.47	-0.45	0.66	-0.12	-0.54
	CER	-0.05	-0.07	-0.16	0.13	-0.03
	CWP	-0.32	-0.26	0.51	0.01	-0.36
	CTT	0.85	0.69	-0.23	0.03	0.32
	CTP	-0.1	-0.38	0.22	-0.47	-0.32
Skardu	CF	-0.69	-0.54	0.64	0.33	-0.29
	COD	-0.69	-0.69	0.80	0.17	-0.66
	CER	-0.36	-0.29	0.13	0.22	-0.1
	CWP	-0.74	-0.71	0.80	0.23	-0.63
	CTT	0.89	0.78	-0.74	-0.32	0.46
	CTP	-0.2	-0.001	-0.30	-0.36	-0.01

5. 4.1 Influence of surface temperature

The obtained results revealed high correlations of surface temperature with CF, COD, CWP, CTP and CER over Diamir and Skardu as shown in Table 5.1. The cloud parameters showed almost negative relationships with temperature, except CTT. The significant relationship between T_{max} and CF is due to the monthly CF anomalies. These anomalies occurred in winter due to the existence of a high pressure, dry and cold air. They eventually prevent the formation of smog (stratus cloud) and ensure the long sunny period in the Himalaya and Karakoram regions. Similarly, the observed inverse response of surface temperature to COD is due to the thinning of clouds with consequent effect of warming [161]. These relationships illustrate the dependency of cloudiness on large scale circulation, local cyclonic low pressure and wind speed with associated increase in winter CF [49]. The positive response with COD occur due to the increasing temperature rate [161]. This increasing rate will also decrease CER because the cloud

microphysical and radiative characteristic change indirectly via scattering and absorption processes [162].

The increase in the concentration of anthropogenic aerosol particles in the atmosphere are the sources of cloud condensation nuclei (CCN), due to which cloud albedo increases, and reducing the size of cloud droplets [127]. The effects of water vapor in the clouds have a very critical role in the formation of precipitation and the cloud life cycle. Genio and Wolf, [163] revealed an inverse relationship of CWP and temperature at mid latitudes. The relationship between CWP and temperature is affected by the energy exchange between surface and atmospheric boundary layer. The results indicated that CWP initially increases with temperature because of growth in the cloud thickness, which occur due to rise in surface moisture during melt season. Several studies have shown that CTP is inversely proportional to surface temperature and have negative correlation with each other. It means that for high temperature (5 °C), the CTP will be smaller (32 hPa) at high altitudes and vice versa. Kaufman *et al.* [164] investigated that surface temperature is one of the major weather parameters that affects the cloud optical properties.

5.4.2 Influence of relative humidity

Relative humidity was found in the same phase with CF, COD and CWP while out of phase with CER, CTP and at some places with CTT. High correlations between RH and CF indicates the presence of clouds at the given pressure level [165]. Relative humidity increases with rise in temperature, due to which the cloud base height and cloud lifting condensation level are decreased [166]. A negative and insignificant correlation was found between CTP and RH at Diamir and Skardu while positive in Gilgit. Devara and Raj, [167] found an increasing rate of growth of cloud droplet due to the variation in RH and temperature. The positive correlation between COD and RH depicts the high value of COD during denser conditions of RH as larger cloud particles have high

contact with water [58]. The correlation between RH and CER is very low and statistically insignificant for the overall period of study during summer, but in winter, a subtle correlation was observed. These correlations indicate that CER is larger during high RH condition (in winter) due to the high hygroscopic growth of aerosols [168]. Jones *et al.* [169] reported that the probability of the growth of existing cloud droplets and activation is directly proportional to the RH. According to Geoffroy *et al.* [170], CWP initially increases to attain the highest value in the droplet collection process and at the end CWP becomes exhausted. Further, CWP affects the earth's climate system through reflection, absorption and emission. The incoming solar radiations are reduced by CWP because of their high relative albedo, absorption of long wave radiation due to water vapor distribution and the effective cloud base height [171]. Similarly, CWP was also found in inverse relationship with wind speed indicate that the concentration of moisture decreases during high winds.

5.4.3 Influence of monthly total rain

Cloud optical properties except CTT and CTP directly influence the monthly total rain at Gilgit. Also, at this site, cloud droplets transform into raindrops. The positive response of MTR with COD illustrates that COD is not the primary reason for rainfall modification. The positive correlation between CER and MTR is due to the changes in the shape of the size distribution of cloud droplets. The reason of changes in the cloud droplet size distributions is possibly due to the different process of growth of cloud droplets in non-precipitating clouds and precipitating clouds [172]. Kobayashi *et al.* [130] reported that during poor rainfall, COD is directly proportional to the rain rate and vice versa. During rainfall, first the concentration of cloud droplet decreases at the time of transformation with quick growth of cloud droplet. The correlation between CER and MTR is positive and almost statistically significant during summer and winter at Diamir and Gilgit, while

at Skardu it was insignificant. A significant and opposite relationship was observed between CTP and MTR. The CTP variation due to cloud reflectivity affects the precipitation (rainfall) behavior through a mechanism described by Myhre *et al.* [173]. This is due to suppression of precipitation, consequently increase cloud lifetime and affect cloud albedo, which can affect the CTP [153, 174].

5.4.4 Influence of wind speed

As clear from the statistical results given in Table 5.2, the wind speed is in inverse relationship with all cloud parameters except CTT. Similarly, a negative and significant correlation between CTP and WS was observed at Diamir and Gilgit, however, at Skardu it was very low. Wind speed depends on the varying pattern of temperature or pressure, while both the temperature and pressure depend on varying CF [175]. Engström *et al.* [165] in their study observed subtle correlation of 0.22 between 10-meter wind speed and CF. WS and COD vary due to the pressure gradient and decreasing rate of temperature. These changes are also driven by the increasing anthropogenic aerosols emissions and precursor gases [176]. Elliott *et al.* [177] recorded for Southeast China the "disappearing wind syndrome" due to vegetation growth and new construction around the meteoroidal stations. Thus the increase in COD reduces the wind speed blow and vertical transport of horizontal momentum, due to stabilities of the air [176]. This reducing process also decreases evaporation and increases the lifetime of cloud. The WS has a negative response to CER, which indicated that the winds brining clean and drier air [178]. Tripathi *et al.* [179] analyzed the relationship between vertical winds and CTP in winter season and observed correlation coefficient (R) of 0.26.

Chapter 6

Conclusions and Future Recommendations

6.1. Conclusions

Atmospheric aerosols play a significant role in the energy balance of Earth-atmosphere system, because the change in the atmospheric aerosol load alter the energy budget of the Earth-atmosphere climate system, the cloud microphysics properties, hydrological cycle, and precipitation rate, directly as well as indirectly. Beside their environmental effects atmospheric aerosols also affected the human health, air quality, ecosystems and visibility. Aerosol helps the cloud formation, and similarly the earth radiative budget is strongly affected by clouds, due to high cloud albedo. Therefore, the study of Aerosol-Cloud Radiative Properties and its Impacts on Climate are the most important and challenging issue of the modern world, due to complex nature of aerosols and clouds, their spatio-temporal variation, and uncertainty in the climate. This thesis examines the five different sites having different climate and environmental condition including Karachi, Lahore for aerosols optical and radiative properties, during Dust Episodes (DE) and Haze Episodes (HE) between 2010 and 2014, and Diamer, Gilgit and Skardu for long-term perspective of cloud optical properties and radiative properties over Himalayan-Karakorum region for the period 2004-2016 using ground and satellite based data-set that cover the following major objectives:

i. To analyze the spatio-temporal and synoptic variability of aerosol and cloud concentration/amount.
ii. To characterize anthropogenic and mineral dust aerosols from aerosol optical properties.

iii. To investigate urban-industrial/mineral dust aerosols' warming or cooling effect at the Earth's surface, at the top of atmosphere and within the atmosphere.

iv. To investigate the effects of aerosols –cloud radiative properties in different regions of Pakistan.

We have achieved the aforementioned objectives successfully with the conclusion of whole thesis in the following noticeable findings in two sections.

6.1.1. Aerosols optical properties and radiative forcing

In the current study the optical and radiative properties of aerosol was carried out during different heavy pollution episodes over two megacities of Pakistan i.e. Karachi and Lahore. These heavy pollution episodes were classified as Dust Episodes (DE) and Haze Episodes (HE) through AOD and AE, which were further confirmed using MODIS fire activity images. The detection of DE was associated with low/high values of AE/AOD over Karachi and Lahore. The case with high AE and high AOD corresponds to HE over Lahore, while no HE was detected over Karachi. During DE, the coarse mode peaks were relatively more pronounced around a radius of 2.24 μm. During HE, the AVSD showed a prominent fine mode peak at a radius of 0.25 μm.

- During DE, the coarse mode peaks were relatively more pronounced around a radius of 2.24 μm. During HE, the size distribution was reported with a prominent fine mode peak at a radius of 0.25 μm.
- SSA abruptly increases with increasing wavelength for DE over Karachi and Lahore. Conversely, during HE, SSA decreases smoothly with increasing wavelength.
- Phase Function PF values were relatively higher at $\theta = 0°$ during the DE, with relatively lower values during HE. During all the episodes, the PF values were a maximum at a

scattering angle of 0°, with a decrease down to a minimum at angles of 131°. A uniform trend was observed at scattering angles>131°.

- For DE, ASY decreases with increasing wavelength at shorter wavelengths (visible region) and slightly increases at longer wavelengths (near-infrared region). For HE, an abrupt decrease in ASY with increasing wavelength was observed.
- RRI remains smooth from 440 to 870 nm and then drops at 1020 nm during DE at both studied sites. On the other hand, during HE over Lahore, the RRI increases with increasing wavelength.
- IRI was found to decrease with increasing wavelength during DE, whereas IRI decreases with wavelength at shorter wavelength, but at longer wavelength the variation was not so pronounced during HE.
- The relationship between AOD and AE revealed that dust aerosols were the dominant aerosol type during DE over Karachi and Lahore, whereas biomass burning activities and urban/industrial aerosols during HE were found vital over Lahore.
- During DE, the daily averaged ARFTOA, ARFBOA, and ARFATM were −15, −48, and 34 W/m2, respectively, with an associated atmospheric heating rate of 1.0 K/day over Karachi. Similarly, during DE over Lahore, the daily averaged values varied from −34, −93, and 58 W/m^2 at ARFTOA, ARFBOA, and ARFATM, respectively, having an atmospheric heating rate of 1.6 K/day. During HE over Lahore, the daily averaged ARF was−38 at ARFTOA, −88 at ARFBOA, and 51 W/m^2 in ARFATM, with a corresponding atmospheric heating rate of 1.4 K/day.

6.1.2. Cloud optical properties, radiative feedback, correlation between cloud optical properties and metrological parameters

Clouds have a major role in determining the energy of the atmospheric system. The role of meteorology in changing the clouds optical properties is one of the challenging problems in cloud physics and climate change. The assessment of spatio-temporal variations in cloud microphysical properties and the influence of radiation fluxes and meteorology is of great importance in the context of climate change. This study utilized collocated remote sensing satellite instruments at high altitudes of Diamir, Gilgit and Skardu in the HK region of northern of Pakistan. The key cloud properties (CF, COD, CWP, CER, CTT and CTP) were retrieved from MODIS. The TOA radiative fluxes and the ground meteorology data were obtained from CERES and PMD. In light of the above discussion, the major findings of the study are:

- Due to the complex topography of the study region, the contrasting variations in the cloud optical properties were observed.
- CF, COD and CWP were observed to be higher in winter months as compared to the summer months. This is due to variation in surface temperature and sunshine hours.
- The correlation between CER and CTP clearly demonstrated the Kelvin effect.
- The correlation between COD and CER is positive and negative for non-precipitating and precipitating clouds respectively. Cold clouds with CTT less than 273K were observed in all seasons over all study areas.
- Maximum values of CF, CER, CWP and COD has been recorded in winter season.
- The relationships between cloud parameters and TOA fluxes showed distinctive characteristics. A Positive correlation between COD and CTP against TOASWCRF illustrate that the cooling effect increases with the increase in COD and CTP at study sites.

Similarly, the increasing and decreasing trends in CWP and CER respectively, with TOASWCRF lead an enhanced reflection of solar radiation with consequent cooling effect.

- The meteorology influenced strongly the cloud properties. The T_{max}/T_{min} and WS are negatively correlated with almost all the cloud properties. However, the MTR and RH showed a contrasting correlation with cloud properties.

6.2. Recommendation for future work

The present study utilized AERONET and satellite observations to study the aerosol optical and radiative properties. Furthermore, cloud optical and radiative properties were analyzed using MODIS and CERES data sets. The following are the recommendations for future studies:

i. In order to study aerosol optical and radiative properties in more details, the ground data of BC and $PM_{2.5}$ will be used with satellite and AEROENT observations. This will reduce the uncertainties in the aerosol optical and the radiative properties, which will help in the accurate estimation of climatic impacts in the region.

ii. In this thesis, cloud optical and radiative analysis was carried out using MODIS, CERES and meteorological observations. The analysis can be further improved using CALIPSO and Sentinel satellites observation, and the Community Atmospheric Model (CAM5) products. This will reduce the uncertainties and possible errors of the derived quantities and will help in better estimation of aerosol-cloud interaction.

References

1. Habib, G., Venkataraman, C., Chiapello, I., Ramachandran, S., Boucher, O., & Reddy, M. S. (2006). Seasonal and interannual variability in absorbing aerosols over India derived from TOMS: Relationship to regional meteorology and emissions. *Atmospheric Environment*, *40*(11), 1909-1921.
2. Prospero, J. M., Ginoux, P., Torres, O., Nicholson, S. E., & Gill, T. E. (2002). Environmental characterization of global sources of atmospheric soil dust identified with the Nimbus 7 Total Ozone Mapping Spectrometer (TOMS) absorbing aerosol product. *Reviews of geophysics*, *40*(1), 2-1.
3. Charlson, R. J., Schwartz, S. E., Hales, J. M., Cess, R. D., Coakley, J. J., Hansen, J. E., & Hofmann, D. J. (1992). Climate forcing by anthropogenic aerosols. *Science*, *255*(5043), 423-430.
4. Gregory, J., Stouffer, R. J., Molina, M., Chidthaisong, A., Solomon, S., Raga, G., ... & Lohmann, U. (2007). Climate change 2007: the physical science basis.
5. Nemmar, A., Hoet, P. H., Dinsdale, D., Vermylen, J., Hoylaerts, M. F., & Nemery, B. (2003). Diesel exhaust particles in lung acutely enhance experimental peripheral thrombosis. *Circulation*, *107*(8), 1202-1208.
6. Jonathan, A. (2003). Vegetation Climate Interaction: How Vegetation Makes the Global Environment.
7. Kaufman, Y. J., Tanré, D., Remer, L. A., Vermote, E. F., Chu, A., & Holben, B. N. (1997). Operational remote sensing of tropospheric aerosol over land from EOS moderate resolution imaging spectroradiometer. *Journal of Geophysical Research: Atmospheres*, *102*(D14), 17051-17067.
8. Pelletier, B., Santer, R., & Vidot, J. (2007). Retrieving of particulate matter from optical measurements: a semiparametric approach. *Journal of Geophysical Research: Atmospheres*, *112*(D6).
9. Jaenicke, R. (1993). Tropospheric aerosols. *Aerosol-cloud-climate interactions*, *1*.
10. Pöschl, U. (2005). Atmospheric aerosols: composition, transformation, climate and health effects. *Angewandte Chemie International Edition*, *44*(46), 7520-7540.

11. Higurashi, A., & Nakajima, T. (2002). Detection of aerosol types over the East China Sea near Japan from four-channel satellite data. *Geophysical research letters, 29*(17), 17-1.

12. Pathak, B., Bhuyan, P. K., Gogoi, M., & Bhuyan, K. (2012). Seasonal heterogeneity in aerosol types over Dibrugarh-North-Eastern India. *Atmospheric environment, 47*, 307-315.

13. Seinfeld, J. H., & Pandis, S. N. (2016). *Atmospheric chemistry and physics: from air pollution to climate change*. John Wiley & Sons.

14. Baker, M. B. (1997). Cloud microphysics and climate. *Science, 276*(5315), 1072-1078.

15. Baker, M. B., & Peter, T. (2008). Small-scale cloud processes and climate. *Nature, 451*(7176), 299-300.

16. Dubovik, O., Holben, B., Eck, T. F., Smirnov, A., Kaufman, Y. J., King, M. D., ... & Slutsker, I. (2002). Variability of absorption and optical properties of key aerosol types observed in worldwide locations. *Journal of the atmospheric sciences, 59*(3), 590-608.

17. Toledano, C., Cachorro, V. E., Berjon, A., De Frutos, A. M., Sorribas, M., De la Morena, B. A., & Goloub, P. (2007). Aerosol optical depth and Ångström exponent climatology at El Arenosillo AERONET site (Huelva, Spain). *Quarterly Journal of the Royal Meteorological Society: A journal of the atmospheric sciences, applied meteorology and physical oceanography, 133*(624), 795-807.

18. Dey, S., Tripathi, S. N., Singh, R. P., & Holben, B. N. (2004). Influence of dust storms on the aerosol optical properties over the Indo-Gangetic basin. *Journal of Geophysical Research: Atmospheres, 109*(D20).

19. Eck, T. F., Holben, B. N., Sinyuk, A., Pinker, R. T., Goloub, P., Chen, H., ... & Reid, J. S. (2010). Climatological aspects of the optical properties of fine/coarse mode aerosol mixtures. *Journal of Geophysical Research: Atmospheres, 115*(D19).

20. Alam, K., Trautmann, T., & Blaschke, T. (2011). Aerosol optical properties and radiative forcing over mega-city Karachi. *Atmospheric Research, 101*(3), 773-782.

21. Gautam, R., Hsu, N. C., Tsay, S. C., Lau, K. M., Holben, B., Bell, S., ... & Payra, S. (2011). Accumulation of aerosols over the Indo-Gangetic plains and southern slopes

of the Himalayas: distribution, properties and radiative effects during the 2009 pre-monsoon season. *Atmospheric Chemistry and Physics*, *11*(24), 12841.

22. Dumka, U. C., N. Tripathi, S., Misra, A., Giles, D. M., Eck, T. F., Sagar, R., & Holben, B. N. (2014). Latitudinal variation of aerosol properties from Indo-Gangetic plain to central Himalayan foothills during TIGERZ campaign. *Journal of Geophysical Research: Atmospheres*, *119*(8), 4750-4769.

23. Alam, K., Trautmann, T., Blaschke, T., & Majid, H. (2012). Aerosol optical and radiative properties during summer and winter seasons over Lahore and Karachi. *Atmospheric Environment*, *50*, 234-245.

24. Adesina, A. J., Kumar, K. R., & Sivakumar, V. (2015). Variability in aerosol optical properties and radiative forcing over Gorongosa (18.97 o S, 34.35 o E) in Mozambique. *Meteorology and Atmospheric Physics*, *127*(2), 217-228.

25. Alam, K., Trautmann, T., Blaschke, T., & Subhan, F. (2014). Changes in aerosol optical properties due to dust storms in the Middle East and Southwest Asia. *Remote sensing of environment*, *143*, 216-227.

26. Yu, X., Lü, R., Kumar, K. R., Ma, J., Zhang, Q., Jiang, Y., ... & Li, M. (2016). Dust aerosol properties and radiative forcing observed in spring during 2001–2014 over urban Beijing, China. *Environmental Science and Pollution Research*, *23*(15), 15432-15442.

27. Michael, M., Yadav, A., Tripathi, S. N., Kanawade, V. P., Gaur, A., Sadavarte, P., & Venkataraman, C. (2014). Simulation of trace gases and aerosols over the Indian domain: evaluation of the WRF-Chem model. *Geoscientific Model Development Discussions*, *7*(1), 431-482.

28. Kaufman, Y. J., Tanré, D., & Boucher, O. (2002). A satellite view of aerosols in the climate system. *Nature*, *419*(6903), 215-223.

29. Solomon, S., Manning, M., Marquis, M., & Qin, D. (2007). *Climate change 2007-the physical science basis: Working group I contribution to the fourth assessment report of the IPCC* (Vol. 4). Cambridge university press.

30. Ramana, M. V., Ramanathan, V., Podgorny, I. A., Pradhan, B. B., & Shrestha, B. (2004). The direct observations of large aerosol radiative forcing in the Himalayan region. *Geophysical Research Letters*, *31*(5).

31. Gadhavi, H., & Jayaraman, A. (2004). Aerosol characteristics and aerosol radiative forcing over Maitri, Antarctica. *CURRENT SCIENCE-BANGALORE-*, *86*(2), 296-304.

32. Takemura, T., Nakajima, T., Dubovik, O., Holben, B. N., & Kinne, S. (2002). Single-scattering albedo and radiative forcing of various aerosol species with a global three-dimensional model. *Journal of Climate*, *15*(4), 333-352.

33. Dey, S., & Tripathi, S. N. (2008). Aerosol direct radiative effects over Kanpur in the Indo-Gangetic basin, northern India: Long-term (2001–2005) observations and implications to regional climate. *Journal of Geophysical Research: Atmospheres*, *113*(D4).

34. Pandithurai, G., Dipu, S., Dani, K. K., Tiwari, S., Bisht, D., Devara, P., & Pinker, R. T. (2008). Aerosol radiative forcing during dust events over New Delhi, India. *Journal of Geophysical Research: Atmospheres*, *113*(D13).

35. Li, Z., Lee, K. H., Wang, Y., Xin, J., & Hao, W. M. (2010). First observation-based estimates of cloud-free aerosol radiative forcing across China. *Journal of Geophysical Research: Atmospheres*, *115*(D7).

36. Singh, S., Soni, K., Bano, T., Tanwar, R. S., Nath, S., & Arya, B. C. (2010). Clear-sky direct aerosol radiative forcing variations over mega-city Delhi. In *Annales Geophysicae* (Vol. 28, No. 5, pp. 1157-1166). European Geosciences Union.

37. Kedia, S., Ramachandran, S., Kumar, A., & Sarin, M. M. (2010). Spatiotemporal gradients in aerosol radiative forcing and heating rate over Bay of Bengal and Arabian Sea derived on the basis of optical, physical, and chemical properties. *Journal of Geophysical Research: Atmospheres*, *115*(D7).

38. Kumar, S., & Devara, P. C. S. (2012). A long-term study of aerosol modulation of atmospheric and surface solar heating over Pune, India. *Tellus B: Chemical and Physical Meteorology*, *64*(1), 18420.

39. Valenzuela, A., Olmo, F. J., Lyamani, H., Antón, M., Quirantes, A., & Alados-Arboledas, L. (2012). Aerosol radiative forcing during African desert dust events (2005–2010) over Southeastern Spain. *Atmos. Chem. Phys*, *12*(21), 10331-10351.

40. Srivastava, R., & Ramachandran, S. (2013). The mixing state of aerosols over the Indo-Gangetic Plain and its impact on radiative forcing. *Quarterly Journal of the Royal Meteorological Society, 139*(670), 137-151.

41. Esteve, A. R., Estellés, V., Utrillas, M. P., & Martínez-Lozano, J. A. (2014). Analysis of the aerosol radiative forcing over a Mediterranean urban coastal site. *Atmospheric research, 137*, 195-204.

42. Taneja, K., Soni, V. K., Attri, S. D., Peshin, S. K., Mor, V., & Sateesh, M. (2014). Seasonal asymmetry of aerosol optical and radiative properties over New Delhi, India using ground-based observations. *Glob. Sustain. Transit. Impacts Innov.*, 124-130.

43. Bhaskar, V. V., Safai, P. D., & Raju, M. P. (2015). Long term characterization of aerosol optical properties: Implications for radiative forcing over the desert region of Jodhpur, India. *Atmospheric Environment, 114*, 66-74.

44. Patel, P. N., & Kumar, R. (2015). Estimation of aerosol characteristics and radiative forcing during dust events over Dehradun. *Aerosol Air Qual. Res, 15*(5), 2082-2093.

45. Kalluri, R. O. R., Gugamsetty, B., Kotalo, R. G., Nagireddy, S. K. R., Tandule, C. R., Thotli, L. R., ... & Surendranair, S. B. (2016). Direct radiative forcing properties of atmospheric aerosols over semi-arid region, Anantapur in India. *Science of the Total Environment, 566*, 1002-1013.

46. Singh, A., Tiwari, S., Sharma, D., Singh, D., Tiwari, S., Srivastava, A. K., ... & Singh, A. K. (2016). Characterization and radiative impact of dust aerosols over northwestern part of India: a case study during a severe dust storm. *Meteorology and Atmospheric Physics, 128*(6), 779-792.

47. Cess, R. D., Potter, G. L., Blanchet, J. P., Boer, G. J., Ghan, S. J., Kiehl, J. T., ... & Morcrette, J. J. (1989). Interpretation of cloud-climate feedback as produced by 14 atmospheric general circulation models. *Science, 245*(4917), 513-516.

48. Van Weverberg, K., Vogelmann, A., Lin, W., Luke, E., Cialella, A., Minnis, P., ... & Jensen, M. P. (2013). The role of cloud microphysics parameterization in the simulation of mesoscale convective system clouds and precipitation in the tropical western Pacific. *Journal of the Atmospheric Sciences, 70*(4), 1104-1128.

49. Cossu, F., Hocke, K., & Mätzler, C. (2015). A 10-year cloud fraction climatology of liquid water clouds over Bern observed by a ground-based microwave radiometer. *Remote sensing*, *7*(6), 7768-7784.

50. Dong, X., Xi, B., Crosby, K., Long, C. N., Stone, R. S., & Shupe, M. D. (2010). A 10 year climatology of Arctic cloud fraction and radiative forcing at Barrow, Alaska. *Journal of Geophysical Research: Atmospheres*, *115*(D17).

51. Seiz, G., Foppa, N., Meier, M., & Paul, F. (2011). The role of satellite data within GCOS Switzerland. *Remote Sensing*, *3*(4), 767-780.

52. Yin, B., & Min, Q. (2014). Climatology of aerosol and cloud optical properties at the Atmospheric Radiation Measurements Climate Research Facility Barrow and Atqasuk sites. *Journal of Geophysical Research: Atmospheres*, *119*(4), 1820-1834.

53. Barrett, E. C., & Martin, D. W. (1981). *Use of satellite data in rainfall monitoring*. Academic press.

54. Bennartz, R., & Rausch, J., (2017). Global and regional estimates of warm cloud droplet number concentration based on 13 years of AQUA-MODIS observations. *Atmospheric Chemistry and Physics*, *17*(16), 9815.

55. Kawamoto, K., & Suzuki, K., (2013, May). Difference in fractional occurrences of precipitation categories in terms of cloud properties. In *AIP Conference Proceedings* (Vol. 1531, No. 1, pp. 424-427). American Institute of Physics.

56. Lin, B., Minnis, P., & Fan, A., (2003). Cloud liquid water path variations with temperature observed during the Surface Heat Budget of the Arctic Ocean (SHEBA) experiment. *Journal of Geophysical Research: Atmospheres*, *108*(D14).

57. Niu, F., & Li, Z. (2012). Systematic variations of cloud top temperature and precipitation rate with aerosols over the global tropics. *Atmospheric Chemistry & Physics*, *12*(18).

58. Liu, Y., De Leeuw, G., Kerminen, V. M., Zhang, J., Zhou, P., Nie, W,. ... & Guo, H. (2017). Analysis of aerosol effects on warm clouds over the Yangtze River Delta from multi-sensor satellite observations. *Atmospheric Chemistry and Physics*, *17*(9), 5623.

59. Patil, N., Dave, P., & Venkataraman, C., (2017). Contrasting influences of aerosols on cloud properties during deficient and abundant monsoon years. *Scientific reports*, *7*, 44996.

60. Liou, K. N., & Wittman, G. D. (1979). Parameterization of the radiative properties of clouds. *Journal of the Atmospheric Sciences*, *36*(7), 1261-1273.

61. Ramanathan, V. L. R. D., Cess, R. D., Harrison, E. F., Minnis, P., Barkstrom, B. R., Ahmad, E., & Hartmann, D. (1989). Cloud-radiative forcing and climate: Results from the Earth Radiation Budget Experiment. *Science*, *243*(4887), 57-63.

62. Rucong, Y., Yongqiang, Y., & Minghua, Z. (2001). Comparing cloud radiative properties between the eastern China and the Indian monsoon region. *Advances in Atmospheric Sciences*, *18*(6), 1090-1102.

63. Machado, L. A. T., & Rossow, W. B. (1993). Structural characteristics and radiative properties of tropical cloud clusters. *Monthly Weather Review*, *121*(12), 3234-3260.

64. Li, J., Mlawer, E., & Chýlek, P. (2011). Parameterization of cloud optical properties for semidirect radiative forcing. *Journal of Geophysical Research: Atmospheres*, *116*(D23).

65. Xi, B., Dong, X., Crosby, K., Long, C. N., Stone, R. S., & Shupe, M. D. (2010, May). A 10-yr Climatology of Arctic Cloud Fraction and Radiative Forcing at Barrow, Alaska. In *EGU General Assembly Conference Abstracts* (Vol. 12, p. 2954).

66. Akbar, M., Ahmed, M., Hussain, A., Zafar, M. U., & Khan, M. (2011). Quantitative forests description from Skardu, Gilgit and Astore Districts of Gilgit-Baltistan, Pakistan. *FUUAST Journal of Biology*, *1*(2 December), 149-160.

67. Holben, B. N., Eck, T. F., Slutsker, I. A., Tanre, D., Buis, J. P., Setzer, A., ... & Lavenu, F. (1998). AERONET—A federated instrument network and data archive for aerosol characterization. *Remote sensing of environment*, *66*(1), 1-16.

68. Dubovik, O., & King, M. D. (2000). A flexible inversion algorithm for retrieval of aerosol optical properties from Sun and sky radiance measurements. *Journal of Geophysical Research: Atmospheres*, *105*(D16), 20673-20696.

69. Smirnov, A., Holben, B. N., Dubovik, O., O'Neill, N. T., Eck, T. F., Westphal, D. L., ... & Slutsker, I. (2002). Atmospheric aerosol optical properties in the Persian Gulf. *Journal of the atmospheric sciences*, *59*(3), 620-634.

70. Remer, L. A., Tanré, D., Kaufman, Y. J., Levy, R., & Mattoo, S. (2006). Algorithm for remote sensing of tropospheric aerosol from MODIS: Collection 005. *National Aeronautics and Space Administration, 1490.*

71. Levy, R. C., Remer, L. A., & Dubovik, O. (2007). Global aerosol optical properties and application to Moderate Resolution Imaging Spectroradiometer aerosol retrieval over land. *Journal of Geophysical Research: Atmospheres, 112*(D13).

72. Kiran, V. R., Rajeevan, M., Gadhavi, H., Rao, S. V. B., & Jayaraman, A. (2015). Role of vertical structure of cloud microphysical properties on cloud radiative forcing over the Asian monsoon region. *Climate dynamics, 45*(11-12), 3331-3345.

73. Draxler, R. R. (2011). Hysplit (hybrid single-particle lagrangian integrated trajectory) model access via NOAA ARL ready website. *http://ready. arl. noaa. gov/HYSPLIT. php.*

74. Kaufman, Y. J., Tanré, D., Remer, L. A., Vermote, E. F., Chu, A., & Holben, B. N. (1997). Operational remote sensing of tropospheric aerosol over land from EOS moderate resolution imaging spectroradiometer. *Journal of Geophysical Research: Atmospheres, 102*(D14), 17051-17067.

75. Ångström, A. (1964). The parameters of atmospheric turbidity. *Tellus, 16*(1), 64-75.

76. Andrews, E., Sheridan, P. J., Fiebig, M., McComiskey, A., Ogren, J. A., Arnott, P., ... & Jonsson, H. (2006). Comparison of methods for deriving aerosol asymmetry parameter. *Journal of Geophysical Research: Atmospheres, 111*(D5).

77. Bohren, C. F., & Singham, S. B. (1991). Backscattering by nonspherical particles: A review of methods and suggested new approaches. *Journal of Geophysical Research: Atmospheres, 96*(D3), 5269-5277.

78. Prasad, A. K., Singh, S., Chauhan, S. S., Srivastava, M. K., Singh, R. P., & Singh, R. (2007). Aerosol radiative forcing over the Indo-Gangetic plains during major dust storms. *Atmospheric Environment, 41*(29), 6289-6301.

79. Sinyuk, A., Torres, O., & Dubovik, O. (2003). Combined use of satellite and surface observations to infer the imaginary part of refractive index of Saharan dust. *Geophysical Research Letters, 30*(2).

80. Zeng, S., Cornet, C., Parol, F., Riedi, J., & Thieuleux, F. (2012). A better understanding of cloud optical thickness derived from the passive sensors

MODIS/AQUA and POLDER/PARASOL in the A-Train constellation. *Atmospheric Chemistry and Physics*, *12*(23), 11245-11259.

81. Hansen, J. E., & Travis, L. D. (1974). Light scattering in planetary atmospheres. *Space science reviews*, *16*(4), 527-610.

82. Horváth, Á., Seethala, C., & Deneke, H. (2014). View angle dependence of MODIS liquid water path retrievals in warm oceanic clouds. *Journal of Geophysical Research: Atmospheres*, *119*(13), 8304-8328.

83. Miller, S. W., Arkin, P. A., & Joyce, R. (2001). A combined microwave/infrared rain rate algorithm. *International Journal of Remote Sensing*, *22*(17), 3285-3307.

84. Koelemeijer, R., B., A., Stammes, P., Hovenier, J. W., & De Haan, J. F. (2002). Global distributions of effective cloud fraction and cloud top pressure derived from oxygen A band spectra measured by the Global Ozone Monitoring Experiment: Comparison to ISCCP data. *Journal of Geophysical Research: Atmospheres*, *107*(D12), AAC-5.

85. Ricchiazzi, P., Yang, S., Gautier, C., & Sowle, D. (1998). SBDART: A research and teaching software tool for plane-parallel radiative transfer in the Earth's atmosphere. *Bulletin of the American Meteorological Society*, *79*(10), 2101-2114.

86. Stamnes, K., Tsay, S. C., Wiscombe, W., & Jayaweera, K. (1988). Numerically stable algorithm for discrete-ordinate-method radiative transfer in multiple scattering and emitting layered media. *Applied optics*, *27*(12), 2502-2509.

87. Eck, T., F., Holben, B. N., Reid, J. S., Dubovik, O., Smirnov, A., O'neill, N. T., ... & Kinne, S. (1999). Wavelength dependence of the optical depth of biomass burning, urban, and desert dust aerosols. *Journal of Geophysical Research: Atmospheres*, *104*(D24), 31333-31349.

88. Holben, B., N., Tanre, D., Smirnov, A., Eck, T. F., Slutsker, I., Abuhassan, N., ... & Kaufman, Y. J. (2001). An emerging ground-based aerosol climatology: Aerosol optical depth from AERONET. *Journal of Geophysical Research: Atmospheres*, *106*(D11), 12067-12097.

89. Tariq, S., & Ali, M. (2016). Satellite and ground-based remote sensing of aerosols during intense haze event of October 2013 over Lahore, Pakistan. *Asia-Pacific Journal of Atmospheric Sciences*, *52*(1), 25-33.

90. Bibi, H., Alam, K., Blaschke, T., Bibi, S., & Iqbal, M. J. (2016). Long-term (2007–2013) analysis of aerosol optical properties over four locations in the Indo-Gangetic plains. *Applied optics*, *55*(23), 6199-6211.

91. Pérez, C., Nickovic, S., Baldasano, J. M., Sicard, M., Rocadenbosch, F., & Cachorro, V. E. (2006). A long Saharan dust event over the western Mediterranean: Lidar, Sun photometer observations, and regional dust modeling. *Journal of Geophysical Research: Atmospheres*, *111*(D15).

92. Dey, S., Tripathi, S. N., Singh, R. P., & Holben, B. N. (2004). Influence of dust storms on the aerosol optical properties over the Indo-Gangetic basin. *Journal of Geophysical Research: Atmospheres*, *109*(D20).

93. Srivastava, A. K., Soni, V. K., Singh, S., Kanawade, V. P., Singh, N., Tiwari, S., & Attri, S. D. (2014). An early South Asian dust storm during March 2012 and its impacts on Indian Himalayan foothills: A case study. *Science of the total environment*, *493*, 526-534.

94. Che, H., Xia, X., Zhu, J., Wang, H., Wang, Y., Sun, J., ... & Shi, G. (2015). Aerosol optical properties under the condition of heavy haze over an urban site of Beijing, China. *Environmental Science and Pollution Research*, *22*(2), 1043-1053.

95. Yu, X., Kumar, K. R., Lü, R., & Ma, J. (2016). Changes in column aerosol optical properties during extreme haze-fog episodes in January 2013 over urban Beijing. *Environmental Pollution*, *210*, 217-226.

96. Eck, T. F., Holben, B. N., Ward, D. E., Dubovik, O., Reid, J. S., Smirnov, A., ... & Slutsker, I. (2001). Characterization of the optical properties of biomass burning aerosols in Zambia during the 1997 ZIBBEE field campaign. *Journal of Geophysical Research: Atmospheres*, *106*(D4), 3425-3448.

97. Tan, J. H., Duan, J. C., Chen, D. H., Wang, X. H., Guo, S. J., Bi, X. H., ... & Fu, J. M. (2009). Chemical characteristics of haze during summer and winter in Guangzhou. *Atmospheric Research*, *94*(2), 238-245.

98. Li, Z. Q., Gu, X., Wang, L., Li, D., Li, K., Dubovik, O., ... & Xie, Y. (2013). Aerosol physical and chemical properties retrieved from ground-based remote sensing measurements during heavy haze days in Beijing winter. *Atmospheric Chemistry & Physics Discussions*, *13*(2).

99. Bergstrom, R. W., Pilewskie, P., Russell, P. B., Redemann, J., Bond, T. C., Quinn, P. K., & Sierau, B. (2007). Spectral absorption properties of atmospheric aerosols.

100. Kumar, K. R., Yin, Y., Sivakumar, V., Kang, N., Yu, X., Diao, Y., ... & Reddy, R. R. (2015). Aerosol climatology and discrimination of aerosol types retrieved from MODIS, MISR and OMI over Durban (29.88 S, 31.02 E), South Africa. *Atmospheric Environment, 117*, 9-18.

101. Bibi, H., Alam, K., & Bibi, S. (2016). In-depth discrimination of aerosol types using multiple clustering techniques over four locations in Indo-Gangetic plains. *Atmospheric Research, 181*, 106-114.

102. Bi, J., Huang, J., Hu, Z., Holben, B. N., & Guo, Z. (2014). Investigating the aerosol optical and radiative characteristics of heavy haze episodes in Beijing during January of 2013. *Journal of Geophysical Research: Atmospheres, 119*(16), 9884-9900.

103. Bi, J., Huang, J., Fu, Q., Wang, X., Shi, J., Zhang, W., ... & Zhang, B. (2011). Toward characterization of the aerosol optical properties over Loess Plateau of Northwestern China. *Journal of Quantitative Spectroscopy and Radiative Transfer, 112*(2), 346-360.

104. Koepke, P., Gasteiger, J., & Hess, M. (2015). Optical properties of desert aerosol with non-spherical mineral particles: data incorporated to OPAC. *Atmospheric Chemistry and Physics, 15*(10), 5947-5956.

105. Cattrall, C., Carder, K. L., & Gordon, H. R. (2003). Columnar aerosol single-scattering albedo and phase function retrieved from sky radiance over the ocean: Measurements of Saharan dust. *Journal of Geophysical Research: Atmospheres, 108*(D9).

106. Andrews, E., Sheridan, P. J., Fiebig, M., McComiskey, A., Ogren, J. A., Arnott, P., ... & Jonsson, H. (2006). Comparison of methods for deriving aerosol asymmetry parameter. *Journal of Geophysical Research: Atmospheres, 111*(D5).

107. Singh, R., P., Dey, S., Tripathi, S., N., Tare, V., & Holben, B., (2004). Variability of aerosol parameters over Kanpur, northern India. *Journal of Geophysical Research: Atmospheres, 109*(D23).

108. Giles, D. M., Holben, B. N., Tripathi, S. N., Eck, T. F., Newcomb, W. W., Slutsker, I., ... & Singh, R. P. (2011). Aerosol properties over the Indo-Gangetic Plain: A

mesoscale perspective from the TIGERZ experiment. *Journal of Geophysical Research: Atmospheres, 116*(D18).

109. Sorooshian, A., Wang, Z., Feingold, G., & L'Ecuyer, T. S. (2013). A satellite perspective on cloud water to rain water conversion rates and relationships with environmental conditions. *Journal of Geophysical Research: Atmospheres, 118*(12), 6643-6650.

110. Kumar, S., Kumar, S., Kaskaoutis, D., G., Singh, R., P., Singh, R., K., Mishra, A., K., ... & Singh, A., K., (2015). Meteorological, atmospheric and climatic perturbations during major dust storms over Indo-Gangetic Basin. *Aeolian Research, 17*, 15-31.

111. Bibi, S., Alam, K., Chishtie, F., & Bibi, H., (2017). Characterization of absorbing aerosol types using ground and satellites based observations over an urban environment. *Atmospheric Environment, 150*, 126-135.

112. Sharma, D., Singh, D., & Kaskaoutis, D., G. (2012). Impact of two intense dust storms on aerosol characteristics and radiative forcing over Patiala, northwestern India. *Advances in Meteorology, 2012*.

113. Sharma, M., Kaskaoutis, D., G., Singh, R. P., & Singh, S., (2013). Seasonal variability of atmospheric aerosol parameters over Greater Noida using ground sunphotometer observations. *Aerosol and air quality research, 14*(3), 608-622.

114. Singh, P., Vaishya, A., Rastogi, S., & Babu, S., S., (2020). Seasonal heterogeneity in aerosol optical properties over the subtropical humid region of northern India. *Journal of Atmospheric and Solar-Terrestrial Physics*, 105246.

115. Sharma, M., Kaskaoutis, D., G., Singh, R., P., & Singh, S., (2013). Seasonal variability of atmospheric aerosol parameters over Greater Noida using ground sunphotometer observations. *Aerosol and air quality research, 14*(3), 608-622.

116. Toledano, C., Cachorro, V., E., De Frutos, A., M., Torres, B., Berjon, A., Sorribas, M., & Stone, R., S., (2009). Airmass classification and analysis of aerosol types at El Arenosillo (Spain). *Journal of Applied Meteorology and Climatology, 48*(5), 962-981.

117. Kumar, S., Kumar, S., Kaskaoutis, D. G., Singh, R. P., Singh, R. K., Mishra, A. K., ... & Singh, A. K. (2015). Meteorological, atmospheric and climatic perturbations during major dust storms over Indo-Gangetic Basin. *Aeolian Research*, *17*, 15-31.

118. Patel, P., N., & Kumar, R., (2015). Estimation of aerosol characteristics and radiative forcing during dust events over Dehradun. *Aerosol Air Qual. Res*, *15*(5), 2082-2093.

119. Chinnam, N., Dey, S., Tripathi, S., N., & Sharma, M., (2006). Dust events in Kanpur, northern India: Chemical evidence for source and implications to radiative forcing. *Geophysical Research Letters*, *33*(8).

120. Srivastava, A., K., Soni, V., K., Singh, S., Kanawade, V., P., Singh, N., Tiwari, S., & Attri, S., D., (2014). An early South Asian dust storm during March 2012 and its impacts on Indian Himalayan foothills: A case study. *Science of the total environment*, *493*, 526-534.

121. Jose, S., Gharai, B., Kumar, Y., B., & Rao, P., V., N., (2015). Radiative implication of a haze event over Eastern India. *Atmospheric Pollution Research*, *6*(1), 138-146.

122. Alam, K., Qureshi, S., & Blaschke, T., (2011). Monitoring spatio-temporal aerosol patterns over Pakistan based on MODIS, TOMS and MISR satellite data and a HYSPLIT model. *Atmospheric environment*, *45*(27), 4641-4651.

123. Alam, K., Trautmann, T., & Blaschke, T., (2011). Aerosol optical properties and radiative forcing over mega-city Karachi. *Atmospheric Research*, *101*(3), 773-782.

124. Yeo, H., Park, S., J., Kim, B., M., Shiobara, M., Kim, S., W., Kwon, H., ... & Choi, T., (2018). The observed relationship of cloud to surface longwave radiation and air temperature at Ny-Ålesund, Svalbard. *Tellus B: Chemical and Physical Meteorology*, *70*(1), 1-10.

125. Tao, W., K., Chen, J., P., Li, Z., Wang, C., & Zhang, C., (2012). Impact of aerosols on convective clouds and precipitation. *Reviews of Geophysics*, *50*(2).

126. Oreopoulos, L., Cho, N., & Lee, D., (2017). Using MODIS cloud regimes to sort diagnostic signals of aerosol-cloud-precipitation interactions. *Journal of Geophysical Research: Atmospheres*, *122*(10), 5416-5440.

127. Twomey, S., (1977). The influence of pollution on the shortwave albedo of clouds. *Journal of the atmospheric sciences*, *34*(7), 1149-1152.

128. Rosenfeld, D., Lohmann, U., Raga, G., B., O'Dowd, C., D., Kulmala, M., Fuzzi, S., ... & Andreae, M., O., (2008). Flood or drought: how do aerosols affect precipitation?. *science*, *321*(5894), 1309-1313.

129. Kay, J., E., L'Ecuyer, T., Gettelman, A., Stephens, G., & O'Dell, C., (2008). The contribution of cloud and radiation anomalies to the 2007 Arctic sea ice extent minimum. *Geophysical Research Letters*, *35*(8).

130. Kobayashi, T., & Masuda, K., (2009). Changes in cloud optical thickness and cloud drop size associated with precipitation measured with TRMM satellite. *Journal of the Meteorological Society of Japan. Ser. II*, *87*(4), 593-600.

131. Hong, Y., & Liu, G., (2015). The characteristics of ice cloud properties derived from CloudSat and CALIPSO measurements. *Journal of Climate*, *28*(9), 3880-3901.

132. Boers, R., & Rotstayn, L., D., (2001). Possible links between cloud optical depth and effective radius in remote sensing observations. *Quarterly Journal of the Royal Meteorological Society*, *127*(577), 2367-2383.

133. Jin, M., Shepherd, J., M., & King, M., D., (2005). Urban aerosols and their variations with clouds and rainfall: A case study for New York and Houston. *Journal of Geophysical Research: Atmospheres*, *110*(D10).

134. Jia, H., Ma, X., Quaas, J., Yin, Y., & Qiu, T., (2019). Is Positive Correlation between Cloud Droplet Effective Radius and Aerosol Index over Land Due to Retrieval Artifacts or Real Physical Processes. *Atmos. Chem. Phys. Discuss., https://doi. org/10.5194/acp-2019-47, in review*, *475*.

135. Albrecht, B., A., (1989). Aerosols, cloud microphysics, and fractional cloudiness. *Science*, *245*(4923), 1227-1230.

136. Han, Q., Rossow, W., B., Zeng, J., & Welch, R., (2002). Three different behaviors of liquid water path of water clouds in aerosol–cloud interactions. *Journal of the atmospheric sciences*, *59*(3), 726-735.

137. Bodas-Salcedo, A., Andrews, T., Karmalkar, A., V., & Ringer, M., A., (2016). Cloud liquid water path and radiative feedbacks over the Southern Ocean. *Geophysical Research Letters*, *43*(20), 10-938.

138. Taylor, S., Stier, P., White, B., Finkensieper, S., & Stengel, M., (2017). Evaluating the diurnal cycle in cloud top temperature from SEVIRI. *Atmospheric Chemistry and Physics*, *17*(11).

139. Punay, J., P., & Perez, G., J., P., (2014). Evaluation of modis cloud product-derived rainfall estimates. *Asian As Remote Sens Proc*, *3*, 1-5.

140. Hanna, J., W., Schultz, D., M., & Irving, A., R., (2008). Cloud-top temperatures for precipitating winter clouds. *Journal of applied meteorology and climatology*, *47*(1), 351-359.

141. Liu, Q., Fu, Y., Yu, R., Sun, L., & Lu, N., (2008). A new satellite-based census of precipitating and nonprecipitating clouds over the tropics and subtropics. *Geophysical research letters*, *35*(7).

142. Gurney, R., J., Foster, J., L., Foster, J. L., Parkinson, C., L., & Gurney, R., J., (1993). *Atlas of satellite observations related to global change*. Cambridge University Press.

143. Bharti, V., I., D., H., I., (2015). *Investigation of extreme rainfall events over the northwest Himalaya Region using satellite data*. Enschede: University of Twente Faculty of Geo-Information and Earth Observation (ITC).

144. Li, S., Joseph, E., Min, Q., & Yin, B., (2014). Long-term observation of aerosol–cloud relationships in the Mid-Atlantic of the United States. *Atmospheric Chemistry and Physics Discussions*, *14*(13), 18943-18960.

145. Qian, Y., Long, C., N., Wang, H., Comstock, J., M., McFarlane, S., A., & Xie, S., (2012). Evaluation of cloud fraction and its radiative effect simulated by IPCC AR4 global models against ARM surface observations. *Atmospheric Chemistry and Physics*, *12*(4), 1785.

146. Ceppi, P., Brient, F., Zelinka, M., D., & Hartmann, D., L., (2017). Cloud feedback mechanisms and their representation in global climate models. *Wiley Interdisciplinary Reviews: Climate Change*, *8*(4), e465.

147. Painemal, D., Minnis, P., & Sun-Mack, S., (2013). The impact of horizontal heterogeneities, cloud fraction, and liquid water path on warm cloud effective radii from CERES-like Aqua MODIS retrievals. *Atmospheric Chemistry & Physics*, *13*(19).

148. Michibata, T., Kawamoto, K., & Takemura, T., (2014). The effects of aerosols on water cloud microphysics and macrophysics based on satellite-retrieved data over East Asia and the North Pacific. *Atmos. Chem. Phys, 14*, 11935-11948.

149. Chakraborty, S., & Maitra, A., (2013). Interrelation between microphysical and optical properties of cloud and rainfall in the Indian region. *92.60. jf; 92.60. nc.*

150. Liu, G., Shao, H., Coakley Jr, J., A., Curry, J., A., Haggerty, J., A., & Tschudi, M., A., (2003). Retrieval of cloud droplet size from visible and microwave radiometric measurements during INDOEX: Implication to aerosols' indirect radiative effect. *Journal of Geophysical Research: Atmospheres, 108*(D1), AAC-2.

151. Hirsch, E., Koren, I., Levin, Z., Altaratz, O., & Agassi, E., (2014). On transition-zone water clouds. *Atmospheric Chemistry & Physics, 14*(17).

152. Chen, R., Chang, F. L., Li., Z., Ferraro, R., & Weng, F., (2007). Impact of the vertical variation of cloud droplet size on the estimation of cloud liquid water path and rain detection. *Journal of the atmospheric sciences, 64*(11), 3843-3853.

153. Alam, K., Khan, R., Blaschke, T., & Mukhtiar, A., (2014). Variability of aerosol optical depth and their impact on cloud properties in Pakistan. *Journal of Atmospheric and Solar-Terrestrial Physics, 107*, 104-112.

154. Cai, Z., & Tian, L., (2016). Atmospheric controls on seasonal and interannual variations in the precipitation isotope in the East Asian monsoon region. *Journal of Climate, 29*(4), 1339-1352.

155. Balachandran, S., & Rajeevan, M., (2007). Sensitivity of surface radiation budget to clouds over the Asian monsoon region. *Journal of earth system science, 116*(2), 159-169.

156. Steli, H., Diouri, M., Marsli, I., & Tahiri, A., (2016). Aerosol and cloud optical depths (AOD and COD) in the equatorial area. *Environ Sci Hikari Ltd, 4*, 39-51.

157. Colman, R., Fraser, J., & Rotstayn, L., (2001). Climate feedbacks in a general circulation model incorporating prognostic clouds. *Climate Dynamics, 18*(1-2), 103-122.

158. Weare, B., C., (1997). Climatic variability of cloud radiative forcing. *Quarterly Journal of the Royal Meteorological Society, 123*(540), 1055-1073.

159. Li, J., Wang, T., & Habib, A., (2017). Observational characteristics of cloud radiative effects over three arid regions in the Northern Hemisphere. *Journal of Meteorological Research, 31*(4), 654-664.

160. Sathiyamoorthy, V., Shukla, B., P., & Pal, P., K., (2011). A study on radiative properties of Indian summer monsoon clouds. *Meteorology and Atmospheric Physics, 113*(1-2), 55-66.

161. Chang, F., L., & Coakley Jr, J., A., (2007). Relationships between marine stratus cloud optical depth and temperature: Inferences from AVHRR observations. *Journal of climate, 20*(10), 2022-2036.

162. Kim, B. G., Schwartz, S. E., Miller, M. A., & Min, Q. (2003). Effective radius of cloud droplets by ground-based remote sensing: Relationship to aerosol. *Journal of Geophysical Research: Atmospheres, 108*(D23).

163. Del Genio, A. D., & Wolf, A., B., (2000). The temperature dependence of the liquid water path of low clouds in the southern great plains. *Journal of climate, 13*(19), 3465-3486.

164. Kaufman, Y., J., Koren, I., Remer, L., A., Rosenfeld, D., & Rudich, Y., (2005). The effect of smoke, dust, and pollution aerosol on shallow cloud development over the Atlantic Ocean. *Proceedings of the National Academy of Sciences, 102*(32), 11207-11212.

165. Engström, A., & Ekman, A., M., (2010). Impact of meteorological factors on the correlation between aerosol optical depth and cloud fraction. *Geophysical Research Letters, 37*(18).

166. Lin, B., Minnis, P., & Fan, A., (2003). Cloud liquid water path variations with temperature observed during the Surface Heat Budget of the Arctic Ocean (SHEBA) experiment. *Journal of Geophysical Research: Atmospheres, 108*(D14).

167. Devara, P., C., S., & Raj, P., E., (1998). A lidar study of atmospheric aerosols during two contrasting monsoon seasons. *Atmosfera, 11*(4), 199-204.

168. Feingold, G., Eberhard, W., L., Veron, D., E., & Previdi, M., (2003). First measurements of the Twomey indirect effect using ground-based remote sensors. *Geophysical Research Letters, 30*(6).

169. Jones, T., A., Christopher, S., A., & Quaas, J., (2009). A six year satellite-based assessment of the regional variations in aerosol indirect effects. *Atmospheric Chemistry and Physics*, *9*, 4091-4114.

170. Geoffroy, O., Brenguier, J., L., & Sandu, I., (2008). Relationship between drizzle rate, liquid water path and droplet concentration at the scale of a stratocumulus cloud system.

171. Saavedra, P., Battaglia, A., & Simmer, C., (2012). Partitioning of cloud water and rainwater content by ground-based observations with the Advanced Microwave Radiometer for Rain Identification (ADMIRARI) in synergy with a micro rain radar. *Journal of Geophysical Research: Atmospheres*, *117*(D5).

172. Kobayashi, T. (2007). Significant differences in the cloud droplet effective radius between nonprecipitating and precipitating clouds. *Geophysical research letters*, *34*(15).

173. Myhre, G., Stordal, F., Johnsrud, M., Kaufman, Y., J., Rosenfeld, D., Storelvmo, T., ... & Isaksen, I., S., (2007). Aerosol-cloud interaction inferred from MODIS satellite data and global aerosol models.

174. Alam, K., Iqbal, M. J., Blaschke, T., Qureshi, S., & Khan, G., (2010). Monitoring spatio-temporal variations in aerosols and aerosol–cloud interactions over Pakistan using MODIS data. *Advances in Space Research*, *46*(9), 1162-1176.

175. Kazil, J., Feingold, G., & Yamaguchi, T., (2016). Wind speed response of marine non-precipitating stratocumulus clouds over a diurnal cycle in cloud-system resolving simulations.

176. Jacobson, M., Z., & Kaufman, Y., J., (2006). Wind reduction by aerosol particles. *Geophysical Research Letters*, *33*(24).

177. Elliott, D., Schwartz, M., & Scott, G., (2004). Wind Resource Base. Encyclopedia of Energy.

178. Tang, J., Wang, P., Mickley, L., J., Xia, X., Liao, H., Yue, X., ... & Xia, J., (2014). Positive relationship between liquid cloud droplet effective radius and aerosol optical depth over Eastern China from satellite data. *Atmospheric Environment*, *84*, 244-253.

179. Tripathi, S., N., Pattnaik, A., & Dey, S., (2007). Aerosol indirect effect over Indo-Gangetic plain. *Atmospheric Environment*, *41*(33), 7037-7047.